Fall 2010

Electrical and thermal behavior of Im7/977-3 Carbon fiber polymer matrix composites subjected to time-varying and steady electric currents

Phillip Eugene Deierling
University of Iowa

ELECTRICAL AND THERMAL BEHAVIOR OF IM7/977-3 CARBON FIBER POLYMER MATRIX COMPOSITES SUBJECTED TO TIME-VARYING AND STEADY ELECTRIC CURRENTS

by

Phillip Eugene Deierling

A thesis submitted in partial fulfillment
of the requirements for the Master of
Science degree in Mechanical Engineering
in the Graduate College of
The University of Iowa

December 2010

Thesis Supervisor: Assistant Professor Olesya I. Zhupanska

Graduate College
The University of Iowa
Iowa City, Iowa

CERTFICATE OF APPROVAL

MASTER'S THESIS

This is to certify that the Master's thesis of

Phillip Eugene Deierling

has been approved by the Examining Committee
for the thesis requirement for the Master of Science
degree in Mechanical Engineering at the December 2010 graduation.

Thesis Committee: Olesya I. Zhupanska, Thesis Supervisor

Albert Ratner

Jia Lu

To my parents, brother and sisters

Strive for perfection in everything you do.
Take the best that exists and make it better.
When it does not exist, design it.

Sir Henry Royce

ACKNOWLEDGMENTS

Special thanks to Professor Olesya I. Zhupanska for her guidance, direction and encouragement throughout this research. The experiences throughout this research will serve priceless in the years to come in my professional engineering career and personal life. Special thanks to Harrison Harnisch for his designing, programming and support for the time-coordinated impact set-up. I would also like to thank all of my friends for their support and guidance. Gratitude is extended to Professors Albert Ratner and Jia Lu for serving on the thesis committee. Finally, deepest thanks to my parents, brother, and sisters for their unwavering support in all of my endeavors.

TABLE OF CONTENTS

LIST OF TABLES

LIST OF FIGURES

CHAPTER 1

INTRODUCTION

1.1 Background Information

A composite is characterized as the combination of two or more constituent materials to create a useful third material (Jones, 1999). These constituent materials can differ greatly from one another in mechanical, electrical, thermal, and other material properties. Properties that can be improved are: strength, fatigue life, stiffness, corrosion resistance, weight, electrical conductivity and thermal conductivity (Jones, 1999). However, when these constituents are combined, a new material is created that can exhibit the best qualities of their constituents and even properties that were not present in the constituents by themselves (Jones, 1999). The combination of different materials will not always create a flawless material. While there may be improvements in particular properties, it will be at the expense of others. This is why the goal is to create a composite material possessing characteristics that are necessary to perform the desired task.

Whether we realize it or not, today's world is surrounded by composite materials. From the plywood used to enclose our homes to the composites used in aircraft that we use to travel the country, to the equipment used to play sports. The idea of combining different materials is not a new one at all. For example, around the 11th century, North African civilizations constructed homes from a mud, straw, and grass combination. This combination of different materials came to be known as cob. Today this material is still being used to construct homes due this combination's sustainability and insulating properties (Mud, 2010). It is this idea of combining materials that provides the motivation to create new composites.

Today, composites differ greatly from the mud and straw combinations of the past. The development of composite materials has begun a revolution in the application of such materials. The high stiffness and strength to weight of fiber ratio as well as mechanical and environmental properties have made composite materials increasingly popular as substitutes for commonly used pure materials (Swanson, 1997). The composite can also aid in the performance of structures or systems, as the designer has the freedom to choose specific fibers, matrix material and orientations to suit the application. Composites today are commonly classified into four groups: fibrous, laminate, particulate and combinations of the three (Jones, 1999). Fibrous materials are those that use many small diameters (μm) of fibers bounded by a matrix. These fibers can be materials such as beryllium, boron, carbon, graphite, steel, and aluminum (Jones, 1999). In these types of composites, the matrix material is just as important as the type of fiber when determining the material properties. An example of such a material is fiberglass as used in such applications as boats and older automobile bumpers. Here a polymer matrix is used to unite millions of fine glass fibers. The laminate consists of at least two or more materials that are bonded together to form a single material. A commonly used example of this type of material is plywood. Plywood is many different types of wood and thicknesses bonded together to form one piece. This allows the material to exhibit qualities that are not present in a single piece of the same dimensions. As the name suggests, particulate composites are composed of particles dispersed within a matrix. A common example of this type of composite is concrete, which consists of gravel, limestone or granite and sand combined in a cement matrix. The final classification for a composite is a combination of fibrous, laminate and particulate. An example of this type of material could be many layers of fibrous materials laid on top of each other to form a laminate.

Due to advancements in production, composites have been seen in many different industries over recent years. These areas include aerospace, military, automotive,

sporting goods and energy, to name a few. Composites were first given the opportunity to display their effectiveness in aerospace and military applications. Composites are naturally an appropriate replacement for traditional materials used in aircraft design due to low weight and high strength characteristics. It has been stated that, "Composites are the most important materials to be adapted for aviation since the use of aluminum in the 1920s" (Composites, 2010). This is emphasized by the fact that the heavier an aircraft is, the more fuel it will burn, making weight reduction a critical design consideration. Military aircraft were the first to utilize composite materials in large quantities, mainly due to manufacturing costs and aircraft maintenance procedures. For example, the V-22 Osprey tilt-rotor aircraft utilizes IM6/3501-6 carbon-fiber for 41% of the primary structure and an additional 8% is fiberglass (Swanson, 1997). This design concept was realized in the commercial sector as early as the 1950s with the Boeing 707 passenger jet. This aircraft incorporated fiberglass in about 2% of the structure (Composites, 2010). This, however, was just the start for Boeing with composite materials. Later models such as the Boeing 777, which is a 400-passenger commercial aircraft, comprises approximately 10% composites by weight with aluminum making up the majority of the remaining material (Swanson, 1997). This utilization of composites has taken another step, in Boeing's latest line of passenger aircraft, the 787 Dreamliner. The Dreamliner will incorporate as much as 50% by weight composite materials, allowing the aircraft to use 20% less fuel than similarly sized planes (Boeing, 2010). It is these implementations of composite materials that have driven a migration to other industries such as automotive and, sporting goods, as well as our infrastructure.

1.2 Literature Review

Over the last several decades, much effort has been focused on improving mechanical properties (e.g., strength-to-weight and stiffness-to-weight ratios) through

various modifications of the composite constituents. However, further improvements in structure weight savings from composite materials are limited, and new transformative paradigms are required for future technological advancements. One of the most recent paradigms is centered around the concept of multifunctionality, which combines multiple subcomponents performing unique functions (carrying load, sensing, control, shielding, etc.) into a single multifunctional component that can result in a significant improvement in overall system efficiency. Composite materials lend themselves naturally to the concept of multifunctionality because of their multiphase nature and inherent tailorability. At the same time, advancements in the design of the multifunctional composite structures require significant strengthening of the scientific base and expanding of our understanding of the complex interactions of multiple physical phenomena in composites, which is the aspect that provides the desired multifunctionality. Many of these phenomena result from multi-field interactions in composites. Thus, studies of coupled electrical, magnetic, thermal, mechanical and other field behavior in composites are critical in the context of multifunctionality.

The carbon fiber polymer matrix composites that constitute the focus of this work consist of electrically conductive fibers and dielectric polymer matrix, and are electrically anisotropic and conductive at the macroscale. Their electrical conductivity prompted development of damage-sensing techniques that are based on monitoring of changes in the electrical resistance that are a result of mechanical damage (Schulte et al., 1989, Angelidis et al., 2005, Wang et al., 2006, Prasse et al., 2007, Chung et al., 2007). The main focus of these studies was on accurate measurement of the composite's electrical resistance, which provides information on whether the composite has experienced damage. The applied electric currents are usually in the microampere range and are innocuous to the composites.

At the other end of the spectrum are studies on lightning striking a carbon fiber polymer matrix composite (Ogasawara, 2010), where electric current is in the kiloampere

range. The focus of those studies is on damage produced by the strike and on damage tolerance of composite structures exposed to lightning strikes.

In the present work, the behavior of carbon fiber polymer matrix composites subjected to steady electric currents up to 100 A is studied. This work is motivated by studies of Telitchev et al. (2008a, 2008b) and Sierakowski et al. (2008), who investigated the impact response of electrified carbon fiber polymer matrix composites and showed that impact resistance of composites can be improved by subjecting them to electrical load at the moment of impact. In the work of Telitchev et al. (2008a, 2008b), 32-ply unidirectional AS4/3501-6 carbon fiber (AS4) polymer matrix (3501-6 epoxy) composite materials were clamped down with a wooden fixture to prevent movement during impact and to provide support for the application of electrical current and a magnetic field. Here, wood was also selected to ensure that all current would pass through the composite material. In an effort to reduce the contact resistance at the composite-copper interface, many electrically conductive materials were investigated. Methods included: an untreated composite-copper interface used as a control, 3M #5012-copper conductive tape, 3M #05085 copper conductive tape, indium foil tape 99.99IN, 3M XYZ electrically conductive tape, and Duralco 120 electrically conductive silver-filled epoxy (Telitchev et al., 2008a). In this investigation, Duralco 120 was found to provide the best decrease in electrical contact resistance. Once the contact resistance was lowered, a steady electrical current of 0, 25 or 50 A was then applied to the composite specimen immediately before and during impact. Preliminary results indicated that the application of current had a significant improvement on the impact resistance of the composite specimens (Telitchev et al., 2008b). Moreover, it was observed that the amount of impact load sustained by the composite was dependent on the magnitude of the electric current. It was found that larger current magnitudes resulted in higher impact load sustained by the composite (Telitchev et al., 2008b).

Additional work performed by Sierakowski et al (2008) investigated the effects of electrical current application to unidirectional and cross-ply carbon fiber polymer matrix composites. The effects of current duration and reduction of contact resistance were of concern. The steady current employed was also 0, 25 or 50 A, with this being limited by the power supply used. The impact results on the electrified cross-ply composites agree with the previous results on the unidirectional composites (Telitchev et al., 2008b). The electrified composites were able to withstand higher impact loads when subjected to short-term application of steady current than the non-electrified samples. Moreover, for cross-ply specimens, electrified composites not only were able to withstand higher impact loads, but also had reduced impact-induced damage.

The work of Sierakowski et al. (2008) also aimed at observing the behavior of composites when subjected to prolonged applications of steady electric current. In these experiments the composites specimens were subjected with steady electric current until a steady-state temperature was reached. The composites were then subjected to an impact load while current was still passing through the specimens. For a unidirectional sample, this steady-state temperature of 35.94^{o}C was reached in 24 min with a steady current of 25 A. In this case, the amount of impact load sustained was increased, but at the cost of reduced absorbed energy resulting in failure. With longer current durations, it was determined that the thermal effects suppress the effects of the electromagnetic coupling, resulting in diminished impact resistance. Thus, it was concluded that the duration of the current application and current-induced heating play an important role in the impact behavior of electrified composites: short-term current application improved the impact response of the tested composite plates and prolonged application of an electric current appeared to have a detrimental effect on the composites. A heat transfer model for electric current-induced heating in composites was proposed by Sierakowski et al. (2008), and analytical and numerical (using finite element modeling) investigation into the thermal heating effects was performed. Analysis showed that a prolonged application

of steady electric currents results in large temperature gradients across the composite plate. It was also determined that the non-uniform temperature distribution across the composites observed in prolonged current applications is a result of the heat generated in electric contact and is not due to the heat produced in current-conducting carbon fibers. On the contrary, in short-term current applications, the temperature in the center of the plate (impact location) is believed to be controlled by the Joule heat produced in the fibers. There was no experimental work done that would confirm these findings.

Magnetic flux density was measured by a Gaussmeter with transverse and axial field probes (Telitchev et al., 2008a). It was determined that the strength of the magnetic field increases with an increase in the current density and at closer distances to the electrical contact interface. The surface temperature of the composites was measured by a non-contact thermometer. Here, it was found that the temperature quickly increases, and then eventually reaches a steady state temperature.

Experiments carried out by Zantout (2009) aimed to further build on the previous work. In addition to confirming the previous results of electrified impact, the electrical characterization of cabron/epoxy composites was performed. Here, different types of materials (AS4/3501-6 and IM7/977-2) of varying ply counts (8, 16 and 32) and fiber orientations (unidirectional and symmetric cross-ply) were studied. Methods of reducing contact resistance and developing a fully automated system were also explored. The electrical contact resistance had proven to be the primary source of temperature distribution in the composite plates subjected to electrical currents. The first goal of this work was to examine different methods that could reduce electrical contact resistance at the composite/copper interface. After experimental trials, a method was developed that resulted in the lowest contact resistance. This method involves: (i) sanding the composite area of electrical contact with 220, 440 and 600 grit sandpaper; (ii) cleaning the specimen with acetone; (iii) treating contact edges with Duralco 120 with hardener and allowing them to completely dry; (iv) lightly sanding treated edges with 600-grit sandpaper; (v)

applying light coat of Duralco 120 without hardener to contact edges. This process was found to produce consistent contact resistances (Zantout, 2009). Additionally, light pressure was used to "clamp" the copper bus bar to the composite, further reducing contact resistance. Furthermore, periodic sanding of the copper bus bars was done to remove corrosion buildup.

Further advancements included developing a completely automated system to apply steady electrical current and real-time measurements of voltage, current, resistance and surface temperature. This set-up allowed for complete control of the sample rates, current magnitude and duration. In addition, all data was outputted in an EXCEL format for post-processing. Advancements were also attempted to further investigate the temperature distribution in the composite plates. Here, five k-type thermocouples were attached to the composite surface near the contact interface to approximately the middle of the composite plate. However, problems were found in consistently attaching the thermocouples to the surface. Lack of secure connection resulted in poor thermal conductivity between the surface and the thermocouple. This resulted in inconsistent surface temperature measurements. However, it was noted that one thermocouple did provide sufficient results for analysis.

The following conclusions were reached (Zantout, 2009). Electrical resistance of the composites was found to decrease with an increase in current magnitude. Furthermore, the resistance was found to monotonically increase with time. Moreover, it was found that an increase in the current magnitude, duration, or electrical resistance resulted in an increase in the surface temperature. A concise report of the electrical characterization results on AS4/3501-6 and IM7/977-2 composite laminates along with the analysis of these results is reported by Zantout and Zhupanska (2010).

The final portion of this work (Zantout, 2009) was to investigate the effects of low-velocity impact on electrified composites. Here it was found that the electrification increased the peak load and the amount of absorbed energy in AS4/3501-6 composites,

regardless of ply count and fiber orientation. The results of electrification for IM7/977-2 composites were found to be inconclusive due to the majority of cases resulting in 3% reduction in peak load and absorbed energy.

The focus of the present thesis is on the experimental study of the electrical and thermal behavior of IM7/977-3 unidirectional and symmetric cross-ply carbon fiber polymer matrix composites subjected to time-varying and steady electric currents. Results on the electrical behavior include electrical resistance as a function of electric load and time and voltage-current characteristics, whereas results on the thermal behavior are mostly concerned with the temporal and spatial temperature distributions, as well as a discussion on heat transfer mechanisms in the electrified composites. Moreover, a new experimental set-up for electrical and thermal characterization of composites subjected to highly dynamic electrical loads was developed as a part of this thesis. This set-up includes the possibility for coordinated application of electrical and impact loads with millisecond time delays between electric current and impact load applications.

1.3 Thesis Objectives

This thesis had four objectives to be achieved. The first objective was to study the electrical response of 32-ply IM7-977-3 unidirectional and symmetric cross-ply carbon fiber polymer matrix composite materials while being subjected to relatively high (up to 100A) electrical currents. The electric currents applied were a time-varying sine wave-form current and steady current. The sine wave-form current was applied under different minimum, maximum and therefore average currents, as well as varying frequencies. The goal was to investigate the effects of electric current magnitude, frequency and duration on the electrical resistance of the composites and their voltage-current characteristics.

The second objective of this thesis was to study thermal response of the electrified 32-ply IM7/977-3 unidirectional and symmetric cross-ply carbon fiber polymer matrix composites via direct measurements of the temperature at the surface of the electrified composite specimens. The goal was to investigate the electric-current-induced heating in the composites and elucidate the effects of resistance and electric current intensity, duration and shape in the thermal response of the electrified composites. As noted earlier, vast amounts of research have been conducted on composite materials. The majority of such research is focused on the damage incurred and the failure modes. However, very few have been concerned with the electrical and thermal response of electrified composites.

The third objective was to design and build a fully automated experimental set-up for real-time measurements of the electric current, resistance, voltage, and temperature in carbon fiber polymer matrix composites, which would allow for the previous two objectives to be completed. This objective included researching equipment such as data acquisition units, temperature measurement devices, and power supplies. Moreover, programming of this equipment had to be performed to ensure that all equipment would be synced together to allow for a completely automated system. Additionally, an experimental procedure needed to be developed to allow for all experiments to be repeated in a consistent manner.

The final objective was to create a system capable of generating an electric current and time-coordinated impact application to the composite specimens with a time resolution of < 100 ms for future low-velocity impact testing. This unit needed to be capable of initiating an impact at a set time during an application of current with minimal alternation of the impact tester.

CHAPTER 2
EXPERIMENTAL SET-UP AND EXPERIMENTAL PROCEDURES

2.1 Experimental Considerations

There were three main considerations in the electrical and thermal characterization that needed to be addressed: (i) effective current application, (ii) surface temperature measurement, (iii) and a reduction in contact resistance.

This work builds upon the accomplishments of Telitchev et al. (2008b), Sierakowski et al. (2008), and Zantout (2009), who studied electrified carbon fiber polymer matrix composites subjected to steady currents. The experimental set-up is a further development of the experimental set-up presented by Zantout (2009), with alterations allowing application of time-varying electric current, more accurate measurements of thermal response of the composites due to electric-current-induced heating, and conducting low-velocity impact tests, which are time-coordinated with electric current applications.

Once the set-up was created, electrical characterization experiments were conducted to understand the effects of time-varying current amplitude, frequency and wave shape on the composite before any impact testing could be conducted. This was an important step in the experimental procedure because it was found that changing the frequency or the shape of the electric load altered the output current of the power supply. Second, a new experimental set-up needed to be developed to allow for the real-time measurement of the temperature distribution across the composite surface. The new set-up was modeled on the set-up that was used previously and utilized five k-type thermocouples connecting directly to the surface of the composite (Zantout, 2009). This set-up needed to be revised due to difficulties in accurately measuring the surface

temperature. The last electrical consideration was reducing the contact resistance at the composite/electrode interface. This reduction in contact resistance would allow for increased current magnitude and duration.

2.2 Contact Resistance

One of the biggest obstacles of previous works (Sierakowski et al., 2007, Telitchev et al., 2008b, Zantout, 2009) was the issue of contact resistance at the interface of the composite and the copper bus bars. The result of contact resistance is excess heating of the composite. This excess contact resistance heating can cause irreversible, detrimental changes in the material properties of the composite. This also limits the magnitude and duration of current that can be applied to the composite during tests, and therefore needs to be minimized.

2.2.1 Causes and Effects of Contact Resistance

This section discusses the causes and effects of contact resistance. Contact resistance is created when two or more electrically conductive materials are brought together and electric current is transferred through them. Contact resistance is due to a number of factors such as small contact area, surface roughness, surface corrosion, dissimilar material electrical resistance and contact surface hardness to name a few. However, the driving force behind most contact resistance studied has been the surface roughness of the two materials. This asperity, or roughness, can vary from large visible surface deformities or inconsistencies down to the atomic scale (Braunovic, 2007). The level of the asperity has a direct effect on the amount of contact area that exists between the two materials. The locations for current to pass through in the contact area are known as "*a*-spots" (Braunovic, 2007). These "*a*-spots" are small when compared to the contact

area, so current encounters resistance to pass through to the other material. This current flow resistance and limited contact area can be seen in Figures 2.1 and 2.2 respectively.

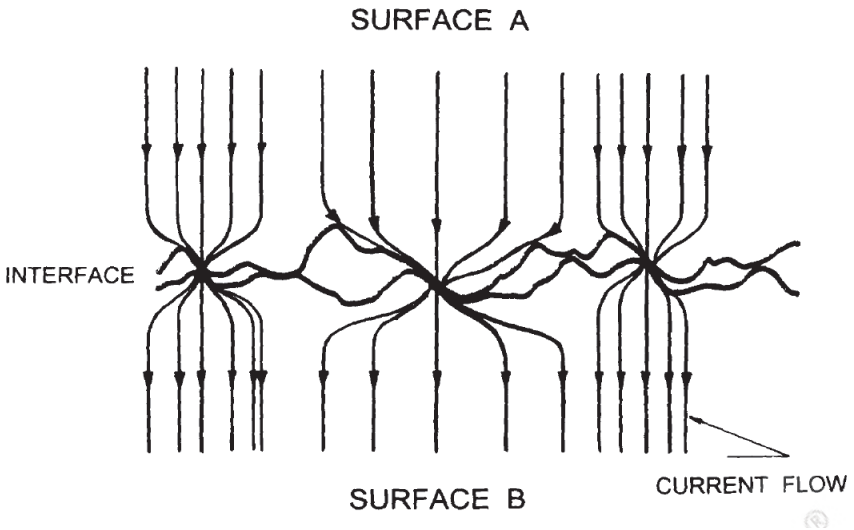

Figure 2.1: Current Flow Resistances (Braunovic, 2007)

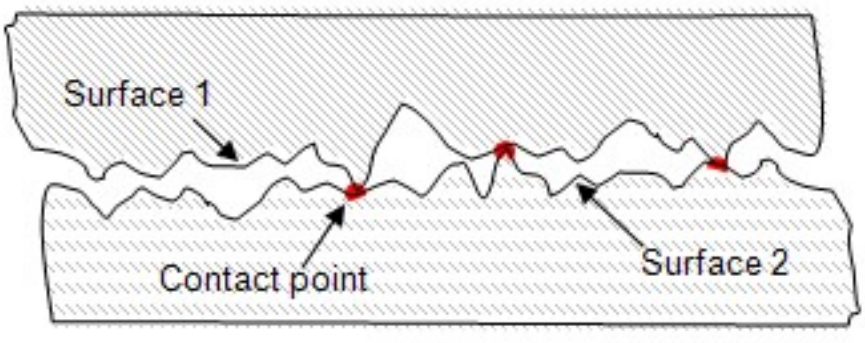

Figure 2.2: Limited Contact Area (Sunstone Engineering, 2010)

Contact resistance consists of two components, the film resistance and the constriction resistance. This relationship can be seen in Equation 2.1 (Joshi, 2004).

$$R = R_c + R_f \tag{2.1}$$

Here, R, R_c and R_f are the contact, constriction and the film resistance, respectively, in ohms. The film resistance is defined as a substance or external layer on the contact surface that has different properties than those of the underlying contact surface (Joshi, 2004). This film resistance could be corrosion, grease, dust, or oxides that have formed on the contact surface (Joshi, 2004). In the case of the composite samples, the film resistance can be assumed to be negligible. The constriction resistance is caused by the contact between the composite and the copper bus bars. This resistance is present because the contact is discontinuous since the fibers are conductive, and the polymer matrix is dielectric (Sierakowski, 2008), and there are contact surface irregularities. The constriction resistance depends on the hardness of the contact members and the contact pressure as expressed in Equation 2.2 (Joshi, 2004).

$$R_c = k\zeta\sqrt{\frac{10H}{F}} \tag{2.2}$$

Here ς is the resistivity of the contact material in ohm-cm, H is the hardness of the contact surface in N/mm^2, F is the contact force in MN, and K is a constant whose value is approximately 100.

This resistance is what ultimately causes heating to occur at the contact interface of the materials. The relationship of contact resistance and heat generation can be seen in Equation 2.3 (Sierakowski et al., 2008).

$$q_c = \frac{I^2 R_c}{A} \tag{2.3}$$

In this equation, I_c is the current passing through the contact surface, A is the contact area, and R_c is the contact resistance. It can be seen that a reduction in the contact resistance or an increase in the area can have a significant reduction in the amount of heat generated at the interface. Since the areas of the composite samples are fixed, a reduction in the contact resistance is what was addressed.

2.2.2 Contact Resistance Reduction Techniques

In this section, techniques to lower contact resistance are evaluated. The primary goal in reducing the contact resistance between two materials is to increase the contact area and therefore increase the size and number of "*a*-spots". There are many different ways of reducing the contact resistance between two materials. The contact resistance can be decreased through any technique that increases the surface contact between the two materials (Slade, 1999). Some suggested techniques and processes are electrodeposition (electroplating, electroless plating) and cladding (Braunovic, 2007). Other techniques include compressive forces, conductive epoxies and conductive silicones/grease. To determine which technique would be used, the proposed suggestions were investigated to determine the feasibility of using them in the lab setting.

2.2.2.1 Electrodeposition

Electrodeposition is a process in which electric current is carried across an electrolyte and a substance is deposited at one of the electrodes (Mohler, 1969). This substance is commonly silver, copper, tin, and gold. The deposition of these materials

onto another material can aid in corrosion resistance, surface hardness and increased electrical conductivity. Electroplating and electroless plating are both processes that describe how the electrodeposition process is taking place. Electroplating uses external electricity to carry out the plating process while electroless uses the deposited metal as a catalyst to fuel the reactions (Mohler, 1969). These processes can create surfaces that are electrically conductive. These surfaces will aid in the increase of "*a*-spots" to decrease contact resistance. This process would not be able to be carried out in the laboratory because of the complex equipment involved, making it not a feasible choice.

2.2.2.2 Cladding

Cladding is covering the contact area of the samples with a material that possesses superior electrical conductivity, such as copper, silver, or nickel (Braunovic, 2007). This technique allows for an efficient transfer of electrical current to the composite samples, thus lowering the contact resistance. However, to secure the cladding to the samples compressive forces would be required to ensure that the cladding is properly adhered to the edge of the sample. These forces could cause changes in the properties of the samples that may alter the response of the composite during testing.

2.2.2.3 Compressive Forces

As shown previously in Equation 1.2, the contact force, F, can increase the electrical contact. By increasing the contact force, a greater contact area can be created. This contact area is created by forcing the irregularities to come together and produce a flatter and larger contact surface. Greater contact area results in more "*a*-spots" and thus reduced contact resistance. However, one drawback of increasing the force at the contact interface is that bending forces and stresses are introduced that were not present to begin

with. Because a continuation of this work will be impact testing, additional forces and stresses could be detrimental and affect the impact results of the composites.

2.2.2.4 Conductive Epoxy, Silicone and Grease

Use of conductive epoxy, silicone, and grease was the last contact resistance reduction method that was investigated. In previous works, conductive epoxy was used at the contact interface to improve the contact resistance. This was found to increase the contact area and electrical conductivity and, therefore, reduce the contact resistance (Zantout, 2009). To build on these findings, conductive epoxies as well as silicones and greases were investigated. Silicones and greases were researched because they offered the ability to flow. This flow would allow for the substance to fill the voids of the contact interface and thus further decrease the contact resistance. Additionally, these techniques are also easy to apply in the laboratory setting as elaborate equipment is not necessary.

Experimental testing of different epoxies, silicones and greases provided feedback for the best method of reducing the contact resistance. In these experiments, the conductive epoxy used in the previous work proved to be the best choice for reducing the contact resistance. The silicone and grease produced a reduction in contact resistance, but not at the levels of the conductive epoxy. Therefore, conductive epoxy was verified as the best method for contact resistance reduction and chosen for the experiments carried out.

2.3 Experimental Set-Up for Testing Composites Subjected to Steady Electric Currents

This section describes the experimental set-up that was previously developed and used for the electrical characterization of carbon fiber polymer matrix composites

subjected to steady electric currents. Also, the type of equipment used and descriptions are provided.

2.3.1 Electrical Characterization for Steady Currents

For the electrical characterization of carbon fiber polymer matrix composites, a fully automated steady current set-up was developed at The University of Iowa by Zantout (2009). The set-up consisted of a power supply, data acquisition switch unit, computer, precision electrical shunt, test fixture and five k-type thermocouples. The entire system of hardware was controlled by Agilent's VEE Pro 8.5 software. This software provided control of the magnitude and duration of the current applied to the composite specimens and defined the sampling rates of the data acquisition system for electrical and thermocouple measurements (Zantout, 2009).

2.3.1.1 Power Supply

The power supply used was an Agilent 6692A 6600 watt model. This power supply is capable of 110 A and 60 V of DC (steady) current application. The 6692A also has a precision programming accuracy of 0.04% +60 mV and 0.1% + 65 mA on the voltage and current, respectively, when operated at 25^{o}C ±5^{o}C (Agilent, 2010). The power supply was chosen because of its high current output, and because it allowed for automated control via a GPIB connection directly to a computer.

2.3.1.2 Data Acquisition

The data acquisition switch unit used was an Agilent 34970A. The 34970A is capable of high precision, 6 1/2 digits (22-bit), and up to 250 channels per second scan

rate (Agilent, 2010). This switch unit also allowed for direct measurements of DC/AC voltage and current, resistance, frequency, period, B, E, J, K, N, R, S, and T type thermocouples, thermisters, and RTDs (Agilent, 2010). This data acquisition unit was used to determine the current supplied to the composite and electrical resistance of the composite specimen by means of Ohm's law as well as to measure and record the temperature from the five k-type thermocouples.

2.3.1.3 Precision Electrical Shunt

The current applied to the sample was determined by measuring the voltage drop across the electrical shunt and then using Ohm's law to determine the current. The Deltec MKB-100-200 precision electrical shunt was used. This shunt was rated at 100 mV and 200 A, resulting in a constant resistance of 0.5 mΩ from 0 to 200 A (Deltec, 2008). The electrical resistance of the composite was determined by measuring the voltage drop across the sample and using Ohm's law once again with the previous determined current to find the resistance. The data acquisition was also used to measure the output signal from the five k-type thermocouples and convert it into the corresponding temperature of the composite surface.

2.3.1.4 Test Fixture

In order to secure the composite specimens during electrical and impact characterization, a fixture needed to be developed. The fixture needed to be capable of bench-top testing as well as fit into the impact-testing fixture. Due to the samples being electrified, a fixture needed to be designed that would ensure that all current passed through the composite samples and not through the fixture itself. This was accomplished by using wood as the construction material, as it is a non-conductive material. The

fixture also had to meet the impact requirements in accordance with ASTM standard D5728-07, ASTM standard D3763-06, and NASA's Standard Tests for Toughened Resin Composites. With these standards, a custom test fixture was designed and constructed. This fixture can be seen in Figure 2.3.

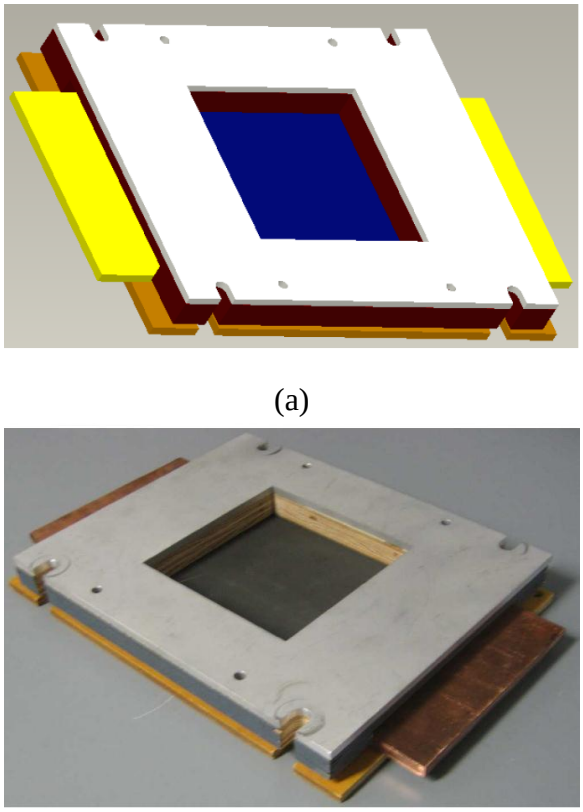

(a)

(b)

Figure 2.3: Test Fixture (a) Modeled in ProEngineer® (b) Fabricated (Zantout, 2009)

Following the standards mentioned previously, the fixture was to allow the composite to be clamped by compression perpendicular to the composite plies (ASTM, 2006). The

composite also needed to be clamped around the entire perimeter of the composite sample with at least one half of one inch overlay for clamping (ASTM, 2007). Lastly, the fixture was to allow the sample being tested to be placed in a NASA impact test stand. This stand exposes a five inch square area to be impacted by the tup impact head (ASTM, 2006). As seen in Figure 2.1, this test fixture is designed to fit into the impact-testing machine fixture. To allow the fixture to be used on the bench, a special mount was designed and constructed to allow the sample to be securely clamped for electrical testing. This bench-top mount can be seen in Figure 2.4.

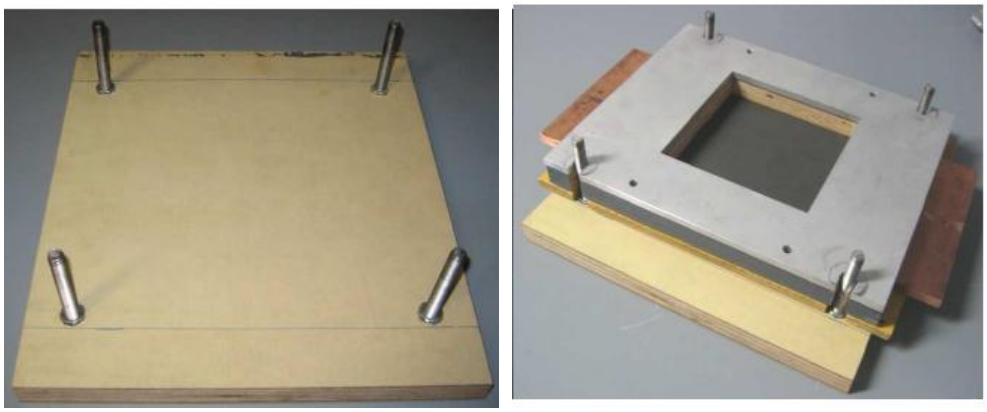

(a) (b)

Figure 2.4: Bench-top Mount (a) Alone (b) With Fixture (Zantout, 2009)

It can also be seen in Figure 2.3 that to provide the electric current to the composite specimens, copper bus bars connected by heavy gauge wire to the power supply were used to complete the electrical connection to the entire length of the contact area. The dimensions of the copper bus bars used were 152.2 x 101.6 mm (6 x 4 in) with a

thickness of 9.5 mm (3/8 in). These dimensions were chosen based on the results from FEM modeling (Zantout, 2009). The copper bus bar material properties can be seen in Table 2.1. Maple and plywood were used on the base and middle plates, respectively, to ensure that all current passed through the composite sample, while aluminum was used on the top to provide structure rigidity (Zantout, 2009).

Table 2.1: Copper Bus Bar Material Properties

Density [kg/m^3]	8700
Specific Heat [J/kg K]	380
Thermal Conductivity [W/mK]	401
Electrical Conductivity [1/Ω^{-1}]	0.58x10^8

2.3.1.5 K-Type Thermocouples

The thermocouples used were Omega k-type twisted and shielded thermocouple wire. These thermocouples allow for a wide range of temperature measurements, -200^o C to 1250^o C (-328^o F to 2282^o F) (Thermocouples, 2010). The shielding of the wire was chosen to reduce the possibility of any noise or false readings due to the magnetic fields created by the power supply during the experiments (Zantout, 2009). The thermocouples were attached to the fixture by a special holder to keep the thermocouples secure to the surface. This holder can be seen in Figure 2.5, while Figure 2.6 shows the complete fixture with the thermocouple holder attached.

All of the measurements and calculations were automated by a computer using Agilent's VEE Pro 8.5 software. The software enabled the user to control the current applied to the composite and set the data acquisition rates of voltage, current, resistance, and temperature measurements. The results of the calculations along with the time of each measurement were exported to a Microsoft EXCEL spreadsheet where data analysis could be performed. A schematic of the set-up can be seen in Figure 2.7.

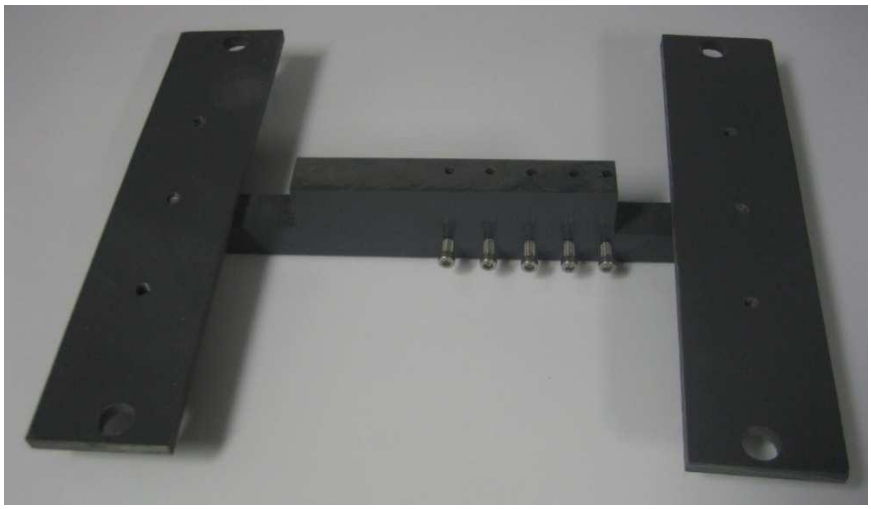

Figure 2.5: Thermocouple Holder (Bottom View) (Zantout, 2009)

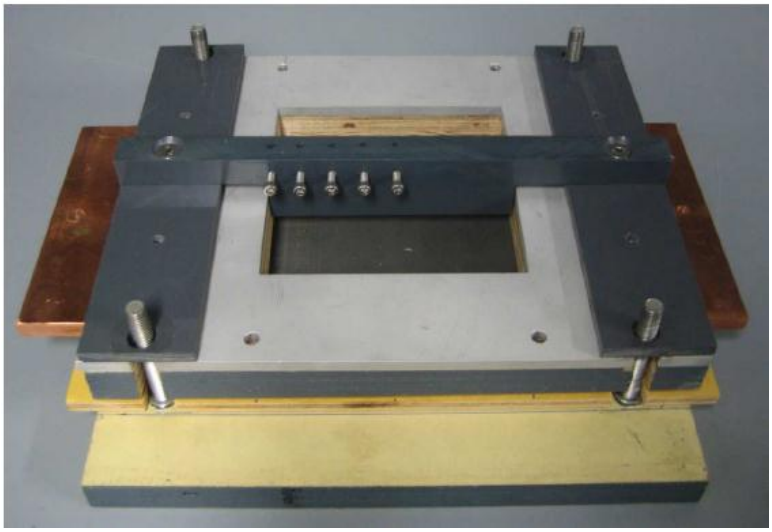

Figure 2.6: Complete Fixture with Thermocouple Holder Attached (Zantout, 2009)

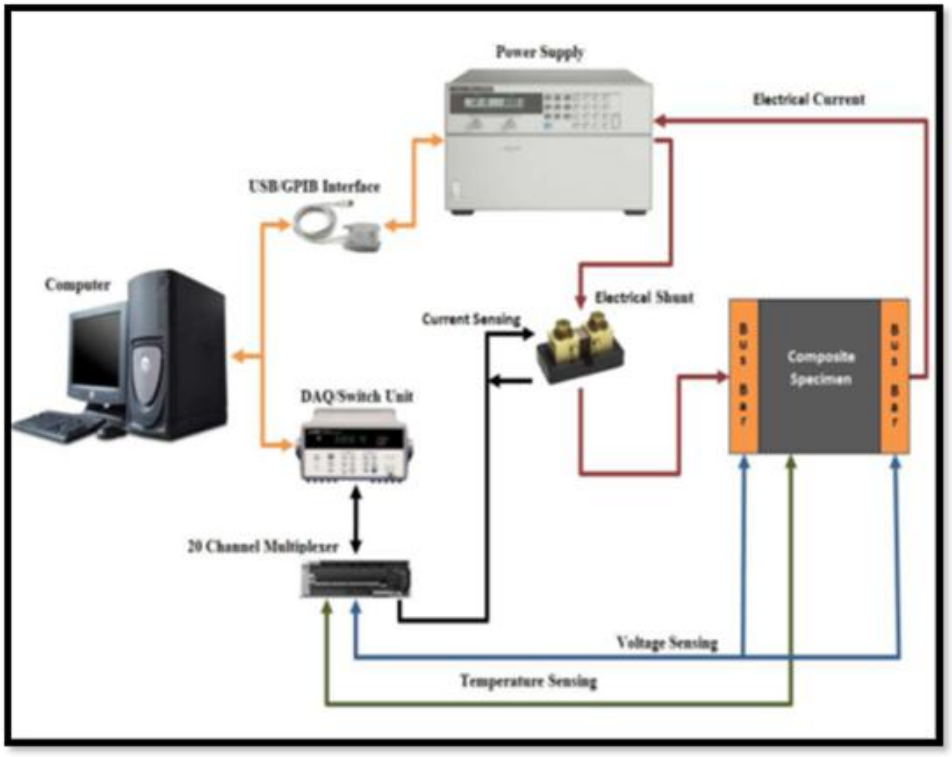

Figure 2.7: Steady Current Electrical Characterization Test Set-Up (Zantout, 2009)

2.3.2 Impact Testing Set-Up for Electrified Composites

Once the electrical experimental set-up was completed, impacting of the composite samples could take place. The purpose of the impact stage of the experiments was to investigate the effects of current application to the composite samples while they were being impacted. Characteristics that were examined were impact energy, impact load, and deflection (Zantout, 2009). These experiments would either confirm or disprove that the material can withstand greater impact energies and loads when electrified vs. non-electrified (Telitchev, 2008b, Sierakowski, 2008). The impact set-up consisted of an impact tester, custom holding fixture, data acquisition, and signal conditioning unit.

2.3.2.1 Impact Testing Machine

The machine used for impact tests was the Instron 8200 Dynatup impact tester. This machine is a low-energy impact tester that was specifically designed for the impact testing of plastics and composites. This machine is capable of performing impact tests in many standards, such as ASTM 3763, Boeing 7620, NASA ST-1, and others. The machine is capable of a maximum velocity of 4.4 m/s (14.5 ft/sec), and an impact energy range of 1.356 J to 132.8 J (1ft-lb to 97.9 ft-lb) (Dynatup, 2010). However, experimental findings have shown the maximum impact energy to be 150 J (Zantout, 2009). This impact tester can be seen in Figure 2.8.

Figure 2.8: Instron 8200 Impact Tester (Dynatup, 2010)

To vary the impact energy and velocity, the height of the carriage and the weight on the carriage are adjusted to produce the desired impact characteristics. The impact tester was also fitted with the optional impact pneumatic rebound brake (Dynatup, 2010). This rebound brake would ensure that only one impact was taking place on the composite by preventing the impact tup from bouncing on the surface. The dimensions of this machine are as follows: 406 mm (16 in) wide, 457 mm (18 in) deep, and a height of 2305 mm (90.8 in).

2.3.2.2 Test Fixture

The fixture used to secure the composite specimens for impact testing is the same fixture used in the electrical characterization as described in Section 2.2.1.3 earlier.

However, during impact testing, the thermocouples and thermocouple holder were removed.

2.3.2.3 Data Acquisition and Signal Conditioner

The Instron 8200 machine also came with its own form of data acquisition and signal conditioning. The data acquisition was used to collect data on impact energy, impact load, deflection, and impact duration. The signal conditioner was used to remove any noise present in the signal. The unit is specifically designed for use with the Instron line of impact-testing equipment. The unit is capable of sample rates from 1.25 to 5 MHz with built-in signal conditioning and filtering (Dynatup, 2010). The unit adds user-friendly operations by incorporating many popular test standards with many preset calculations already selected depending on the type of impact test that is selected. The unit is used in conjunction with the Impulse ^{TM} software supplied with the DAQ. This software has the capabilities of generating plots of impact load, deflection, or any plot that may be desired. The data acquisition unit can be seen in Figure 2.9 below. The unit is triggered to start acquisition by a flag and photogate on the impact machine. The flag is a two-pronged piece of metal attached to the falling carriage. The photogate is a beam that remains fixed on the impact machine. Once the first prong on the flag passes through the photogate, a signal is sent to the DAQ to begin sampling data. Next the second prong on the flag passes through the photogate. Once the second prong has passed through the photogate, the velocity of the falling carriage can be calculated. This is done by knowing the width of the flag (distance) and the amount of time between each passing of the photogate. All of these calculations are done just slightly before the impact. The photogate can be adjusted by moving it up or down to compensate for different material thickness. The flag and photogate trigger can be seen in Figure 2.10.

To determine the absorbed energy and the impact load, a load cell is attached to the bottom of the crosshead of the impact machine. The complete instrumented load cell assembly includes a striker that is connected to a strain gage transducer (tup), which is then attached to a mounting plate, which is finally attached to the bottom of the crosshead of the impact machine. This instrumented load cell can be seen in Figure 2.11. A consideration that needed to be addressed was the standard striker that is supplied with the impact machine. This striker is 12.7 mm (0.5 in) in diameter with a hemispherical shaped head made of steel. The problem with this striker is that it is electrically conductive, which will pose a problem due to some samples being electrified during impact. To overcome this obstacle, a special impact-resistant striker was used that was also an electrical insulator. The striker chosen was constructed from DELRIN® material with a flat head and 12.7 mm (0.5 in) diameter. The material has a Rockwell Hardness of 94 (HR 120), making it suitable for repeated impacts (DuPont, 2010). Both the standard and the DELRIN® striker heads can be seen in Figure 2.12.

Figure 2.9: Impact Data Acquisition Unit

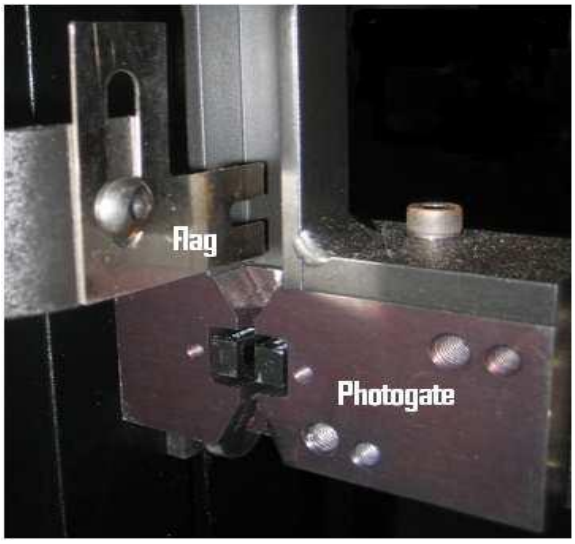

Figure 2.10: Data Acquisition Trigger Flag and Photogate (Zantout, 2009)

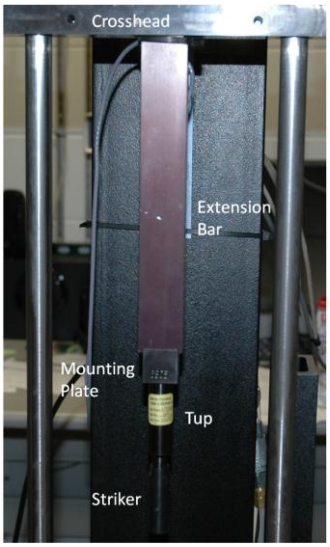

Figure 2.11: Complete Instrumented Load Cell Assembly

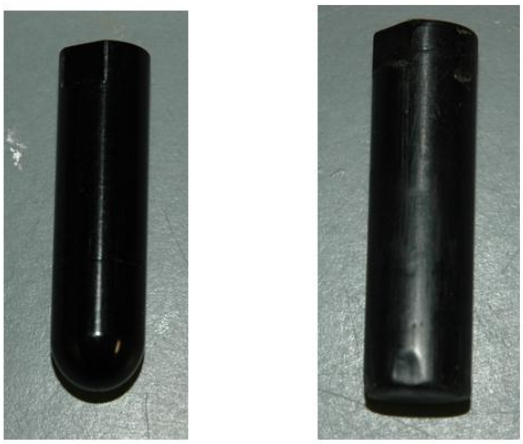

(a) (b)

Figure 2.12: Impact Striker Heads: (a) Standard Steel (b) DELRIN®

2.4 A New Experimental Set-Up for Testing Composites Subjected to Time-Varying Electric Currents and Impact Loads

2.4.1 Requirements for the Experimental Set-Up

The previous experimental set-up (as described in Section 2.2) could not be used in the application of the time-varying electrical current due to limitations. One of the clear limitations of the previous set-up was that it only allowed for the application of steady currents. Because time-varying currents were desired, this was one motivation to develop a new set-up. Furthermore, the previous set-up also did not give accurate or repeatable results of the surface temperature distribution. Because the surface temperature distribution was a crucial measurement in the experimental procedure, this needed to be altered to allow for more accurate and consistent results. Moreover, the speed of the data acquisition system was not capable of capturing a time-varying signal.

Sampling rates for the previous set-up would only be capable of capturing the real-time response of the composite subjected to a time-varying load at low operating frequencies. Lastly, the system was unable to allow for a time-coordinated impact with the electrical load. In previous work, this was done by simply estimating the time of current application and manually releasing the impact carriage on the machine. These limitations of this system are only because the design was intended for steady current applications only and was not anticipated to be used in another manner.

The experiments carried out in this work involved the electrical characterization of carbon fiber polymer matrix composites subjected to time-varying electric loads. The electrical characterization involved four key measurements that were needed to characterize the response to time-varying loads. These measurements include: current, voltage, resistance, and surface temperature distribution. In order to effectively capture these measurements, the experimental set-up needed to adhere to the following requirements: (i) effective application of time-varying current; (ii) real-time measurements of current, voltage, and resistance; (iii) real-time surface temperature measurement; (iv) current and time-coordinated impact; (v) completely automated system. To fulfill these requirements, a custom experimental set-up was developed to complete the experiments in this work.

The set-up for the time-varying electrical characterization needed to be capable of supplying high current to the tested composite samples, since it was noticed in previous steady current studies (Sierakowski et al., 2007) that there was a direct relationship between the impact response and the amount of current applied to electrified composite samples. In the present work, the maximum electric current magnitude was also 100 A. The maximum current magnitude was limited by the power supply used, which was the same as in the work of Zantout (2009).

Although the increase in current magnitude has shown to have positive effects on the impact response of electrified composites, the application of high current leads to

large amounts of heat that is generated within the composite sample. Additionally, heating is also a result of lower current magnitudes for extended application duration. This heating is caused by contact resistance at the composite-copper interface and heating within the fibers (Joule heating) (Slade, 1999). If excess heating is introduced, it has been shown to have detrimental effects on the impact resistance of the composite (Telitchev et al., 2008b). As a result, finding methods to lower the contact resistance was an important step in the experimental set-up. This Joule and contact heating also made monitoring the composite surface temperature crucial during experiments so the composite samples would not be excessively heated and cause permanent damage to the material. The use of time-varying electrical loads is proposed to have both the benefits of improving the damage resistance of composites and reducing the detrimental heating effects (Zhupanska, 2009).

A further requirement for the experimental set-up was to have the capability of time-coordinated impacts. The set-up had to be capable of accurately and consistently releasing the impact carriage. This time-coordinated impact required small time increments (< 100 ms) related to the application of the time-varying electrical load. Maintaining a time-coordinated impact with the application of electrical current ensures that accurate data and relationships, if any, between the effects of time-varying electrical load and impact could be established.

In order to satisfy the above requirements, two new experimental set-ups were created: (i) electrical characterization (ii) and time-coordinated impact testing. The two set-ups needed to have the ability to work together as well as independently from one another.

2.4.2 Time-Varying Electric Current Characterization Set-Up

The custom electrical characterization set-up included a function generator, power supply, test fixture, data acquisition system, precision electrical shunt, and temperature measurement. The complete electrical characterization set-up can be seen in Figure 2.13. A few of the components of the time-varying electric current characterization set-up were used from the previous steady electrical current characterization set-up. These components include the computer, power supply, and shunt resistor, which are all described in Section 2.2.1. The following descriptions and specifications only include new components that were added to the time-varying electric current characterization set-up.

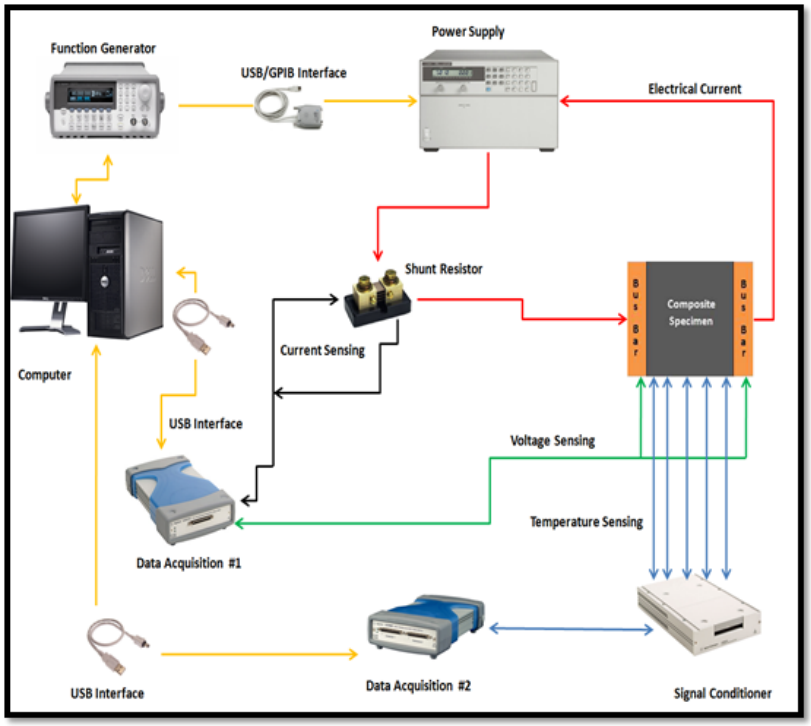

Figure 2.13: Time-Varying Electric Current Characterization Set-Up

2.4.2.1 Test Fixture

To provide the electric current to the composite samples, a fixture needed to be utilized to hold the sample in place for both electrical characterization and impact testing. As well as being capable of bench-top and impact testing, this fixture needed to be constructed of a non-electrically conductive material to ensure that no electrical shorts were present to make sure all of the current would flow through the composite specimens. The test fixture used in the steady electrical characterization tests was examined to determine if it would be a suitable test fixture for the experiments to be performed. After investigation it was found that the text fixture suffered from charring and chipping of the wood surface. Furthermore, it was found that when placing the composite sample in the fixture, the position had to be measured to ensure that each sample was placed in the same position for every experiment. Moreover, it was determined that in impact testing the copper bus bars could "jump" out of contact with the composite, causing a momentary loss of current supply if not secured properly. These discoveries led to a redesign of a testing fixture to accommodate electrical and impact characterization requirements as described in Section 2.2.1.3. For bench-top testing, the previous bench mount developed by Zantout (2009) was used. The newly Pro/E designed fixture as seen in Figure 2.14 is based mostly on the previous design but includes improvements to aid in simplifying experiments. One such improvement is the implementation of alignment bars to eliminate the need to measure the placement of the composite specimen in the fixture. The second addition is end clamps to ensure that the copper bus bars cannot "jump" out of contact when impact is taking place. These two additions can be seen in Figure 2.15. The completely assembled fixture with bench mount can be seen in Figure 2.16.

The fixture is composed of three main components, the base, middle plate, and top plate, as seen in Figure 2.14. The base plate and middle plate needed to be

constructed of a non-electrically conductive material to ensure that all current was forced to flow though the composite. The type of material chosen was poplar. This type of wood was chosen because of its rigidity and good machining characteristics. The top plate did not have any electrical conductivity issues that needed to be addressed as no current would be passing through the material. Therefore, the top plate was machined from a solid piece of 6061-T6 aluminum. Aluminum was chosen because it would add additional strength and rigidity to the rest of the fixture. Additionally, aluminum provides light weight with excellent machining characteristics. Two versions of the top plate were fabricated, one for electrical characterization, and one for impact testing. The electrical characterization top plate incorporated openings to allow for the five infrared k-type thermocouples to be inserted. This top plate can be seen with the five infrared thermocouples installed in Figure 2.17.

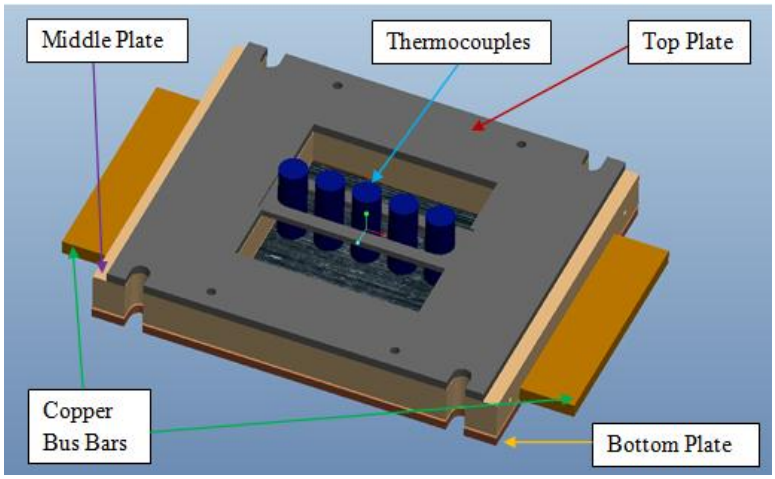

Figure 2.14: Pro/E Designed Fixture

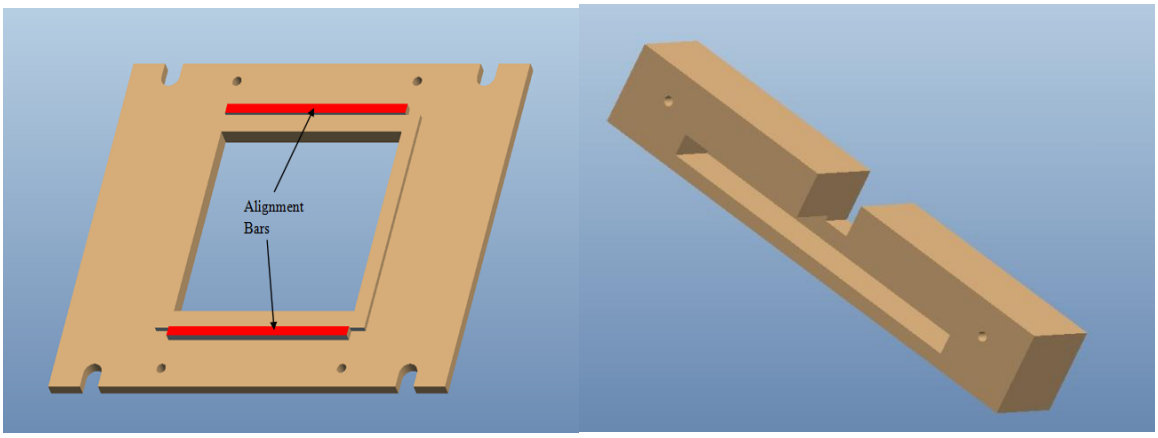

(a) (b)

Figure 2.15: Fixture Additions: (a) Alignment Bars (b) End Clamp

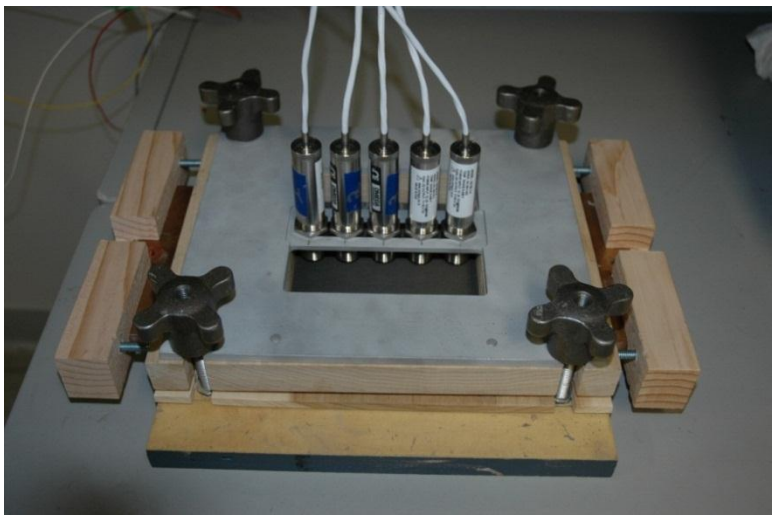

Figure 2.16: Completely Assembled Fixture with Bench Mount

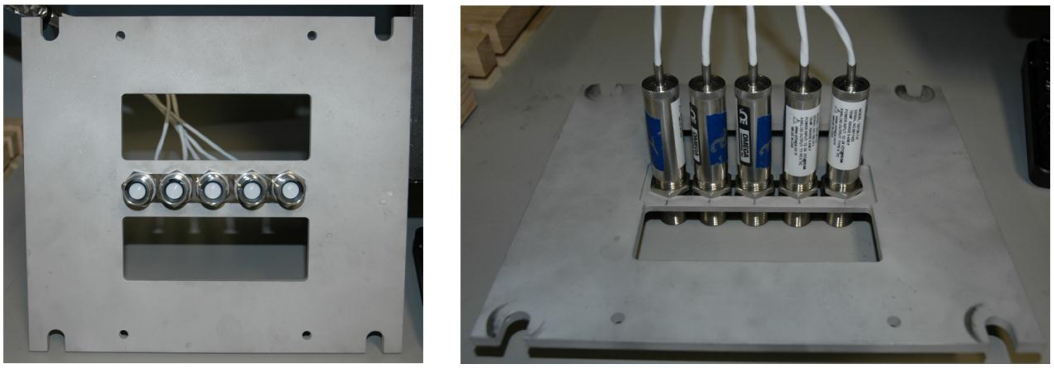

(a) (b)

Figure 2.17: Top Plate: (a) Bottom View (b) Top View

The second top plate was used only for impact testing. This top plate had a 5x5 inch (127x127 mm) pocket machined to ensure that it would not interfere with the impact. This impact top plate can be seen in Figure 2.18.

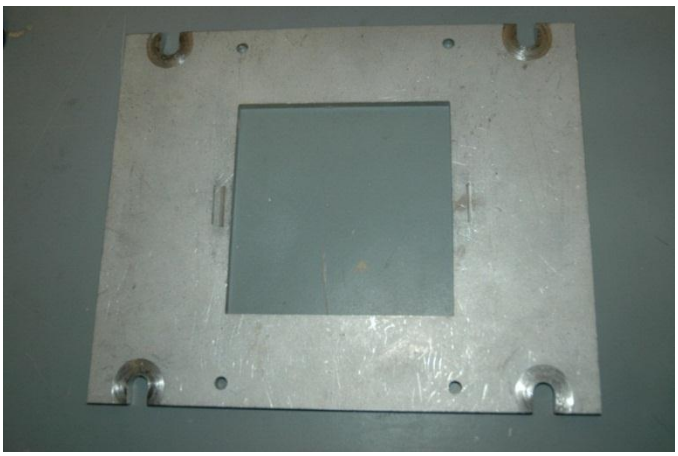

Figure 2.18: Impact Top Plate

2.4.2.2 Function Generator

In order to apply time-varying current, an Agilent 33250A 80 MHz Function/Arbitrary Wave Generator was chosen in conjunction with the previous Agilent 6692A 6600-watt power supply used in steady current tests. This function generator was used as an analog input for the power supply. The function generator is connected to the power supply via analog inputs on the back of the power supply. Once the function generator output is connected to the power supply, the power supply will transform the output to mimic the input by using an internal switching system incorporated within the power supply. Once the waveform is chosen from the function generator, the power supply will supply the composite with the input waveform up to approximately 1000 Hz depending on the current amplitudes desired. The relationship between the analog input voltage and the output current of the power supply can be seen by Equation 2.4.

$$\frac{FGV}{5V} = \frac{PSA}{110A} \tag{2.4}$$

where *FGV* is the voltage from the function generator and *PSA* is the output current of the power supply in amps.

This function generator has the capabilities to produce sine, square, ramp, noise, pulse and user-defined waveforms with variable frequencies and rise/fall times (Agilent, 2010), allowing the user to specify the type of time-varying load applied to the specimen. The function generator can also be connected and controlled by a computer via a General Purpose Interface Bus (GPIB), allowing the entire system to be synced together.

2.4.2.3 Data Acquisition

To capture the real-time changes in electric current and voltage, a data acquisition (DAQ) unit was used. The first step was to determine if the previous DAQ system used for the steady current tests could be used for the experiments with the time-varying electric currents. The previous DAQ was an Agilent 34970A data acquisition/switch unit. This unit is capable of high precision, 6 1/2 digits (22-bit), internal digital multi-meter, thermocouple signal conditioning, and up to 250 channels per second scan rate (Agilent, 2010). This DAQ would have been an ideal choice because the unit was already implemented into the entire system. Upon reviewing the operating manual on the unit, it was found that the maximum sample rate was approximately 250 samples per second operating on one channel. This DAQ operated on 2-7 channels depending on the experiment; therefore, the realistic maximum sampling rate would be 125 samples per second. The Nyquist theory was used to determine what sampling rates the DAQ would be capable of operating at (Agilent, 2010). The Nyquist theory states that the minimum sampling rate should be 2x the highest frequency of the incoming signal that is being measured. Moreover, it is suggested to use 5-10x the highest frequency being measured if permitted (Agilent, 2010). Using the Nyquist theory with the minimum of 2x sampling rate, only 125 samples per second could be achieved. This sample rate resulted in a maximum frequency of 62.5 Hz. This was also verified experimentally to ensure that the unit would not be sufficient for the time-varying experiments. Therefore, an alternative DAQ unit would have to be investigated. After looking into different manufacturers' products, the U2531A USB Modular Simultaneous Data Acquisition from Agilent Technologies was chosen. This unit allowed for up to 14 bits of resolution, four analog input measurements, four digital input measurements, and 2M and 1M samples per second on each analog and digital input, respectively (Agilent, 2010). From 0-55^{o} C the U2531A has an offset error of ± 2 mV and a gain error of ± 6 mV. The DAQ unit is

controlled via a USB 2.0, allowing for the unit to be controlled and synced together with other equipment via the computer. Data acquisition is controlled by the Agilent Measurement Manager (AMM) software included with the unit. The key benefit of choosing this unit is the high sampling rate of each channel. This allowed for up to 1 MHz of input signal at the minimum of 2x sampling rate and effective acquisition of the time-varying signals the composites are subjected to. The resistance of the composite is determined indirectly by using Ohm's law as seen in Equation 2.5.

$$R = V / I \tag{2.5}$$

where R is the resistance of the composite, V is the voltage drop across the composite, and I is the current through the composite. This method to determine the resistance of the composite had to be utilized as the U2531A DAQ only allows for voltage measurements. To determine the current passing through the composite sample, a precision electrical shunt was used before the sample to produce a voltage drop. This voltage drop was measured by the DAQ and then the current was calculated using Ohm's law. The same Deltec MKB-100-200 0.5 mΩ precision electrical shunt used in the steady current electrical set-up (Section 2.2.1), was used for the time-varying electrical set-up.

2.4.3 Temperature Measurement

It has already been pointed out that understanding the temperature distribution across the composite sample was crucial for both interpreting electrical characterization results and understanding the relationship between the applied electric current and the impact resistance of the carbon fiber polymer matrix composites. It was also crucial to avoid any permanent thermal damage to the composite samples during electric current applications. Previous methods for measuring the temperature distribution at the surface

of the composite specimens included five k-type thermocouples spaced across the composite monitored by the DAQ with built-in k-type signal conditioning (Zantout, 2009). This method proved to be inconsistent in temperature measurements. One of the tasks of the present study was to determine the cause of this inconsistency and develop a better temperature measurement system that can provide consistently accurate temperature measurements. A thorough investigation showed that errors in the measurements were due to lack of proper contact with the composite surface. Previously, Arctic Silver was used between the thermocouple and composite interface (Zantout, 2009). Arctic silver is a thermally conductive compound that contains 99.9% pure silver and is designed to increase the heat conduction between two materials (Arctic Silver, 2010). In the present work, in an attempt to achieve a consistent contact between the thermocouple and composite surface, a thermally conductive adhesive was used to ensure proper contact was being made. The McMaster-Carr Part #US1150 was used. This adhesive has a temperature range of -65^{o} C to 125^{o} C, thermal conductivity of 0.486 W/m*k (McMaster-Carr, 2010). Performing experiments with this adhesive holding the thermocouples to the composite surface did produce better results of temperature measurement. However, this process was found to be time consuming as it was recommended to wait for a period of 48 hours for the adhesive to reach full strength (McMaster-Carr, 2010). Additionally, this method would not permit the thermocouples to be removed after they were adhered to the composite surface. Not being able to find a reasonable solution to the contact problem of the k-type thermocouples led to an investigation of non-contact measurement devices.

2.4.3.1 Infrared K-Type Thermocouples

A non-contact measurement device utilizes infrared wavelengths to measure temperature of a surface. The first step involved determining what products were

available and if they would be a feasible choice. To aid in the selection, a set of constraints needed to be adhered to. These constraints involved temperature measurements from at least 20 to 150^{o} C, small size scale, and being easily adaptable to the newly designed experimental set-up. After looking into different manufacturers' products, the OS136-1-K infrared thermocouple from Omega engineering was chosen. This OS136-1-K model allows for temperature measurements from -18 to 202^{o} C (0 to 428^{o} F) with a k-type thermocouple output signal, 150 ms response time, accuracy of 3% of reading, a fixed emissivity of 0.95, and 12-24 Volts @ 50 mA of power required. Furthermore, the units are packaged in a 19 mm (0.75 in) OD by 89 mm (3.5 in) stainless steel housing making them durable as well as compact (Non-Contact, 2010). A picture of the infrared thermocouple can be seen in Figure 2.19. This unit was an ideal choice because the temperature range fit into the desired criteria and the small size allowed for up to 5 units to be placed evenly across the composite surface. The thermocouples also would fit into the newly designed test fixture with minimal alteration.

Figure 2.19: Infrared K-Type Thermocouple (Non-Contact, 2010).

To ensure that any external noise would not affect the signal output of the thermocouples, an external shielding was used to completely enclose all of the wires from

the thermocouples. The shielding that was chosen was McMaster-Carr part # 7940K33 EMI/RFI wire shielding. This shielding protects wire from electromagnetic and radio frequency interference, with an operating temperature of -40 to 107^{o} C (-40 to 225^{o} F) (McMaster-Carr, 2010). To record the temperature in real time, an additional power supply, signal conditioner and data acquisition unit were needed.

2.4.3.2 Infrared Thermocouple Power Supply

In order for the infrared thermocouples to operate, a 12-24 V constant voltage was needed to function properly. To supply this constant voltage, the Agilent 6612C 40 watt power supply was chosen. This unit is capable of 20 volts and 2 amps (Agilent, 2010). This unit is also capable of providing enough power to supply all five of the thermocouples at once, eliminating the need for additional power supplies. This power supply can be seen in Figure 2.20.

Figure 2.20: Infrared Thermocouple Power Supply (Agilent, 2010).

2.4.3.3 Signal Conditioner

To obtain accurate temperature measurements, the output voltage from the thermocouples needed to be amplified to allow for the data acquisition to acquire the small changes in the signal. The signal conditioner chosen for the set-up was the Agilent U2802A 31 channel thermocouple input signal conditioner. This conditioner is capable of conditioning low input signals from J,K,R,S,T,N,E and B type thermocouples into higher output signals, which can then be recorded using a data acquisition system. The unit also incorporates a built-in thermistor for cold junction compensation to simplify temperature measurements (Agilent, 2010). The error for the gain and offset are 0.06% and 6 μV, respectively. The cold junction compensation has an accuracy of ± 1^{o}C. These errors combine for an accuracy of ± 1.5^{o}C for k-type thermocouple measurements (Agilent, 2010). This unit can be seen in Figure 2.21.

Figure 2.21: Agilent U2802A 31 Channel Thermocouple Signal Conditioner (Agilent, 2010).

2.4.3.4 Temperature Data Acquisition Unit

The final piece of equipment is the Agilent U2356A 64 channel data acquisition unit. This unit was chosen because it is specially designed to be compatible with the U2802A signal conditioner. The unit is capable of 500,000 samples per second and 16 bits of resolution, allowing for fast sampling of the varying temperatures (Agilent, 2010). Both the U2356A and U2802A are synced with the rest of the equipment and computer via USB 2.0 connections and with the use of the AMM software. The temperature data acquisition unit can be seen in Figure 2.22. The unit has a gain and offset error of ± 1 mV and ± 2 mV, respectively. With the additional temperature measurement equipment in place, the temperature could be easily measured and recorded in real time to determine the temperature distribution across the composite surface.

Figure 2.22: Agilent U2356A 64 Channel Data Acquisition Unit (Agilent, 2010)

2.4.3.5 Experimental Limitations

During testing of the time-varying electrical characterization set-up, there were a few limitations of the system that were discovered. The frequency that can be applied to the composite is limited by the internal switch of the power supply and by the current applied. The operating manual of the power supply suggests a maximum internal switching speed of 1000 Hz. A thorough testing of the characterization set-up revealed that this value was closer to 750 Hz in order to achieve consistent wave shapes. Furthermore, the frequency was found to be a function of the current and vice versa. Here, signals with minimum and maximum current levels closer together or "shrunk" would permit a higher frequency to be applied. This was found to be the inverse for signals with minimum and maximum current levels far apart. Therefore, if signals with large separation in the current peaks are desired, the frequency at which the power supply will be able to produce a consistent wave is significantly reduced. This reduction is only determined by experimental verification. One solution that was found to overcome this wave reduction was to overdrive the current peaks by setting the upper and lower voltage limits higher and lower, respectively. This would allow for the power supply to produce the desired current peaks at higher frequencies. Additionally, it was found during experiments that the time-varying load will not be applied from the same starting point for every experiment. This was found to be due to the position of the waveform and the initiation of the power supply output. An example of this would be with one wave starting at a minimum and another starting at a maximum. This difference in start location produces two similar waveforms in different phases. This difference in phase can be seen in Figure 2.23.

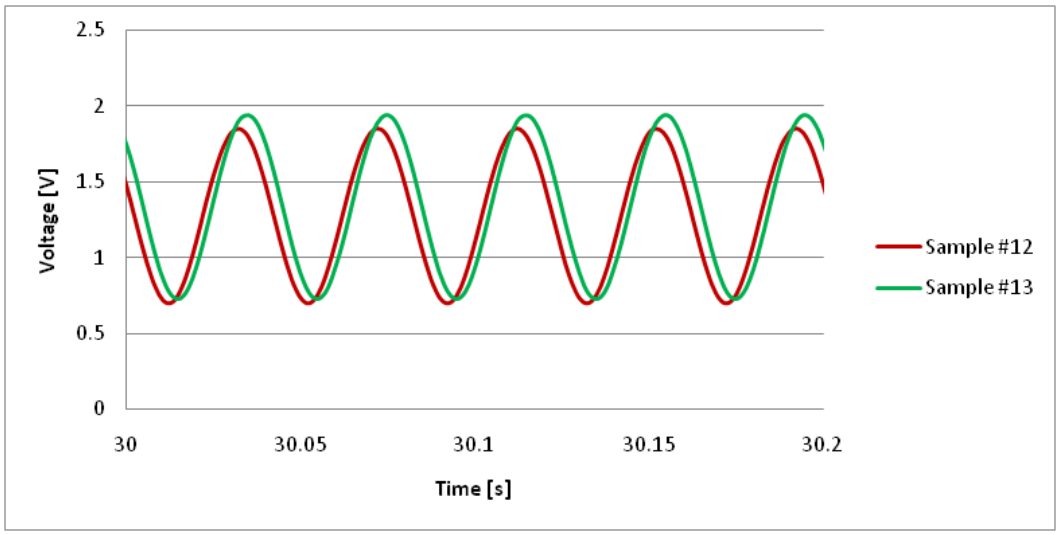

Figure 2.23: Voltage vs. Time, Difference in Phase

As seen in Figure 2.23, the voltage measurements with respect to time are out of phase between the samples #12 and #13. These measurements were taken on two different samples with identical waveforms of 50 A average currents and at a frequency of 25 Hz.

For temperature measurements, there were limitations as well. The infrared thermocouples operated at a response time of 150 ms, resulting in a maximum response rate of approximately 7 Hz. To keep measurements standard for all experiments, sampling rates of 20 times the frequency being tested were always used even for the temperature data acquisition. This was done to simplify the acquisition and data analysis as the same time step would be taken for both the electrical characterization and thermal response. Since the sampling frequency was higher than the operating frequency of the infrared thermocouples, data filtering and reduction was incorporated to remove repeated values due to oversampling. Additionally, during experiments, it was required to keep the surface temperature of the composite specimen under 177^{o} C as this is the glass

transition temperature for IM7/977-3 composites (Cycom, 2010). Furthermore, it was found in previous work that 150^{o} C was the temperature at which the wooden fixture would begin to char (Zantout, 2009). This charring temperature was assumed to be the same for the newly designed testing fixture even though a different type of wood was used and would therefore be the limiting temperature in experiments.

2.4.3.6 Thermocouple Calibration Verification

An additional experiment was carried out that involved determining the accuracy of each infrared thermocouple compared to the manufacturer's specifications. The experiment consisted of using the Agilent U2802A signal conditioner, U2356A DAQ, 6612C 40 watt power supply, and an Omega BB703 Black Body Calibrator. The BB703 is a portable, miniature black body calibrator that is useful for calibrating infrared temperature equipment with temperature ranges of ambient +10^{o} C to 400^{o} C (ambient +20^{o} F to 752^{o} F) with a built-in 29 mm (1.125 in) black body target (Portable Blackbody, 2010). The accuracy of the calibrator is specified as ± 1.4^{o} C (± 2.5^{o} F) (Portable Blackbody, 2010). The procedure for this experiment was as follows: (i) set the black body calibrator to a specific temperature; (ii) record 10 measurements from each infrared thermocouple; (iii) repeat from 30 to 190^{o} C in increments of 20^{o} C. From here, the data was gathered and an analysis was performed to determine the accuracy of each of the thermocouples. The determined accuracy for each thermocouple and temperature can be seen in Table 2.2.

Table 2.2: Thermocouple Accuracy

Thermocouple	Accuracy	
	Minimum	Maximum
1	96.3	99.1
2	97.2	98.9
3	96.8	99.5
4	95.2	97.6
5	96.4	98.1

2.4.4 Time-Coordinated Impact Characterization Set-Up

The time-coordinated impact testing set-up included an impact machine, data acquisition system, air-actuated cylinder, electric air solenoid, and custom computer-controlled release timer. This set-up allowed for the drop weight of the impact tester to be released at exact times coordinated with the application of electrical load. Since the samples were tested electrified and non-electrified, a custom fixture, as described in Section 2.3.2.1, was designed to replace the metal fixture provided with the impact machine. This would ensure that the electric current would be forced to pass only through the composite samples during experiments. The complete impact testing set-up can be seen in Figure 2.24.

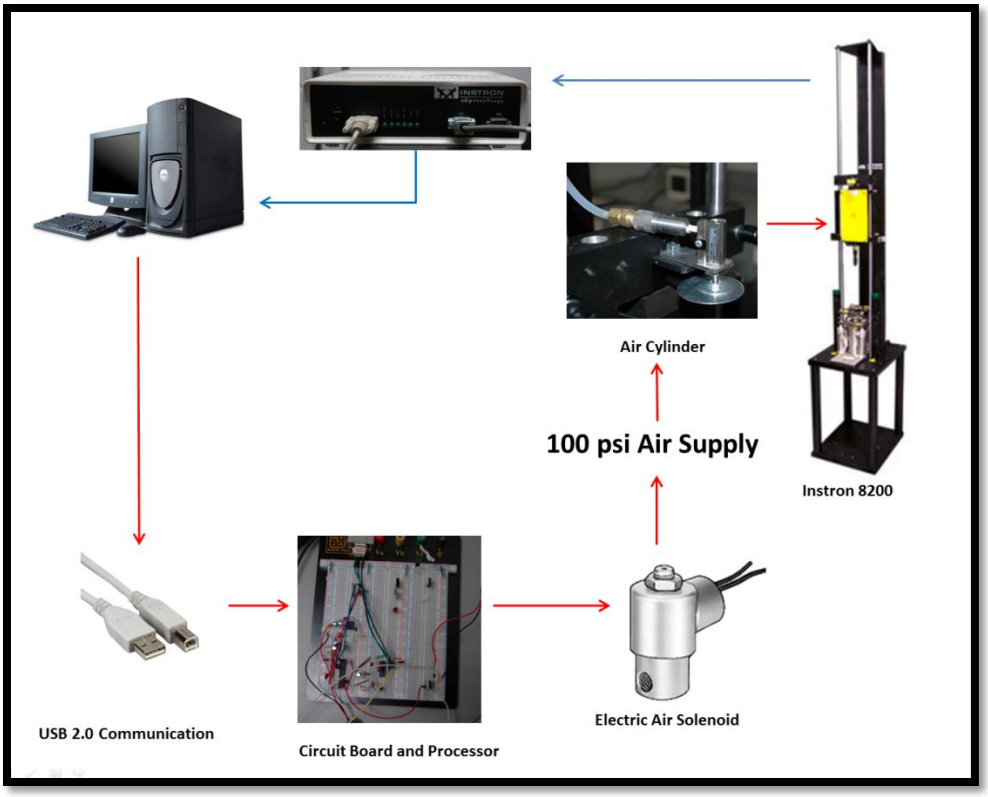

Figure 2.24: Time-Coordinated Impact Test Set-Up

Most of the components of the previous impact set-up were used for the current impact set-up. These components include the computer, impact tester as mentioned in Section 2.2.2.1, data acquisition, and signal conditioner as mentioned in Section 2.2.2.2. The following descriptions and specifications include only new components that were added to the new time-coordinated impact set-up.

2.4.4.1 Air-Actuated Cylinder

To initiate impact, a mechanism needed to be designed to release the carriage. The original design of the machine used a button that was pushed to release the drop

carriage. Since it was undesirable to alter the machine in anyway, a removable system was designed that would release the carriage at a desired time. The device that releases the carriage is an air-actuated cylinder. The force needed to actuate the button was found to be approximatley 4 lbs. This force was found by actuating the release mechanism with a force spring scale as shown in Figure 2.25. With the known force for release, a suitable air cylinder could be chosen.

Figure 2.25: Use of Spring Scale

The air cylinder that was chosen was the McMaster-Carr part# 59155K12, miniature brass air cylinder. This cylinder produces 9 lbs of force @ 100 psi with a stroke length of 6.35 mm (0.25 in) and a 9.53 mm (0.375 in) bore (McMaster-Carr, 2010). This air-actuated cylinder can be seen in Figure 2.26. The air cyliner operates by

extending the actuator to hit the release button on the impact tester when 100 psi of air is supplied. Once the air supply is shut off, the actuator releases the button. The actuation of the cylinder is what determines when the impact will be inititated. The supply of air to the cylinder is controlled by an electronic air solenoid. The air cylinder implemented on the impact tester can be seen in Figure 2.27.

Figure 2.26: Air-Actuated Cylinder (McMaster-Carr, 2010)

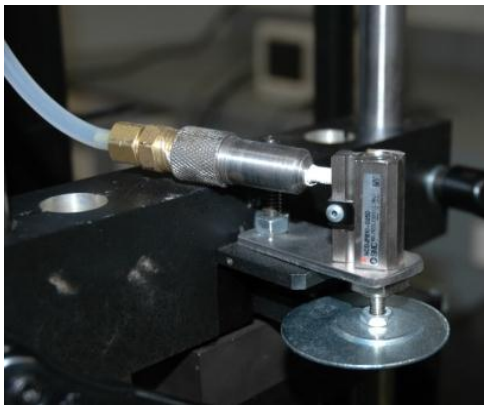

Figure 2.27: Air Cylinder Implemented

2.4.4.2 Electric Air Solenoid

To control the application of the air supply to the air cylinder, a valve needed to be used between the air supply and the cylinder. This valve would control when the air would be supplied to the air cylinder and hence, the drop time. This valve would need to be electrically actuated so that it could be controlled remotely. The selected valve was the McMaster-Carr part# 61245K84, solenoid air control valve. This solenoid valve has an operating range of 0-120 psi, one inlet, and one outlet port with 1/8 NPT. The solenoid valve can be seen in Figure 2.28.

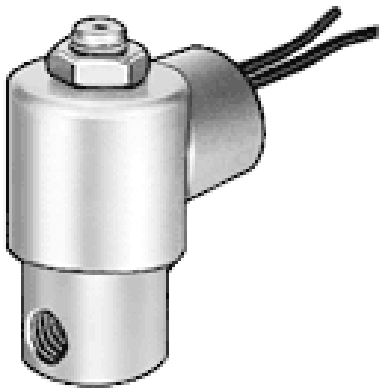

Figure 2.28: Solenoid Valve (McMaster-Carr, 2010)

The valve requires 12 VDC and draws 0.67 watts of power to operate, with a simple two-wire connection (McMaster-Carr, 2010). This valve was also chosen due to its small size, with a width of 30.48 mm (1.2 in) and height of 58.42 (2.3 in) (McMaster-Carr, 2010), making it easy to implement into the impact tester. The solenoid valve would need to be controlled by a system that could sync the opening and closing with the

rest of the system, such as the power supply, function generator, and data acquisition units. This timing was accomplished through the use of a custom designed and built timing unit. The solenoid valve implemented onto the back of the impact tester can be seen in Figure 2.29.

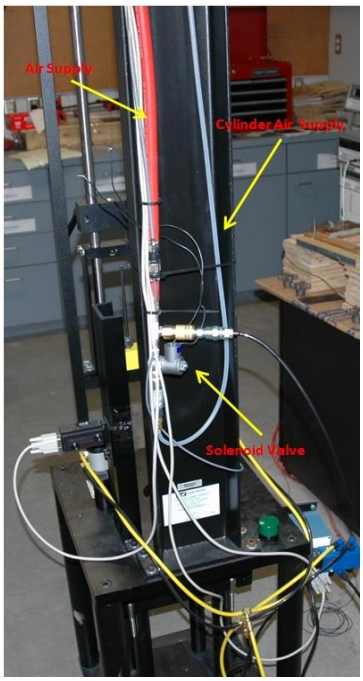

Figure 2.29: Solenoid Valve Implemented onto Back of Impact Tester

2.4.4.3 Computer-Controlled Release Timer

The opening and closing of the solenoid valve was controlled by a custom designed and built timing unit. The basic components of the unit are: (i) microcontroller; (ii) USB communication; (iii) 20 MHz crystal oscillator; (iv) 12 VDC power supply. The

timing unit works by receiving user input comands from a computer via the Agilent VeePro software. These commands are processed by a PIC18F4550 – Microchip 40 pin microcontroller. The communication between the computer and the microcontroller is handled by USB connection via emulated virtual COM port. The input comands are the drop height, delay time and desired drop time. The drop height, in m, is the value at which the impact is desired to take place. The delay time is an experimentally found value that accounts for the delay time for the solenoid, air cylinder and other components to operate. The drop time is time, in seconds, at which the impact is requested to occur. The time input has a resolution of 1 ms. The input for the height is used to calculate the fall time for the impact in seconds. The time is calcuated using Equation 2.6.

$$t = \sqrt{\frac{2h}{g}} \tag{2.6}$$

Here, h is the drop height in m and g is the acceleration due to gravity. This time calculation is then subtracted from the desired fall time inputted by the user to produce an impact that occurs at the actual desired time.

2.4.4.4 Summary of Time-Coordinated Impact Characterization Set-Up

Combining the custom programed microcontroller, electric solenoid, and air actuated cylinder, the complete time-coordinated impact set-up was complete. Testing of this set-up confirmed that the impact was occurring when desired in relation to current application with a 1 ms time resolution and an accuracy of ± 0.5 ms and repeatability of ± 0.01 ms as determined experimentally. Future use of this time-coordinated impact will

enable a researcher to accurately and consistently ensure impact occurs at a desired time with respect to current application.

2.5 Experimental Procedures

This section describes the procedure for how the experiments were carried out and repeated to ensure every test was performed following the same procedure. Because the electrical characterization and the impact response of an electrified composite incorporated much of the same components, the procedure for experimental testing was very similar between the two. One of the differences is that surface temperature measurements could not be performed during impact tests because the infrared thermocouples are positioned in such a way that they hinder impacts to the composite surface.

2.5.1 Composite Sample Preparation

The composite samples were prepared individually before each experiment to ensure that accurate and consistent results could be obtained. This was done to ensure that each sample would have similar electrical contact resistance. The composite materials that were supplied for testing came in large approximately 1397x1117.6 mm (55x44 in) sheets. Because the size required for testing was 152.4 mm (6 in) squares, the sheets needed to be cut into appropriate sizes. To do so, the sheets were first measured and marked to the appropriate size with silver paint markers. Once each sheet was marked with the proper dimensions, the specific type of material, the fiber orientation and the number of plies was written on the surface to clearly identify each specimen. To cut the large sheets into the individual 152.4 mm (6 in) squares, a table saw with a fine-tooth

finishing blade was used along with masking tape on both sides of the cut line to minimize any fraying during the cutting process.

After the large sheets were cut, the samples were ready to be prepared for electrical characterization. The process of preparing samples for electrification began by sanding and cleaning the edges that would be in contact with the copper bus bars. The sanding process was multi-step one, starting off with a 220 grit to remove any large imperfections, then a 440 grit to remove the 220 grit sand marks, and finally a 600 grit to create a smooth surface. To clean the composite surface and edges, acetone was used. Extreme care was taken not to expose the composite to the acetone for extended periods of time because the chemical was found to dissolve the polymer matrix of the composite specimens. To aid in placement of the specimen into the fixture, two lines were drawn onto the composite surface 11 mm (7/16 in) from each contact edge using silver paint markers to ensure that equal distances from each electrode were maintained. This was done to produce consistent results in the temperature distribution. This placement can be seen in Figure 2.30.

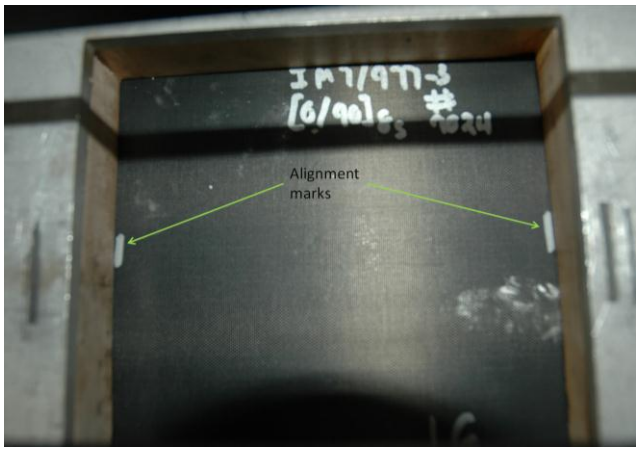

Figure 2.30: Sample Alignment Marks

Now that the composite samples were smooth and clean, the edges were treated to reduce the contact resistance at the composite/bus bar interface. To reduce the contact resistance, Duralco 120 was applied to the edges of the specimens. Duralco 120 is an electrically conductive epoxy that contains over 70% ultra-fine active silver. The epoxy also has a volume resistivity of 0.00008 ohm-cm at 500^{o} F operating temperature and cures at room temperature (Duralco 120, 2010). To apply the epoxy, the amounts of silver paste and hardener were measured to obtain the proper 100/3.5 weight ratio of paste to hardener as specified by the manufacturer. After thoroughly mixing, a thin, uniform coat of the mixture was applied to both edges of the sample. The epoxy was then given a minimum of 24 hours to cure and harden. After the epoxy hardened, a rough surface was created. This surface was then lightly sanded using a 600 grit sandpaper to flatten the surface and cleaned using acetone.

After the epoxy was sanded smooth and cleaned, a final coat of Duralco 120 was applied to both sample edges as well as both copper bus bars without the hardening agent mixed in. This was done because it was found in previous work to increase the contact areas and hence decrease the contact resistance (Zantout, 2009). As described earlier in Section 2.2.1, an increase in surface area and reduction in contact resistance results in a reduction in heat generation during the electrification process. The composite samples were now ready to undergo the electrification experimental procedure. The sample preparation for impact was the same for the electrical characterization except the back side of the samples were first given a thin coat of white spray paint. White paint was chosen because it was found that this aids in increasing the visibility of any damage that would be created during impact testing (Zantout, 2009). After the paint had dried, the sample preparation was continued.

2.5.2 Time-Varying Electrical Characterization

Experimental Procedure

The time-varying electrical characterization of electrified composite samples involved all of the equipment that was described previously in Section 2.4.2. To begin the electrical characterization, the electrical test fixture was assembled. This process included placing the plywood base plate down onto risers, to raise the base plate approximately 150 mm (6 in) off of the bench-top. The base plate was raised to allow for air to flow under the composite sample to aid in cooling. This additional height significantly cut down the amount of time for the sample to cool and return to ambient temperature. Next, the plywood mid plate was placed onto the base plate. A composite sample was then chosen and placed onto the mid plate. The top wood plate was then placed on top of the composite. Next the top aluminum plate, which holds the five infrared thermocouples, was placed on top of the top wood place to complete the assembly. The position of the composite plate was adjusted so that the lines drawn on the sample were aligned within the fixture so that each sample would be placed in the same location every time. The copper bus bars, with the lead wires from the power supply and sensing wires to the DAQ attached, were then given a thin coat of Duralco 120 and placed onto each end of the fixture in order to make contact with the composite specimen. Now the end clamps were assembled onto the ends of the copper bus bars and the nuts were tightened to a torque of 2.71 J (2 ft-lb). The final step of the process was to evenly torque the tightening nuts to 13.56 J (10 ft-lb) by using the torque wrench.

Now that the sample preparation and fixture assembly was complete, the composite specimen was ready to have electrical current passed through it. All of the equipment mentioned earlier in Section 2.4.2 was given a minimum of 30 minutes of warm-up time compared to the manufacturer recommended time of 20 minutes (Agilent, 2010). This, however, did exclude the infrared thermocouples as only a minimum of 1

minute is recommended for warm-up (Non-Contact, 2010). The output of the function generator was then connected to the analog input of the power supply. This was accomplished by connecting the function generator positive output wire to the IP+ connector and negative output wire to the IP- and ↓IP connector located on the back of the power supply. When a steady current output was desired for comparison tests, these connections were removed. This connection can be seen in Figure 2.31.

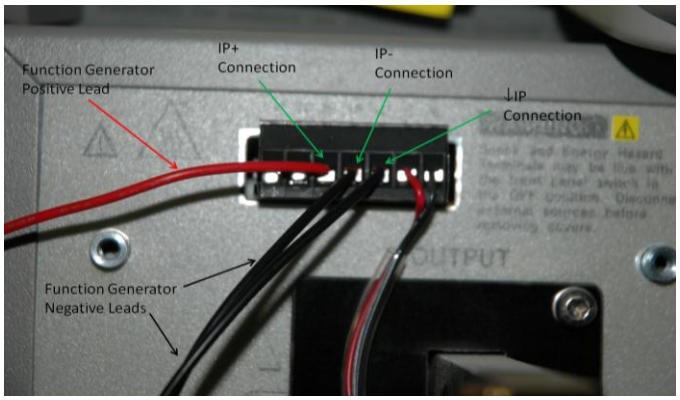

Figure 2.31: Power Supply Analog Input Connections

The power supply was now placed into constant current mode by setting the maximum allowable voltage to 50 V, which was higher than what would be observed during testing. This was done by pressing the buttons on the front face of the power supply in the following sequence: pressing "Local," then choosing "Output on/off" to ensure the output was off, then pressing "Voltage" and typing "50," then "Enter". Now parameters for the function generator such as wave shape, frequency, maximum (peak) current, and minimum current could be specified for the experiment with the front panel

of the function generator. For example, if a 50 Hz sine wave with maximum and minimum current values of 100 A and 50 A, respectively, were desired, the frequency, wave shape and voltage limits would be entered on the front panel of the function generator. The voltage limits, along with Equation 2.4, controlled the current magnitudes during the experiment. To obtain the 100 A and 50 A maximum and minimums, voltage limits of 4.545 V and 2.273 V were specified in the software. The parameters for the power supply were specified by the VEE software, by setting the output current to "0" and setting the time application of current in seconds. Here it was crucial to have the output of the power supply in constant current mode and with 0 amps of output, as any additional current would add to the total current output of the wave shape.

Both of the data acquisition units, temperature and electrical, could now be set up. This was done by opening the Agilent Measurement Manager (AMM) software. In the AMM software, the data acquisition rates can be specified in samples per second. For time-varying electrical currents, the sampling rate was always chosen to be 20 times the frequency of the waveform being tested. This was done to ensure that enough data points would be captured to prevent aliasing of the signal and to follow the recommendations of the manufacturer. This was done for both of the DAQs in the experiments even though the infrared thermocouple response time does not allow for such acquisition, as discussed earlier in Section 2.4.3.5. For steady current tests, the sampling rate was always selected to be 10 samples per second for both DAQs. This was selected because it was not necessary to sample at high rates for a constant signal. The final procedure before any experiments were performed was to verify that the electrical resistance was similar from sample to sample. This was done by subjecting the sample to 1 A steady current for 5 seconds. Once this was complete, the resistance was compared to the other samples tested. The experiment would proceed if the resistance was similar; if not, adjustments would be made to obtain similar values. These adjustments include adjusting the copper bus bar placement and/or applying more conductive epoxy. All experiments were carried

out on a single specimen before it was allowed to be removed from the fixture. This was done because it was found that it was difficult to obtain the same resistance values if the specimen was removed and reinserted. The samples and copper bus bars were allowed to cool down to as close to ambient temperature as possible. The temperature was verified by using a handheld infrared thermometer, seen in Figure 2.32. Once the temperature was thought to be in the correct range, the five infrared thermocouples mounted on the fixture were used to verify that the temperature across the composite surface was uniform.

Figure 2.32: Handheld Infrared Thermometer

CHAPTER 3

EXPERIMENTAL RESULTS

This chapter describes materials and experiments, reports experimental results and provides analysis and discussion of the experimental findings.

3.1 Materials Tested

The carbon fiber polymer matrix composite specimens that were tested consisted of 32-ply IM7/977-3 carbon-reinforced polymer matrix composite laminates. In this material notation, IM7 distinguishes the type of carbon fiber used in the material design (Hexcel, 2010). The 977-3 denotes the type of epoxy matrix used (Hexcel, 2010). All of the specimens arrived as large plates that were cut into smaller samples with the same 152.4 x 152.4 mm (6 x 6 in) dimensions as discussed in Section 2.4.1. Specimens had thickness varying from 4.953 mm to 5.004 mm (0.195 in to 0.197 in). Material specifications can be seen in Table 3.1. The materials were all tested following the procedures outlined for the electrical characterization and time-coordinated impact characterization as described in Chapter 2 Sections 2.4.2 and 2.4.3, respectively.

Table 3.1: Materials and Dimensions

Material Type	Fiber Orientation	Length mm [in]	Width mm [in]	Thickness mm [in]
32-ply IM7/977-3	[0]	152.4 [6]	152.4 [6]	4.953 [0.195]
32-ply IM7/977-3	$[0/90]_s$	152.4 [6]	152.4 [6]	5.004 [0.197]

In Table 3.1, the "Fiber Orientation" denotes the direction of the individual plies in the composite laminate. For example, [0] denotes that each ply in the composite is in the 0^o direction (i.e., fiber direction). The 32-ply $[0/90]_s$ alternates the orientation of each layer by 90^o with 8 layers in the 0^o and 8 in the 90^o direction and this composite is a symmetric laminate, which is indicated by subscript "s."

3.2 Summary of the Experiments

The objective of testing was two-fold: to determine the electrical and thermal behavior of the electrified carbon fiber polymer matrix composites at different current magnitudes and frequencies. The sine wave current ranging from 50 to 100 A in magnitudes, 25 to 150 Hz in frequencies, and 1 minute in duration was applied to the composite specimens. Effects of the current magnitude, frequency, and duration were investigated. In the case of unidirectional plates, an electric current was applied in the 0^o direction (fiber direction), and in the case of cross-ply plates, the current was applied in either 0^o or 90^o directions.

Each sample tested was subjected to three different types of experiments. The first was to understand the electrical and thermal response of specimens when subjected to a sine waveform with a constant frequency of 25Hz and three different average currents of 50 A (I_{max} = 75 A, I_{min} = 25 A), 70 A (I_{max} = 100 A, I_{min} = 40 A), and 75 A (I_{max} = 100 A, I_{min} = 50 A) for 1 minute. The experiments were then carried out in the same fashion for 50 and 150 Hz. The average currents were computed by averaging the maximum and minimum current applied to the specimen as shown in Figure 3.1.

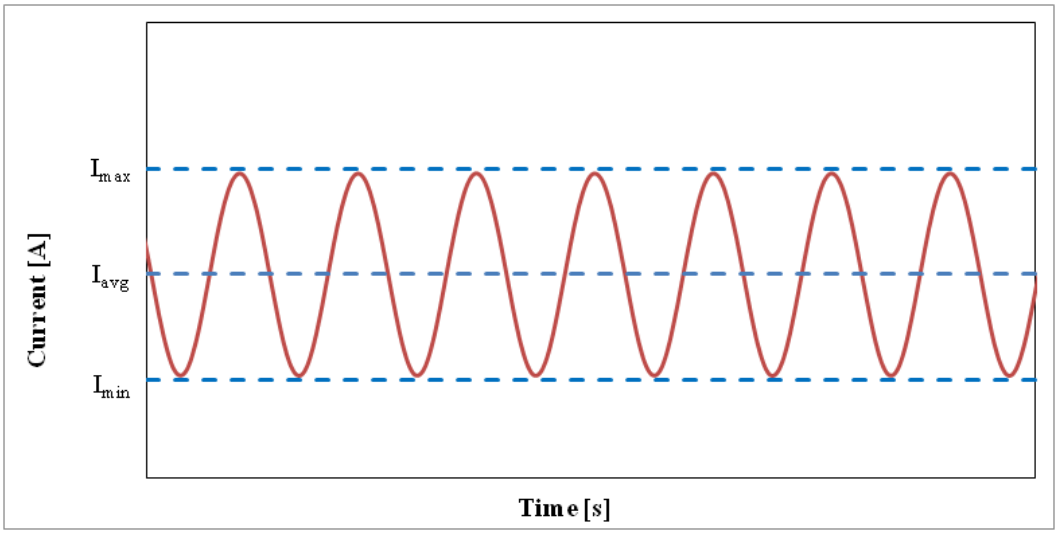

Figure 3.1: Sine Waveform Displaying I_{max} , I_{min} and I_{avg}

The maximum and minimum currents and frequencies selected for the experiments were constrained by the limitations of the system as described in Section 2.3.3.3. Experiments were performed while the power supply was in a constant current mode with the current peaks fixed. These fixed current peaks would allow for the voltage and resistance to vary depending on the changes in the electrical contact and the properties of the composite specimen. To simplify reference to the different time-varying currents, only average currents (I_{avg}) will be indicated in this thesis from now on. Thus, an electrical current with maximum and minimum of 75 A and 25 A will be referred to as I_{avg} = 50 A current, a current with maximum and minimum of 100 A and 40 A will be referred to as I_{avg} = 70 A current, and a current with maximum and minimum of 100 A and 50 A will be referred to as I_{avg} = 75 A current. The "ω" symbol will be used to denote the frequency (Hz) of the time-varying current.

Besides time-varying currents, composite specimens were also tested at a steady DC current (with a frequency of zero, ω = 0) applied for 1 minute. The current magnitudes

applied were the same as the average current as tested in the time-varying current experiments, 50, 70 and 75 A. Note that in the experiments performed in this work, time-varying current is in fact a form of DC current due to the flow of current from the anode to cathode (negative to positive), which is the same direction as the steady DC current. Therefore, for reference purposes, "steady" or "steady current" will be used to denote this DC current with zero frequency ($\omega = 0$) in this thesis from now on.

During testing, an electric current, voltage, and temperature were measured and recorded. Each experiment was repeated on at least three samples. The three samples tested were first subjected to a 1 A steady current for 5 seconds to ensure that all three samples had similar contact resistance. If a sample did not have similar resistance to the others, sample preparation (as described in Section 2.4.1) was repeated. A summary of the specimens tested is listed in Table 3.2. A summary of the experiments, including current magnitudes, duration, and frequencies, is given in Table 3.3.

The surface temperature of the composite specimens was monitored throughout each experiment to determine the thermal response of the composites subjected to the varying current magnitudes and frequencies. Temperature measurements were performed using the equipment as described in Section 2.3.3.

Table 3.2: Summary of the Specimens Tested

Material Type	Fiber Orientation	Specimens Tested
32-ply IM7/977-3	[0]	#12, #13, #14
32-ply IM7/977-3	$[0/90]_s$	#15, #16, #17, #22

Table 3.3: Summary of the Experiments

Specimens Tested	Current Duration, min	Average Current Value, I_{avg}, [A]	Minimum Current Value, I_{min}, [A]	Maximum Current Value, I_{max}, [A]	Frequency, ω, [Hz]
#12, #13, #14, #15, #16, #17	1	50	25	75	25
					50
					150
		70	40	100	25
					50
					150
		75	50	100	25
					50
					150
#12, #13, #14, #15, #16, #17, #22	1	50	50	50	0, Steady
		70	70	70	0, Steady
		75	75	75	0, Steady

3.3 Results of 32-Ply Unidirectional IM7/977-3 Composites

3.3.1 Electrical Response of 32-Ply Unidirectional IM7/977-3 Composites to Time-Varying Currents

Three 32-ply unidirectional IM7/977-3 composite specimens were used to investigate the electrical and thermal response when subject to time-varying and steady electrical loads using the fully instrumented system as described in Section 2.3.2. The specimens tested were samples #12, #13, and #14. To ensure that the correct waveform and current amplitudes were being applied to the composite specimens by the power supply, a fourth sample (#11) was tested. This sample was also used to ensure that the temperature increase due to the applied current was below the glass transition level of the specimens and charring temperature of the wooden fixture as noted in Section 2.3.3.3. According to the procedure outlined in Section 3.2, samples #12, #13, and #14 were first subjected to a 1 A steady current for 5 seconds to ensure that all three samples had similar contact resistance. If a sample did not have similar resistance to the others, sample preparation (as described in Section 2.4.1) was repeated. The resistance of the composite samples subjected to the steady current can be seen in Table 3.4. Sample-to-sample variation in resistance at 1 A steady current was found in the acceptable range, and all samples were then subjected to sine-wave time-varying currents.

Table 3.4: 1 A Steady Current Resistance for Unidirectional Composites

Resistance [Ω]			
Sample	Average	Maximum	Minimum
#12	0.04819	0.04836	0.04780
#13	0.05667	0.05703	0.05564
#14	0.04524	0.04538	0.04502

The shape of the voltage and current, as measured by the DAQ system for sample #13 subjected to sine wave current with ω = 25 Hz and I_{avg} = 50 A sine wave current, can be seen in a reduced time step in Figures 3.2 and 3.3, respectively.

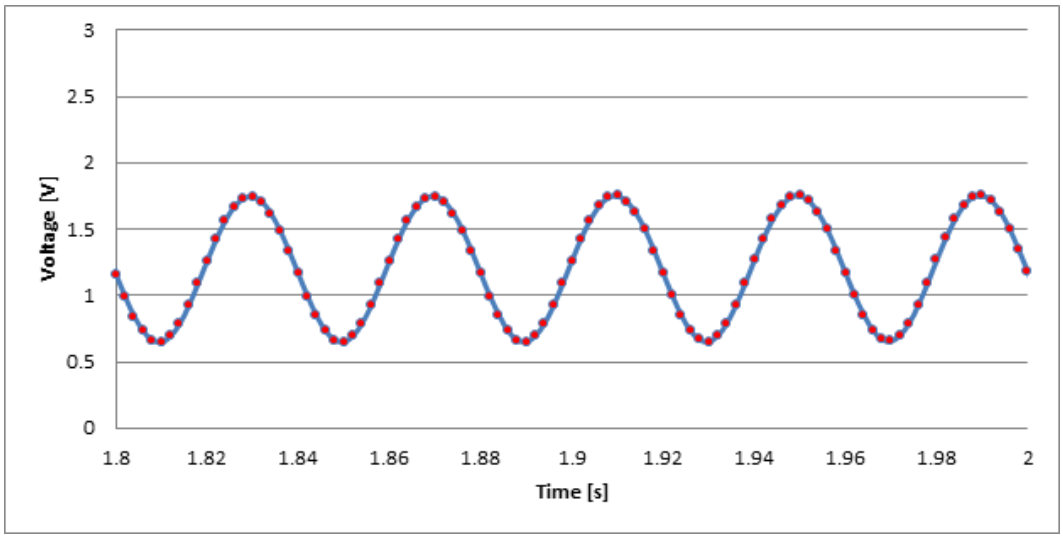

Figure 3.2: Unidirectional Sample #13: Voltage vs. Time, ω = 25 Hz, I_{avg} = 50 A

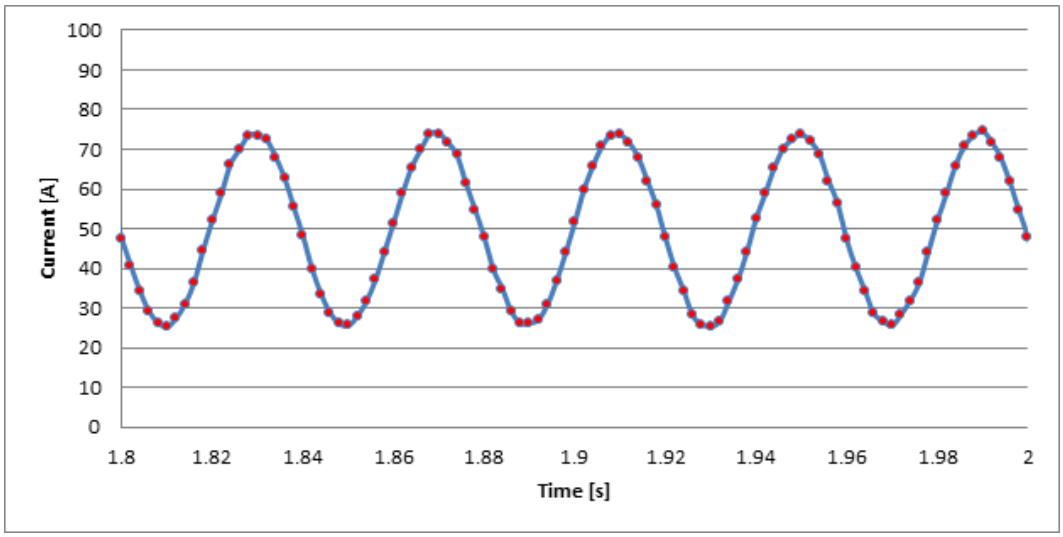

Figure 3.3: Unidirectional Sample #13: Current vs. Time, ω = 25 Hz, I_{avg} = 50 A

The plots of voltage and current as functions of time clearly show that the experimental setup is capable of measuring time-varying electrical current applications. Red markers on both plots indicate where each measurement was taken during the experiment. Using the voltage and current measurements, the electrical resistance of the composites subjected to time-varying electrical load was obtained.

Variation of the resistance with time for sample #13 subjected to varying current magnitudes (with I_{avg} = 50 A, 70 A and 75 A) at 25 Hz frequency can be seen in Figure 3.4.

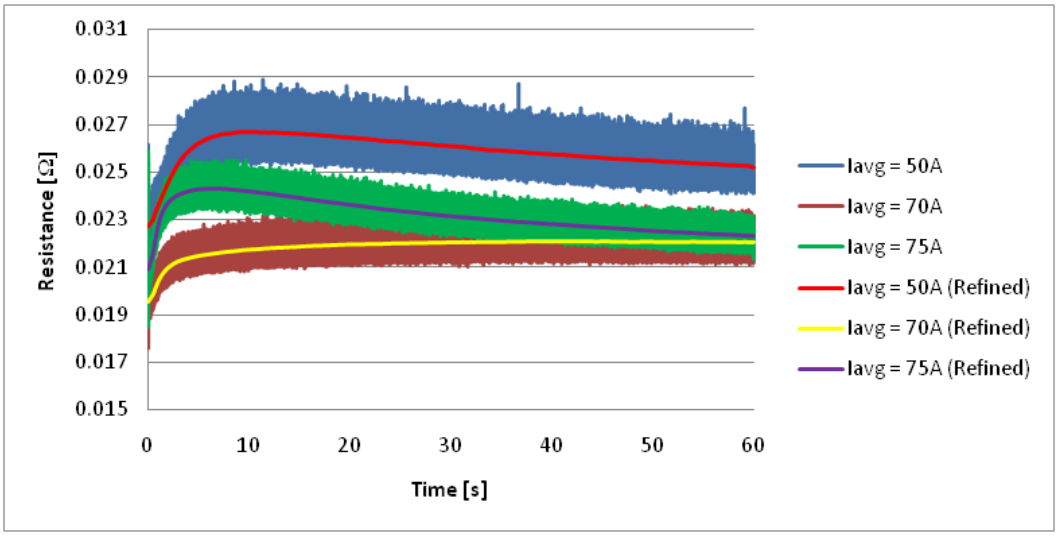

Figure 3.4: Unidirectional Sample #13: Resistance vs. Time, ω = 25 Hz

The trend of the resistance, as shown in Figure 3.4, reveals that the resistance is not constant and also depends on the electric current magnitude. The resistance tends to rise for a short period of time, and then eventually come to a lower steady value at the end of the 60 second current application. It is also noted that the 50 A average current resulted in the highest resistance values when compared to 70 and 75 A average current applications. The results for samples #12 and #14 were very similar to those shown in Figure 3.4.

Due to high sampling rates for extended periods of time, a large number of data points were captured and plotted, which was not always practical. To simplify the data analysis, the resistance data was post-processed. The average resistance values were calculated by smoothing the original data with a moving average filter and then by reducing the amount of data points. The technique used for this is described in detail in APPENDIX A. Therefore, Figure 3.4 also displays the average resistance values and

trend with respect to time imposed onto the measure values, labeled as "Refined." Future plots shown will only display the average resistance trend.

Analyzing the average resistance trends shown in Figure 3.4, one can see that the resistance increases for all average currents to approximately 17-13% and 11-7% from the initial to peak and final values, respectively. The percentage difference from the initial to highest and initial to final measured resistance values for each experiment can be seen in Table 3.5. The initial, highest, and final measured resistances are denoted as "Initial," "High," and "Final," respectively.

Table 3.5 shows that there was some scatter in the resistance values from sample to sample. All three samples had increases from the initial electrical resistance, with some being higher than that of others. These differences can be attributed to two different causes. First, sample preparation was performed in a manner to produce as consistent a contact resistance as possible. This, however, did not always produce the same contact resistance from sample to sample at the same current magnitude, as seen in Table 3.4. Second, the composite materials form a discontinuous electrical contact with the copper bus bars. This is due to the carbon fibers being electrical conductive and the polymer matrix being dielectric. The discontinuous contact produces contact resistance by forcing current to flow through carbon fibers. Therefore, it would be expected that some variation in resistance will exist from sample to sample. More information on contact resistance can be found in Section 1.3.

Figure 3.4 shows the general time trend of the resistance, but it does not show the wave shape of the resistance. Once would expect that the shape would follow the same shape as the current and voltage because Ohm's law (Equation 2.5) is also valid for time-varying currents. This was found to be the case in the experiments performed. The shape of the resistance wave is seen when a small time step was taken to produce a clear visual image of the wave. This wave for sample #13 at $\omega = 25$ Hz, $I_{avg} = 50$ and 75 A can be seen in Figure 3.5.

Table 3.5: Percent Increase in Resistance for Unidirectional Composites, ω = 25 Hz

Sample #12						
Frequency [Hz]	Average Current [A]	Initial [Ω]	High [Ω]	Final [Ω]	Initial-High % Difference	Initial-Final % Difference
25	50	0.02591	0.03166	0.02883	22.17	11.25
	70	0.01879	0.02429	0.02429	29.27	29.27
	75	0.02179	0.02822	0.02396	29.48	9.95

Sample #13						
Frequency [Hz]	Average Current [A]	Initial [Ω]	High [Ω]	Final [Ω]	Initial-High % Difference	Initial-Final % Difference
25	50	0.02273	0.02667	0.02518	17.35	10.80
	70	0.01955	0.02210	0.02206	13.04	12.83
	75	0.02089	0.02430	0.02230	16.31	6.75

Sample #14						
Frequency [Hz]	Average Current [A]	Initial [Ω]	High [Ω]	Final [Ω]	Initial-High % Difference	Initial-Final % Difference
25	50	0.02364	0.02741	0.02737	15.95	15.77
	70	0.02095	0.02473	0.02472	18.02	17.96
	75	0.02282	0.02735	0.02381	19.83	4.32

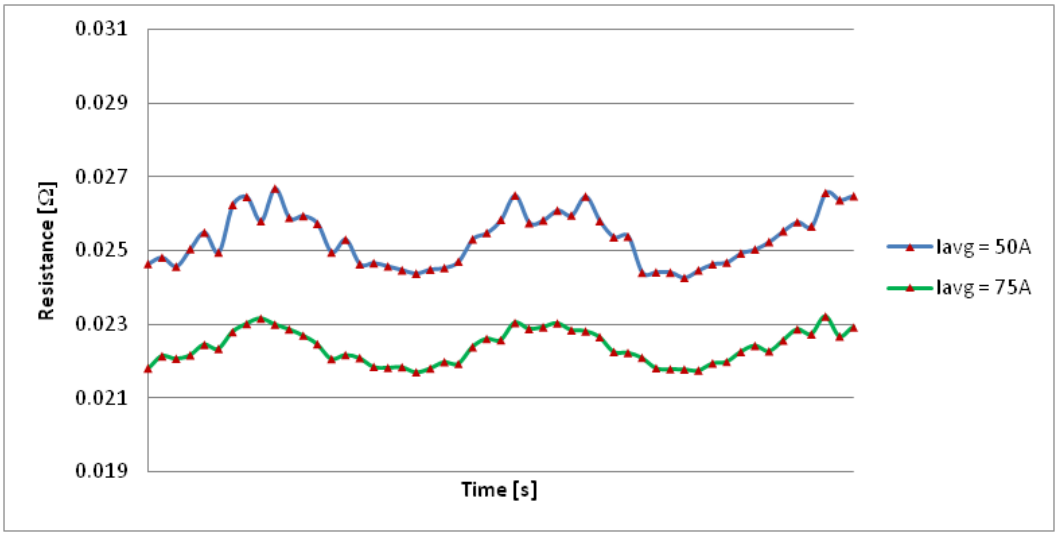

Figure 3.5: Unidirectional Sample #13: Wave Shape, Resistance vs. Time, ω = 25 Hz

In Figure 3.5, the resistance waves have been time shifted so the resistance peaks for both time-varying currents (I_{avg} = 50 A and I_{avg} = 75 A) can be seen at the same time. The time step is not shown for this reason. The shift was done to analyze the effects of the current amplitude (if any) on the resistance. Here the markers indicate where each measurement during the experiment was taken. It can also be seen, as stated earlier, that the 50 A average current results in higher resistance when compared to the 75 A average current application. The shape of the resistance shown in Figure 3.5 does not appear as a smooth sine wave like the voltage and current waves shown previously. This is likely due to the resistance being calculated numerically from the current and voltage measurements using Ohm's law. These calculations result in very small changes in resistance (approximately ± 2.5%) at neighboring points. These small changes in resistance make plotting difficult when interpolation is used to connect data points. Also, any errors in voltage measurements by the U2531A DAQ unit will have a greater error effect on the resistance calculation (a detailed description of the error calculation is

discussed in APPENDIX B). When comparing the "amplitude" of the resistance, it can be seen that the 50 A average current resulted in greater amplitude of resistance when compared to the 75 A average current. Both of these average current values, 50 A and 75 A, had the same peak-to-peak current of 50 A. This trend was found to be true for all samples subjected to sine wave current. In Figure 3.6, the resistance amplitude can be seen for 70 and 75 A.

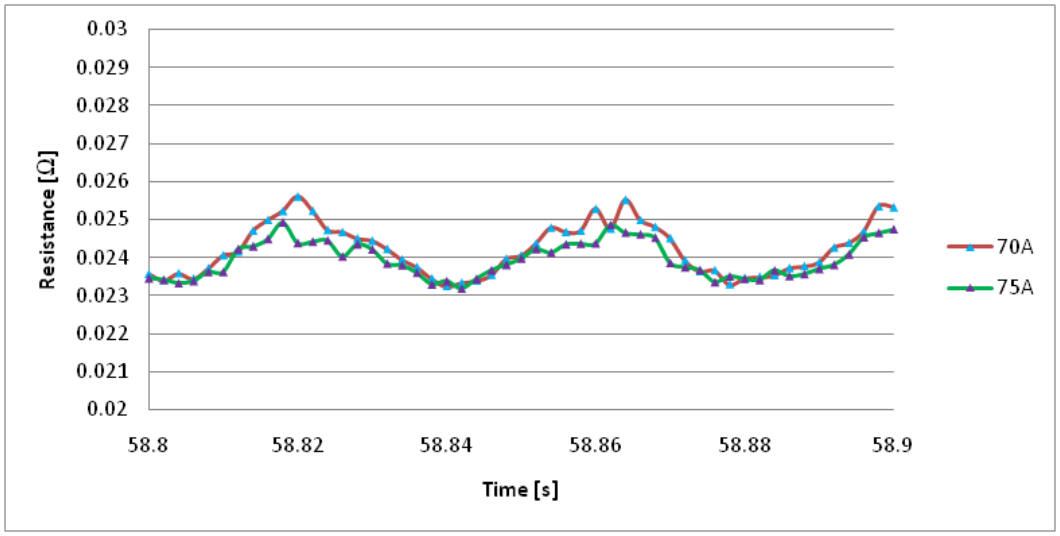

Figure 3.6: Unidirectional Sample #12: Wave shape, Resistance vs. Time, ω = 25 Hz

As seen in Figure 3.6, the amplitude of the resistance is greater for the 70 A average current than that for 75 A. In this case, both current values have different peak resistance at minimum current. This is due to 70 A and 75 A having different minimum currents (40 A and 50 A, respectively). The minimum resistance values occurred at the maximum currents. In this case, it was 100 A for both 70 A and 75 A average current

applications. At this same peak current, the resistance values were very similar to one another. This was found to be the same for samples #12 and #13. Sample #14 was found to have lower minimum resistance for 75 A than for 70 A at the same maximum current value of 100 A. Markers are used to indicate moments of time when the actual measurements for current and voltage were recorded and the resistances were calculated.

During the experiments, it was also important to ensure that the current, voltage, and resistance were being measured in the same phase by the DAQ system. This was verified by scaling the current and the resistance to the voltage and plotting them together. This process was performed on many of the experiments to ensure the phase synchronization. A 25 Hz example of such scaling and phase plotting can be seen in Figure 3.7. This plot also shows that the electric resistance is directly related to the amplitude of the applied time-varying current: resistance is in phase with the current, and there is an increase in the resistance as the current magnitude decreases.

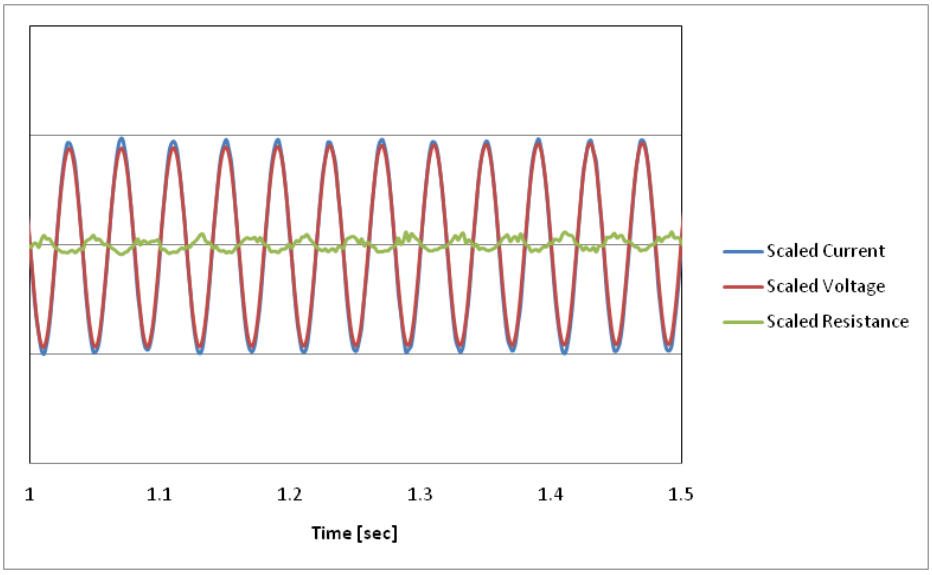

Figure 3.7: Unidirectional Sample #13: Scaled Current, Voltage, and Resistance vs. Time, $\omega = 25$ Hz

3.3.2 Electrical Response of 32-Ply Unidirectional IM7/977-3 Composites to Steady Currents

In addition to time-varying currents, steady currents of zero frequency ($\omega = 0$ Hz) were applied to the composite specimens Figures 3.8-3.10 show the resistance vs. time for samples #12, #13, and #14. Similarly to time-varying current, electrical resistance under steady currents does not stay constant. However, changes in the electrical resistance under steady currents are smaller when compared to time-varying currents (see Fig. 3.4, 3.8-3.10). Resistance measured at 50 A steady current tends to be lower than that measured at 70 A and 75 A currents. Moreover, electrical resistance under steady current monotonically increases with time, whereas electrical resistance under time-varying currents was not a monotonic function of time. Furthermore, the variation in the resistance from sample to sample increases as the current magnitude increases. Figure 3.11 shows resistance vs. time for all three samples subjected to a 75 A steady current.

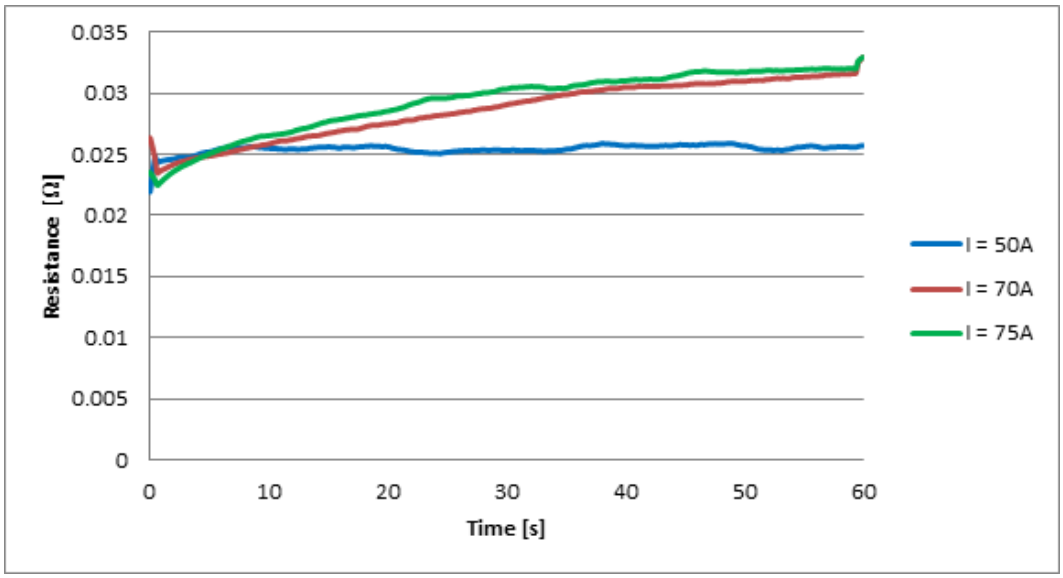

Figure 3.8: Unidirectional Sample #12: Resistance vs. Time, Steady Current

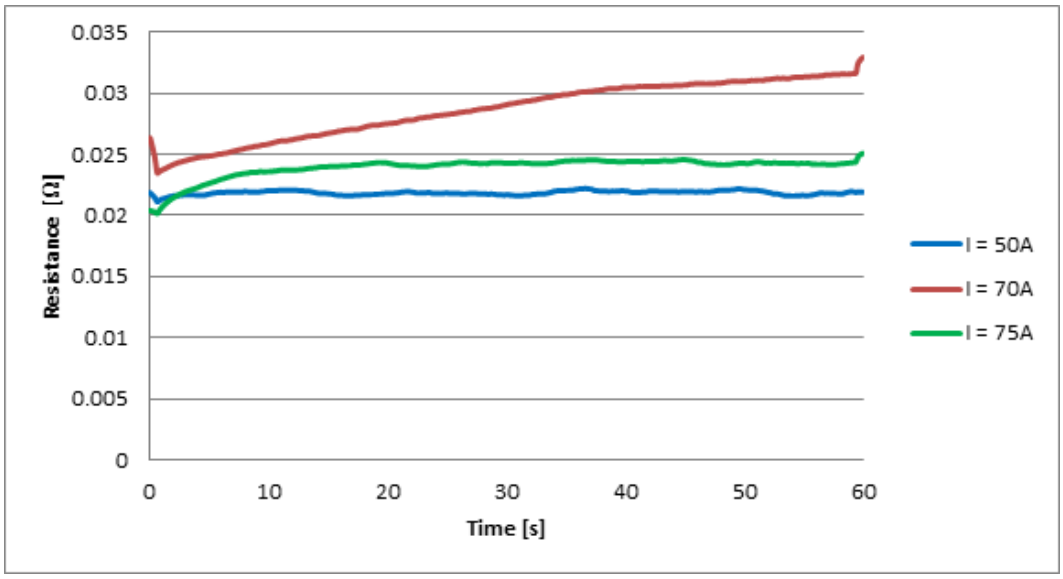

Figure 3.9: Unidirectional Sample #13: Resistance vs. Time, Steady Current

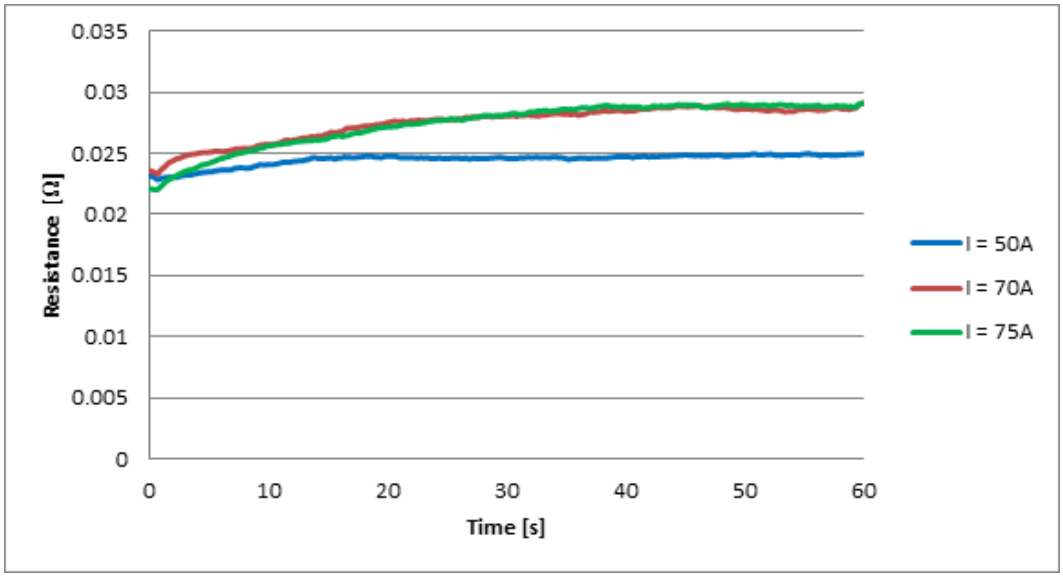

Figure 3.10: Unidirectional Sample #14: Resistance vs. Time, Steady Current

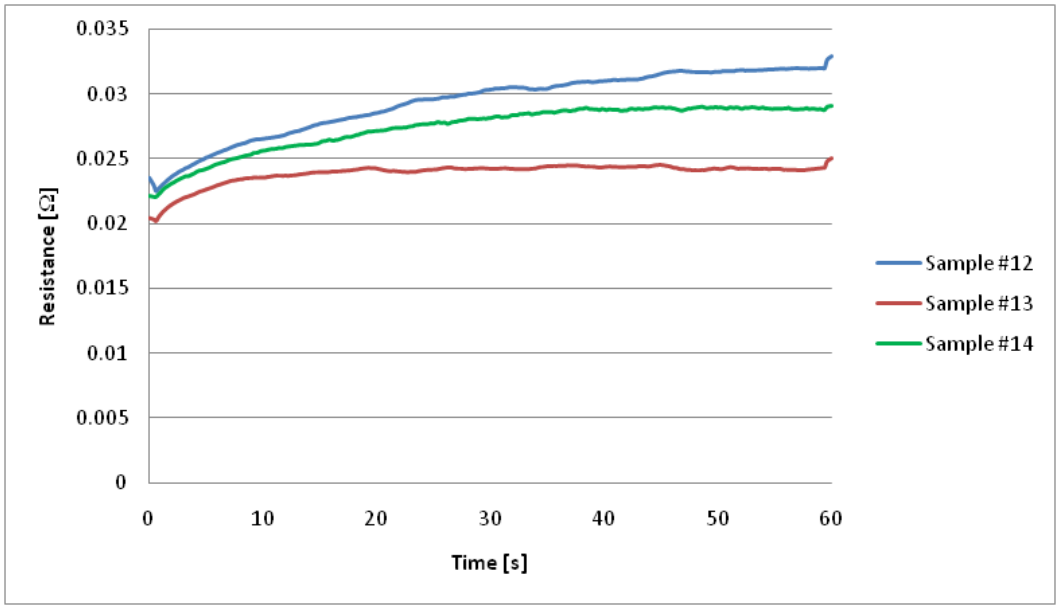

Figure 3.11: Unidirectional Samples: Resistance vs. Time, Steady Current, I = 75 A

Table 3.6 shows maximum and minimum values of the resistance in samples #12, #14, and #14 subjected to 50, 70, and 75 A steady currents for 1 minute.

Table 3.6: Minimum and Maximum Values of Resistance for Unidirectional Composites, Steady Currents

Sample #12				
Frequency [Hz]	Average Current [A]	Minimum [Ω]	Maximum [Ω]	Percent Difference
0	50	0.0220	0.0259	17.94
	70	0.0235	0.0330	40.25
	75	0.0225	0.0330	46.65

Sample #13				
Frequency [Hz]	Average Current [A]	Minimum [Ω]	Maximum [Ω]	Percent Difference
0	50	0.0211	0.0222	5.23
	70	0.0235	0.0330	40.25
	75	0.0202	0.0251	24.51

Sample #14				
Frequency [Hz]	Average Current [A]	Minimum [Ω]	Maximum [Ω]	Percent Difference
0	50	0.0228	0.0250	9.44
	70	0.0233	0.0292	25.26
	75	0.0220	0.0291	32.08

In addition to analyzing the behavior of the electrical resistance, voltage-current characteristics were examined for all specimens at the onset of the electric current applications and after the electric current had been applied for 1 minute. Recall that each specimen undergoing testing was treated following the procedure described above to reduce contact resistance. After that, the specimen was placed into the fixture, and a steady electric current was applied for 1 minute while current, voltage, and surface temperature were measured. After the current application, the specimen was cooled to ambient temperature (if necessary) and the next test under a higher current magnitude was conducted. The minimum tested current was 1 A, which corresponded to the current density of 1312 A/m^2, and the maximum current applied was 75 A, which corresponded to the current density 98425 A/m^2. The current densities were computed by using the composite sample dimensions as shown in Table 3.1 and computing the total contact area by using the thickness and width.

Figures 3.12 and 3.13 show voltage-current relationships for the unidirectional composite specimens measured at the onset of the electric current applications (beginning of the experiments, t = 0 sec) and after electric currents were applied for 1 minute (end of experiment, t = 60 sec).

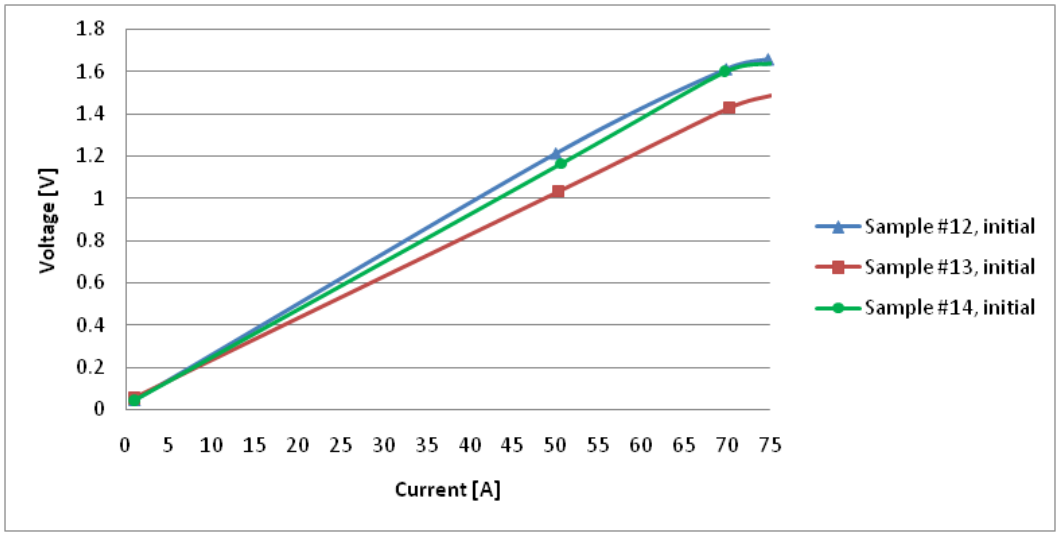

Figure 3.12: Unidirectional Samples: Voltage vs. Current, Steady Currents

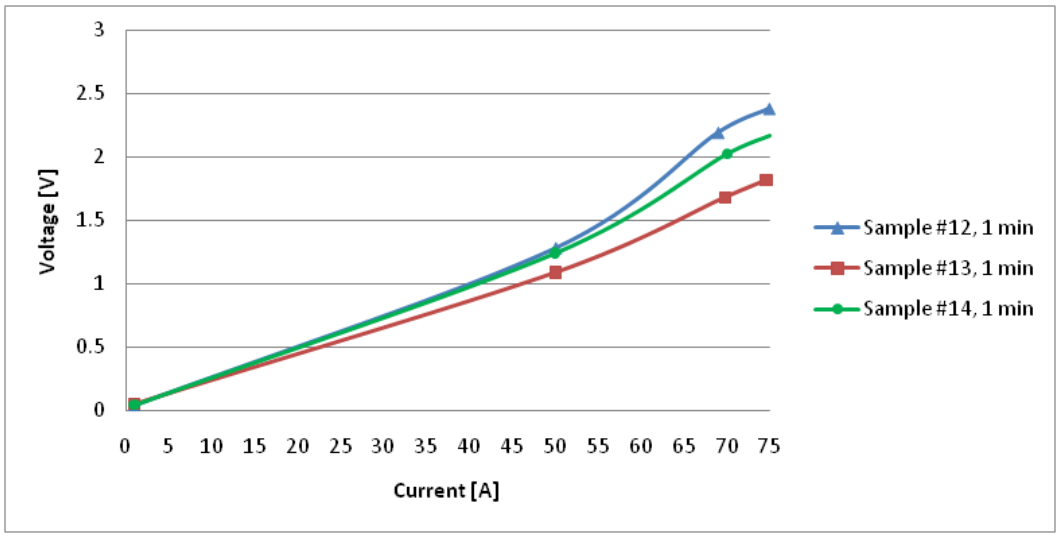

Figure 3.13: Unidirectional Samples: Voltage vs. Current, Steady Currents

From Figures 3.12 and 3.13 shown above, it can be seen that the change in resistance with respect to time results in the composite specimens having a dynamic resistor effect

and not a static or Ohmic resistance. Moreover, there is a critical value of the current above which linear Ohm's law fails and the voltage-current relationship becomes nonlinear. In the experiments conducted in this study, this critical value was 50 A, which corresponded to a 65617 A/m^2 current density (as described previously). Furthermore, it was noticed that below 50 A, electrical resistance changed little over time, while above this value there was an increase in the resistance with time.

3.3.3 Current-induced Heating of 32-Ply Unidirectional IM7/977-3 Composites

Heating in the electrified composites is caused by electrical conduction (Joule heating) and contact resistance heating generated at composite electrode interface, which are equally significant for the response of electrified composites. This section presents results of temperature measurement on 32-ply unidirectional IM7/977-3 composites (samples #12, #13, and #14) subjected to electric currents of various magnitude, frequency, and duration. As mentioned before, the temperature distribution on the surface of composite specimens was measured by five thermocouples. These thermocouples are denoted by either "Thermocouple #1," "Thermocouple #2," etc., or "TC #1," "TC #2," etc. Figure 3.14 shows the position of thermocouple as well as the copper electrodes and composite specimen location.

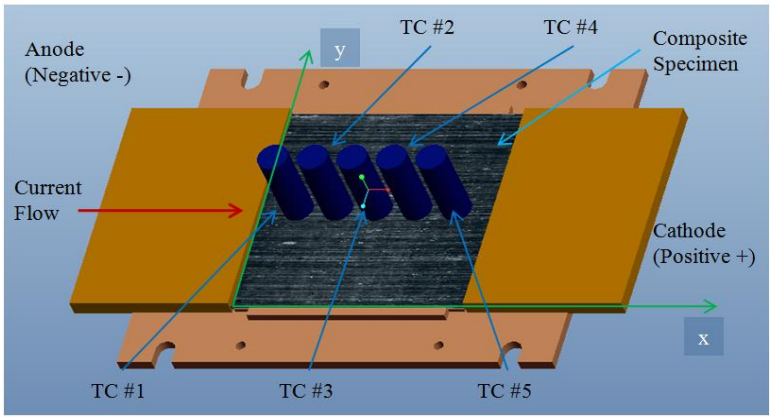

Figure 3.14: Thermocouple Location

As seen in Figure 3.14, the middle plate and the top plate have been hidden from view to enable a clear view of the thermocouples' copper bus bars and composite specimen. Here "x" represents the distance from the left edge of the composite and copper contact interface and "y" represents the length along the contact interface. As mentioned in Section 2.3.2.1, the thermocouples are separated by 25.4 mm (1 in) from each center axis. The current flow is from anode to cathode (negative to positive). The distances of the thermocouples with respect to the left side copper-composite interface and the desired distance can be seen in Table 3.7.

Table 3.7: Thermocouple Location for Unidirectional Composites

Thermocouple Distance from Interface, x [mm]					
Sample #	TC #1	TC #2	TC #3	TC #4	TC #5
12	19.5	44.9	70.3	95.7	121.1
13	22.8	48.2	73.6	99.0	124.4
14	23.7	49.1	74.5	99.9	125.3
Desired	25.4	50.8	76.2	101.6	127.0

Note that this thermocouple placement was not symmetric with respect to the middle of the specimens with smaller distance between thermocouple #1 and the copper bar attached on the left and larger distance between thermocouple #5 and the copper bar attached on the right (see Figure 3.14 for details).

Figure 3.15 shows temperature change, ΔT, measured by the infrared thermocouples (TC #1, TC #2, TC #3, TC #4, and TC #5) vs. time in the 32-ply unidirectional IM7/977-3 composite (sample #12) subjected to a 25 Hz sine wave electric current with $I_{avg} = 50$ A. The initial temperature, T_{in}, was $T_{in} = 18^{o}$ C and $\Delta T = T - T_{in}$.

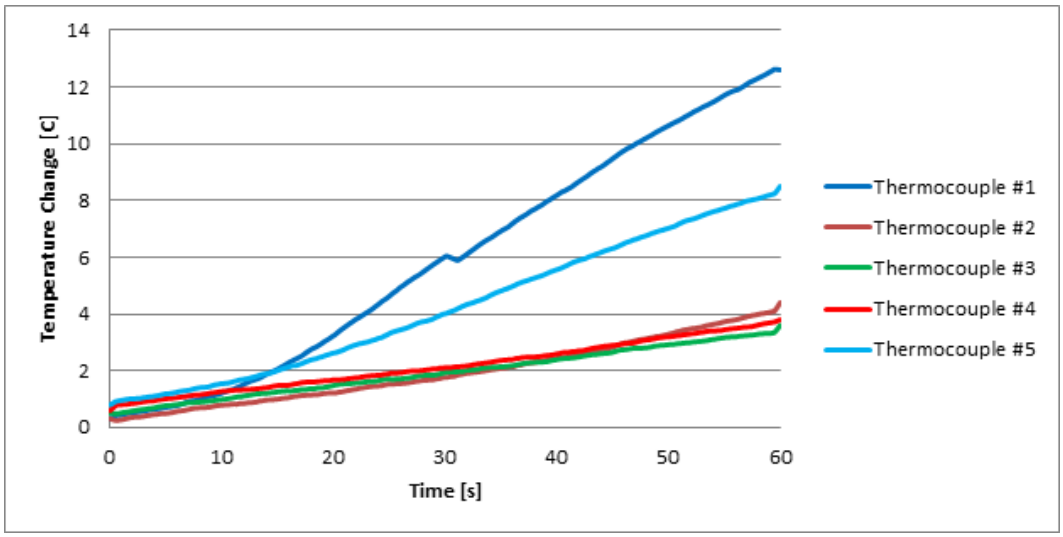

Figure 3.15: Unidirectional Sample #12: Temperature Change vs. Time: ω = 25 Hz, I_{avg} = 50 A

As seen in Figure 3.15, the temperature of thermocouples #1 and #5 measure the highest temperature on the composite surface, #2 and #4 the next highest, and #3 the lowest temperature. This was found to be the same for all samples tested. Thus, there was a temperature gradient in the composite produced across the composite by current-induced heating. Moreover, this gradient is formed in the direction of the applied current and is a result of the heating due to the electrical contact resistance as will be explained in detail in the later sections of this thesis.

Figure 3.16 shows the temperature distribution in sample #12 subjected to a 25 Hz sine wave and I_{avg} = 50 A, after the electric current was applied for 1 minute. As seen, the temperature distribution in the plate is not symmetric with the temperature being higher at the left end. This is due to the fact that, in all experiments performed in this work, the copper bus bar attached to the left end served as the anode and the copper bar attached to the right end served as a cathode (see Figure 3.14 for details). In both steady and time-

varying current experiments, the direction of the current flow did not change, thus leading to different temperatures at the left and right ends of the specimen with the temperature at the anode being higher than at the cathode. Also any error present in temperature measurement can yield differences in the temperatures at the ends of the plate.

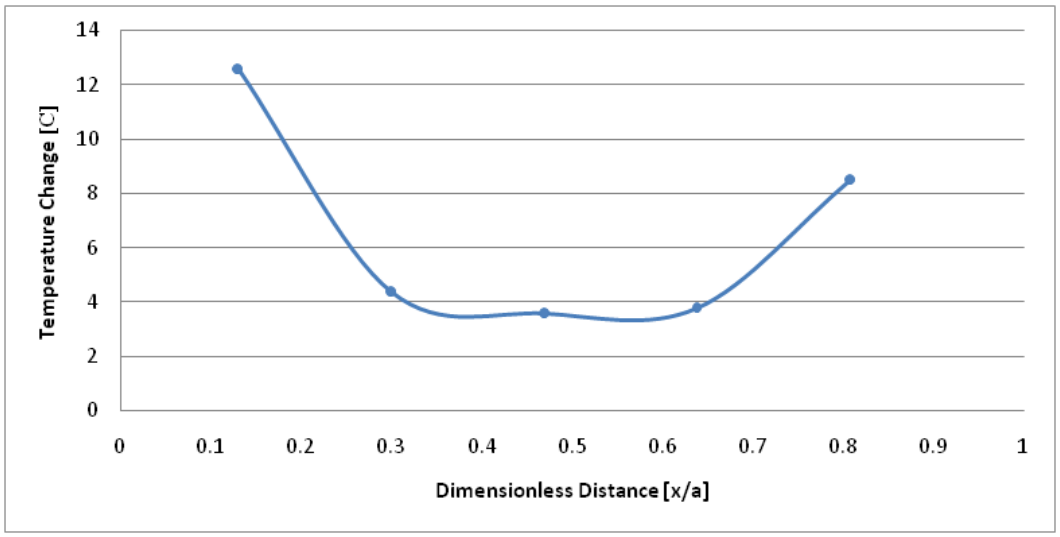

Figure 3.16: Unidirectional Sample #12: Temperature Change vs. Dimensionless Distance: $\omega = 25$ Hz, $I_{avg} = 50$ A

Note that in Figure 3.16 the temperature is plotted versus dimensionless distance from the electric contact interface. This "dimensionless distance" is computed by normalizing the distance of the thermocouple measuring location (x) with the total length of the plate (a) from the anode to the cathode. In the case of the samples tested, a = 150 mm (5.91 in). Also, markers indicate the location (dimensionless distance) at which the temperature

measurement was taken by the infrared thermocouples on the composite surface. The arrangement of the thermocouples can be seen as shown previously in Figure 3.14.

Similar temperature measurements have been conducted at other current magnitudes and frequencies listed in Table 3.3. Figure 3.17 shows the results of different current magnitudes of a sine wave with ω = 25 Hz for sample #13.

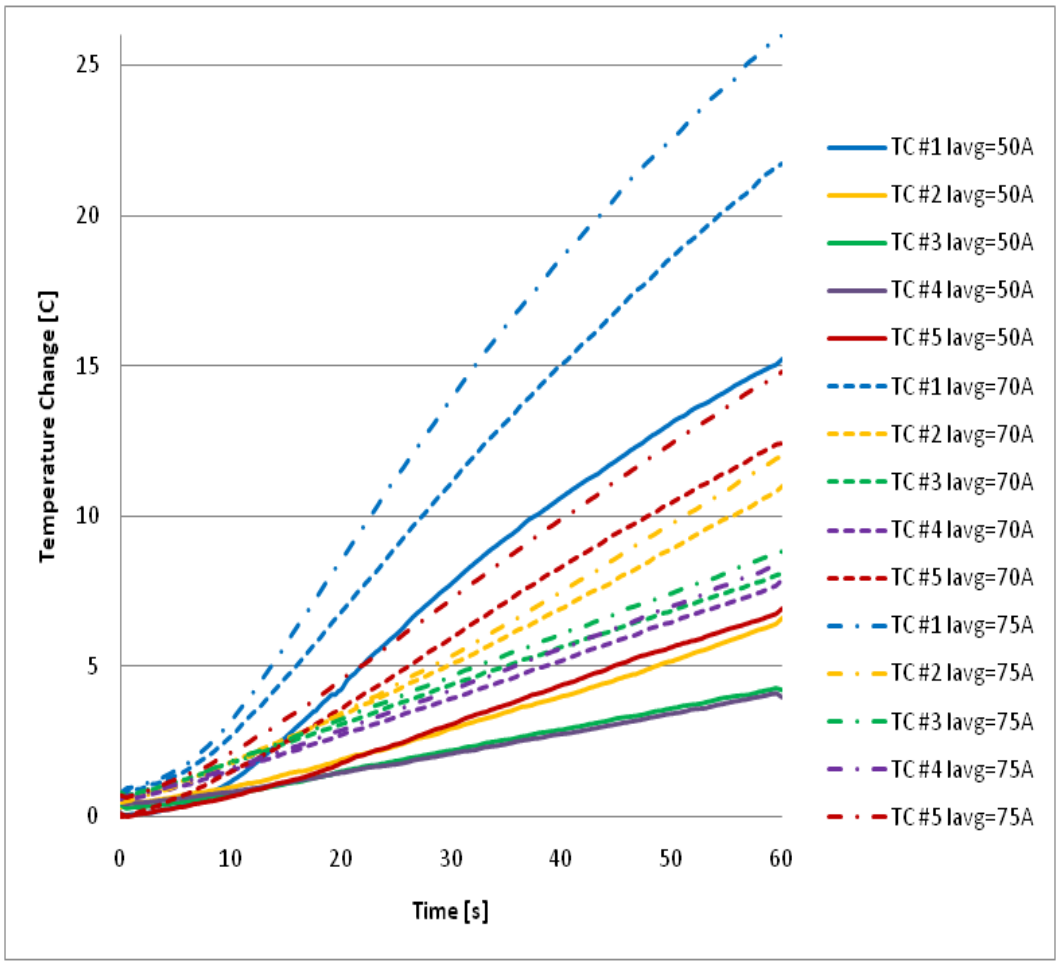

Figure 3.17: Unidirectional Sample #13: Temperature vs. Time: ω = 25 Hz

Figure 3.17 reveals the relationship between the average current and temperature change at 25 Hz. It can be seen that the higher the current magnitude and the closer the proximity to the contact interface, the greater the change of the composite surface temperature. Figure 3.18 displays the temperature change with respect to the dimensionless distance of the thermocouple from the composite and copper bus bar contact interface, with markers indicating the location at which each measurement was taken. The results are shown for all three unidirectional samples, #12, #13, and #14, subjected to a 50 Hz sine wave and I_{avg} = 75 A.

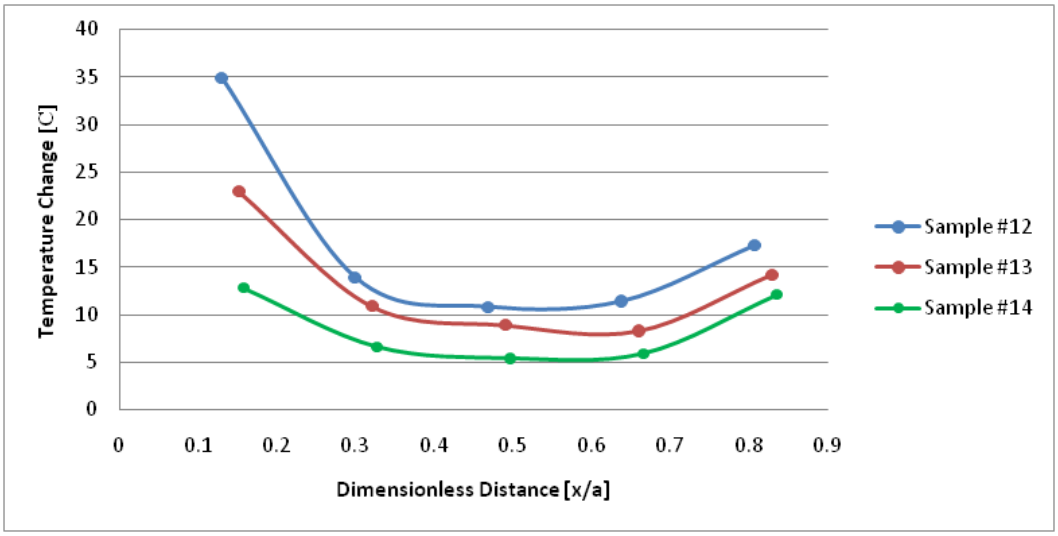

Figure 3.18: Unidirectional Samples: Temperature vs. Dimensionless Distance: ω = 50 Hz, I_{avg} = 75 A

As shown in Figure 3.18, each sample had different temperature distributions under the same experimental conditions. It is assumed that this difference in the temperature

distribution came from the difference in electrical contact resistance from sample to sample. It would be expected that samples with the highest initial resistance would have the highest temperature after 60 seconds of current application. This was not found to be the case for these samples in these experiments. Figure 3.19 displays the time history of the resistance of samples #12, #13, and #14 subjected to the sine wave current ω = 50 Hz, I_{avg} = 75 A.

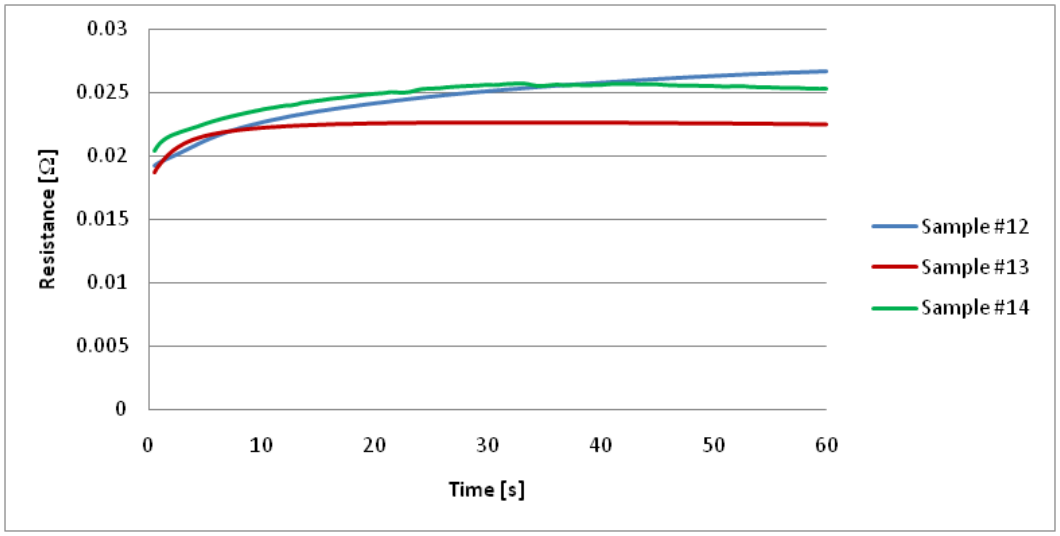

Figure 3.19: Unidirectional Samples: Resistance vs. Time: ω = 50 Hz, I_{avg} = 75 A

Table 3.8 shows the initial, average, and final resistance for samples #12, #13, and #14 subjected to I_{avg} = 75 A and ω = 50 Hz sine wave current.

Table 3.8: Initial, Average, and Final Resistance for Unidirectional Composites, ω = 50 Hz and I_{avg} = 75 A

Resistance [Ω]			
Sample	Initial	Average	Final
#12	0.0193	0.0246	0.0268
#13	0.0191	0.0224	0.0225
#14	0.0207	0.0249	0.0254

Analyzing Figures 3.18 and 3.19 and Table 3.8, one can see that the sample #13 had the lowest resistance through the experiments, but did not have the lowest temperature. Moreover, samples #12 and #14 had similar resistance values, but did not have similar temperatures. At the same time, it can be seen that the resistance for sample #12 continued to rise throughout the entire experiment, while the resistance of sample #13 increased initially and then remained fairly constant from approximately 20 seconds to the end of the experiment (60 seconds). Sample #14 increased initially until approximately 30 seconds then lowered until the end of the experiment. After 1 minute, sample #12 had the highest resistance of the three samples tested. This high resistance also corresponded to the highest change in temperature seen after 1 minute of current application among the three samples, as seen in Figure 3.18. This trend, however, was not confirmed with samples #13 and #14. Here sample #13 had lower resistance than sample #14, but the change in temperature was higher for sample #13. Thus it can be concluded that the entire time history of the resistance influences the temperature change in the electrified composite.

These same findings were also investigated for steady current applications. The time history of the change in surface temperature with respect to time for a 75 A steady current application can be seen in Figure 3.20.

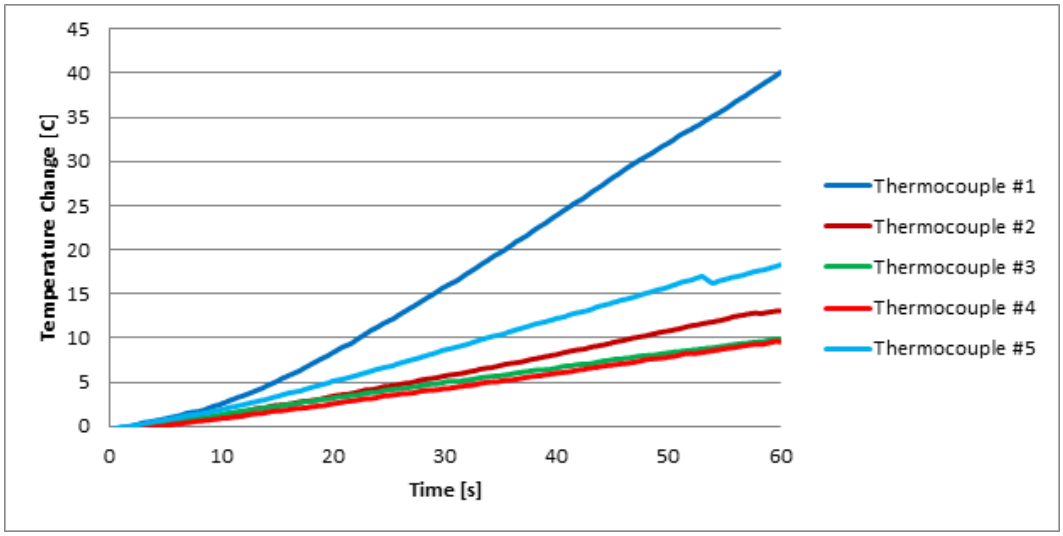

Figure 3.20: Unidirectional Sample #12: Temperature Change vs. Time, Steady Current: I = 75 A

As can be seen in Figure 3.20, a temperature gradient is present. Figure 3.21 displays the temperature distribution for a 75 A steady current application. The time history of the resistance for the same experiment can be seen in Figure 3.22.

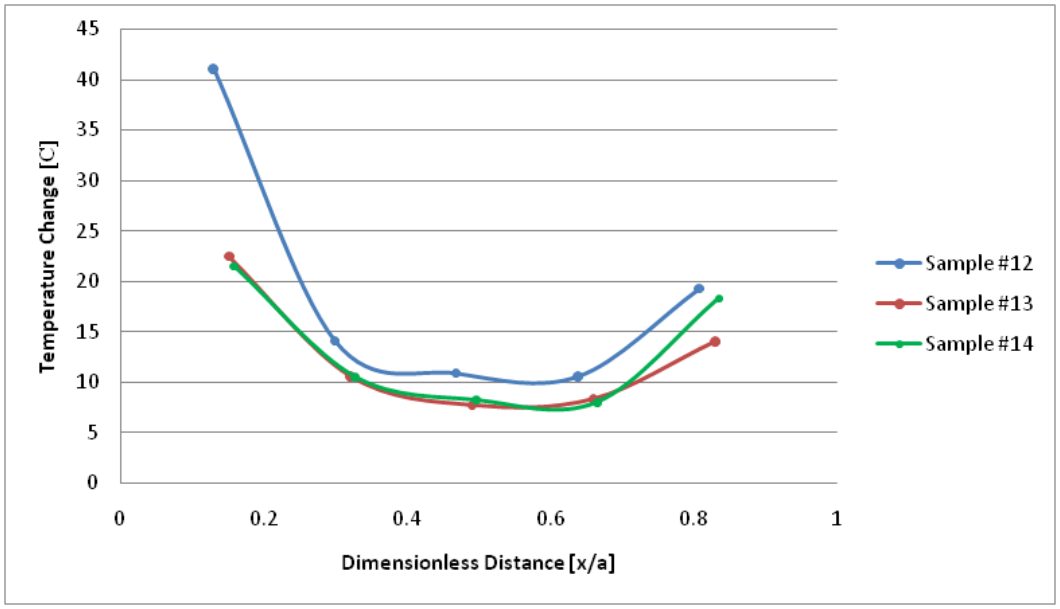

Figure 3.21: Unidirectional Samples: Temperature vs. Dimensionless Distance, Steady Current: I = 75 A

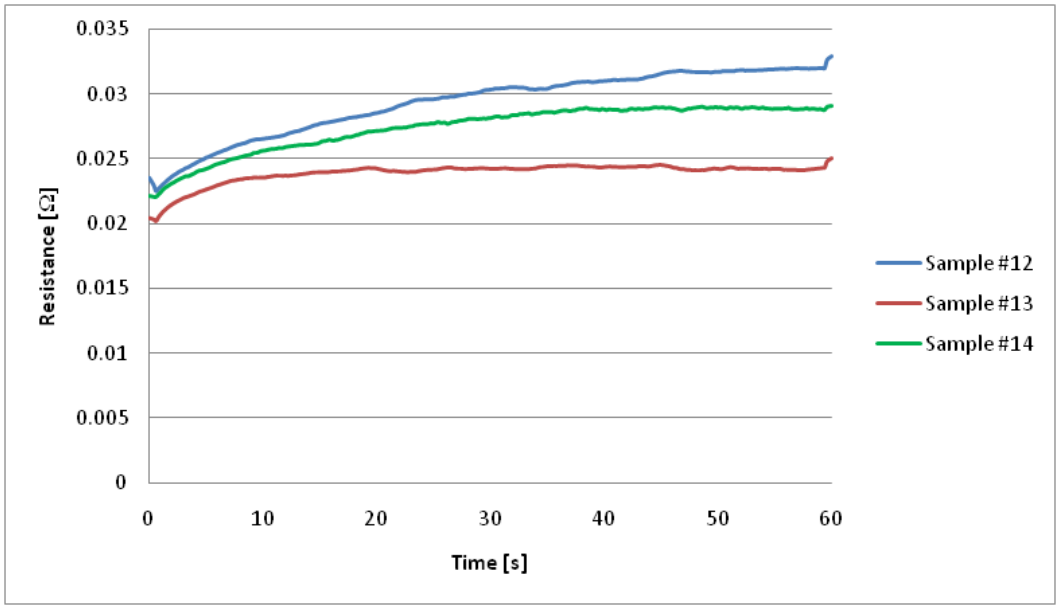

Figure 3.22: Unidirectional Samples: Resistance vs. Time, Steady Current: I = 75 A

When comparing Figures 3.21 and 3.22, one can see that the highest resistance measured was for sample #12, which correlated to the highest change in temperature as well. However, this was not the case for samples #13 and #14. The difference in the final resistance (after 1 minute) between samples #13 and #14 was 16%. Consequently, this difference in resistance only attributed to a 4.5% and 3.5% difference in temperature as measured by thermocouples #1 and #3, respectively. This was unexpected as the difference in resistance between samples #12 and #14 was only 11.7%. This smaller difference in resistance corresponded to a 48% and 25% increase in temperature as measured by thermocouples #1 and #3, respectively.

It is believed that no correlation was observed between the resistance values and the temperature change due to relatively small difference in the resistance of three tested samples. Thus, experiments involving samples with significantly different resistances needed to be carried out (described later in Section 3.3.4) to establish the relationship between the resistance and the temperature.

It was also verified, as one would expect, that a decrease in the average current would result in a decrease in specimen surface temperature. This temperature decrease can be seen in Figure 3.23 as well as the resistance time history in Figure 3.24.

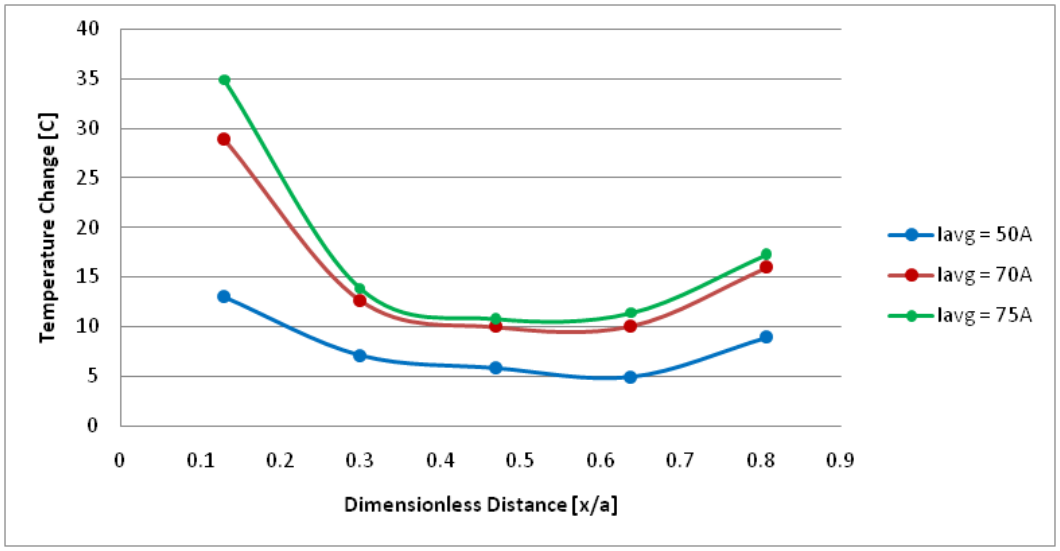

Figure 3.23: Unidirectional Sample #12: Temperature vs. Dimensionless Distance: ω = 50 Hz

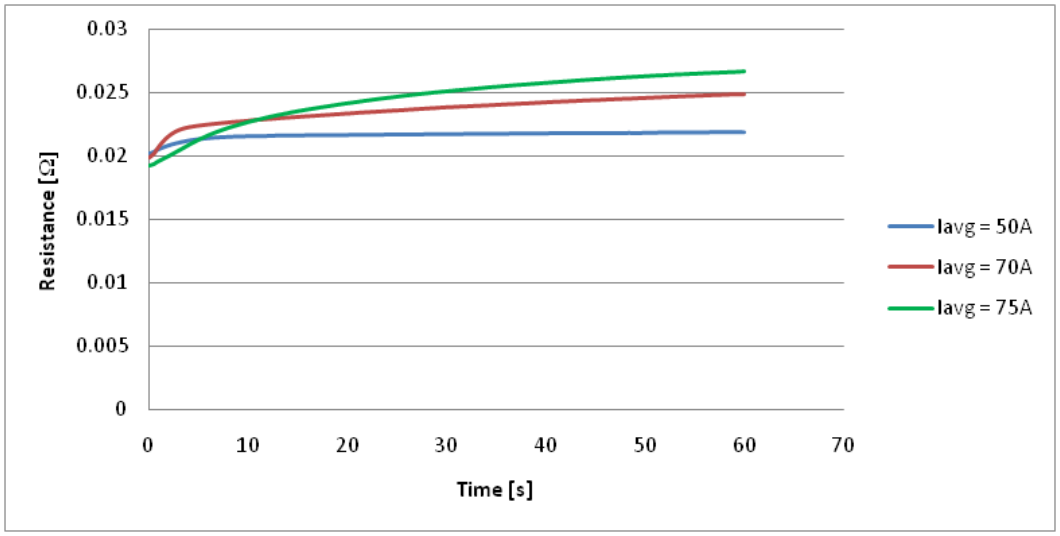

Figure 3.24: Unidirectional Sample #12: Resistance vs. Time: ω = 50 Hz

In Figure 3.23 it can be seen that a decrease in average current (75 A to 50 A) resulted in a decrease of surface temperature of approximately 22° C and 5° C as measured by thermocouple #1 and thermocouple #3, respectively. Furthermore, it can also be noticed that the higher the average current, the greater the change in surface temperature of the composite specimens. This trend was found to hold true for all frequencies tested. In Figure 3.24 the resistance time trend for ω = 50 Hz and I_{avg} = 50 A remains mostly constant throughout the entire experiment when compared to the continually rising resistance of I_{avg} = 70 and 75 A.

Once again it was found that a decrease in the current magnitude resulted in a decrease of surface temperature for steady current applications. Figure 3.25 displays the temperature distribution for steady current application, while Figure 3.26 shows the resistance time history.

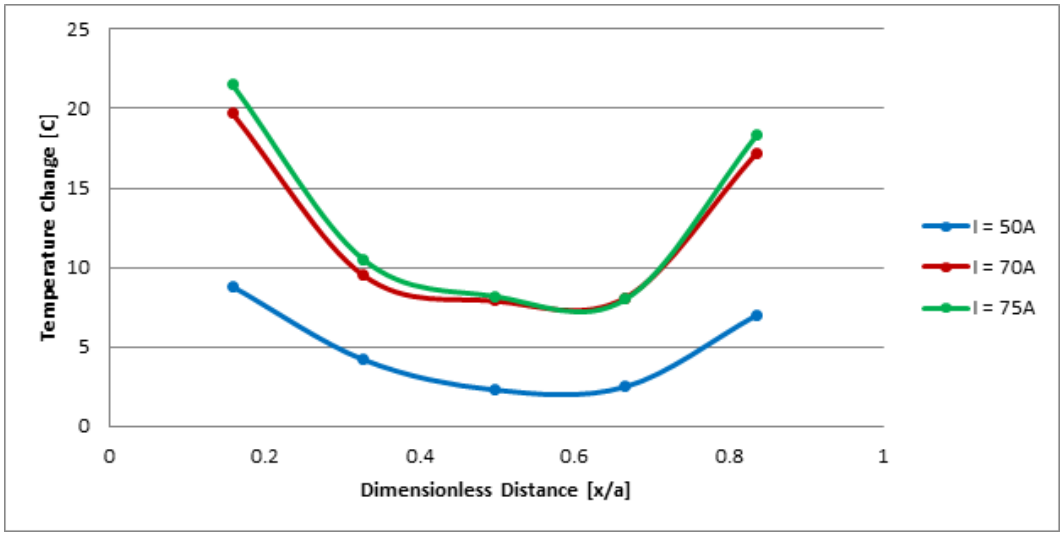

Figure 3.25: Unidirectional Sample #14: Temperature vs. Dimensionless Distance, Steady Current

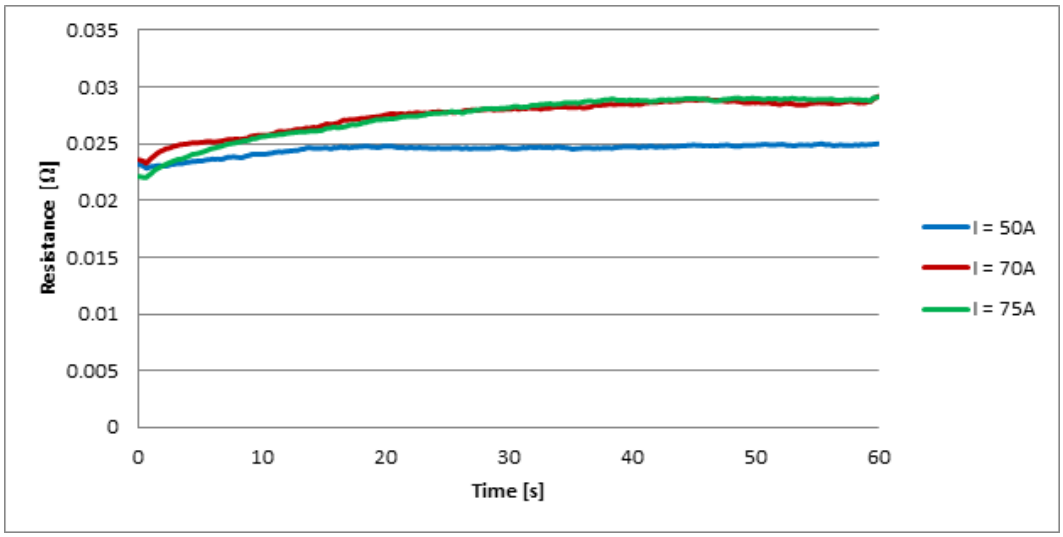

Figure 3.26: Unidirectional Sample #14: Resistance vs. Time, Steady Current

In Figure 3.25 it can once again be seen that a decrease in current (75 A to 50 A) resulted in a decrease of surface temperature of approximately 6^{o} C and 1^{o} C as measured by thermocouple #1 and thermocouple #3, respectively, for sample #12. As shown in Figure 3.26, the resistances for all three current magnitudes are very similar to one another with a maximum difference of 0.007 Ω between all three currents.

The effect of frequency on the change in temperature for sample #13 can be seen in Figure 3.27 with markers indicating the location of the temperature measurement. The time history of the resistance can also be seen in Figure 3.28. As noted previously, the temperature distribution is not symmetric throughout the plate. Figure 3.27 also reveals that frequency does not have a noticeable effect on the temperature distribution of the composite specimens. This was also found to be the case for samples #12 and #13. However, for sample #14, it was found that for all frequencies (ω = 25, 50, 150 Hz) and average currents (I_{avg} = 50, 70 and 75 A) tested, there was a reduction in the overall temperature change from steady current application. The remainder of experiments did

not reveal any trend of temperature as a function of frequency. Therefore, it can be concluded that temperature is not a function of frequency. A summary of the differences in temperature from steady to time-varying current (70 A) can be seen in Table 3.9.

Table 3.9: Percent Change in Temperature for Unidirectional Composites from I = 70 A Steady Current to I_{avg} = 70 A Time-Varying Current

Percent Change in Temperature From 70A Steady Current						
Frequency, ω [Hz]	Sample	TC #1	TC #2	TC #3	TC #4	TC #5
25	#12	-27.7	-72.7	-64.0	-62.4	-50.9
	#13	8.5	11.1	9.5	12.9	1.6
	#14	-50.3	-49.5	-49.4	-44.4	-50.0
50	#12	-16.5	-3.8	0.0	0.0	-7.5
	#13	4.5	0.0	2.7	10.0	0.0
	#14	-35.5	-41.1	-31.6	-37.0	-37.2
150	#12	-9.2	-3.8	-8.0	-11.9	-10.4
	#13	-11.5	-16.2	-12.2	-5.7	20.5
	#14	-61.9	-66.3	-74.7	-70.4	-65.1

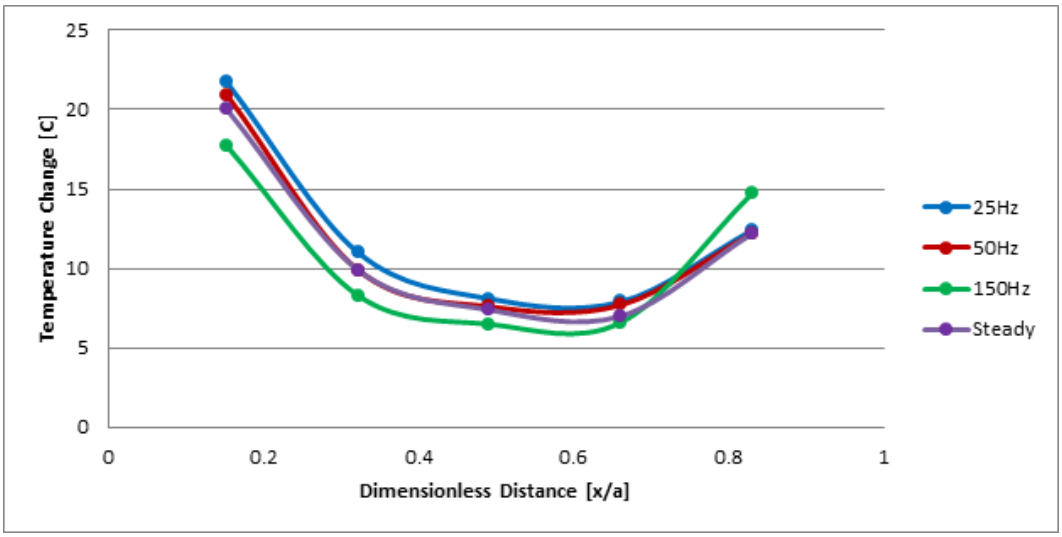

Figure 3.27: Unidirectional Sample #13: Temperature vs. Dimensionless Distance: I_{avg} = 70 A

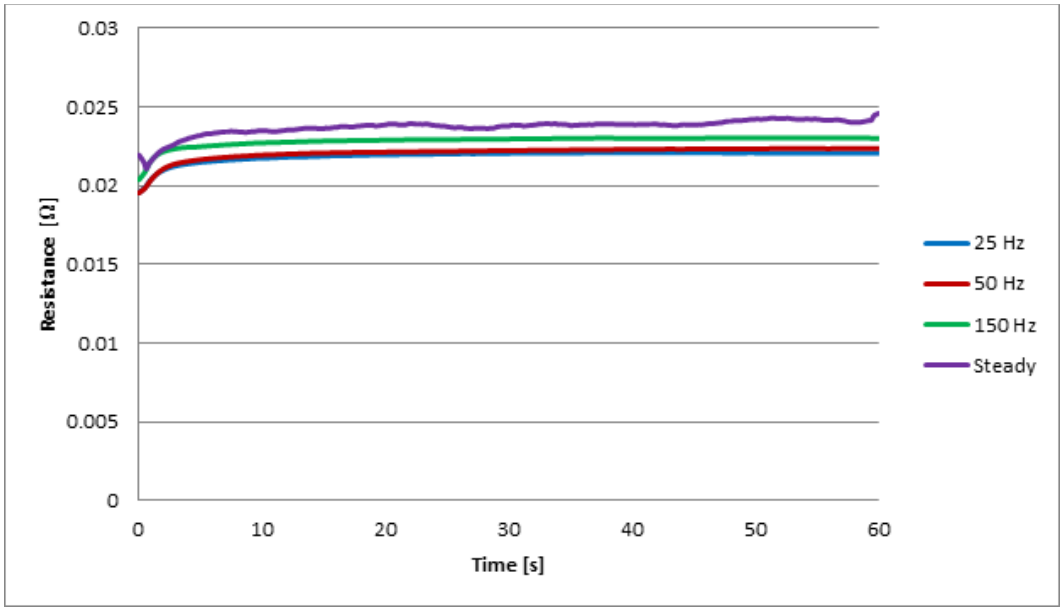

Figure 3.28: Unidirectional Sample #13: Resistance vs. Time: I_{avg} = 70 A

When comparing Figures 3.27 and 3.28, it can be seen that frequencies with lower resistance had corresponding higher changes in temperature, and vice versa for higher resistances. As mentioned previously, the relationship between the contact resistance and change in surface temperature is not well defined due to samples having very similar resistance values.

3.3.4 Electrical Response and Current-induced Heating of 32-Ply Unidirectional IM7/977-3 Untreated Composites

To understand the effect of contact resistance and the change in surface temperature, an additional 32-Ply Unidirectional IM7/977-3 composite sample was tested. The specimen was subjected to steady current magnitudes of 1, 10, 20, 30, 40, and 50 A and varying application times. This sample differed from samples #12, #13, and #14 by not being subjected to sample preparation as described in Section 2.4.1. The samples were only "lightly" sanded with a 440 and then 600 grit sand paper on the contact surface to remove any frayed or loose material. As noted previously, the samples were subjected to steady currents for varying times while measurements of the current, voltage, and resistance were recorded. The application time of the current was determined by the surface temperature of the sample. If the temperature became higher than 140^{o} C, the experiment was stopped as soon as possible due to the fixture temperature limitations as described in Section 2.3.3.3. The time history of the resistance for this untreated sample can be seen in Figure 3.29.

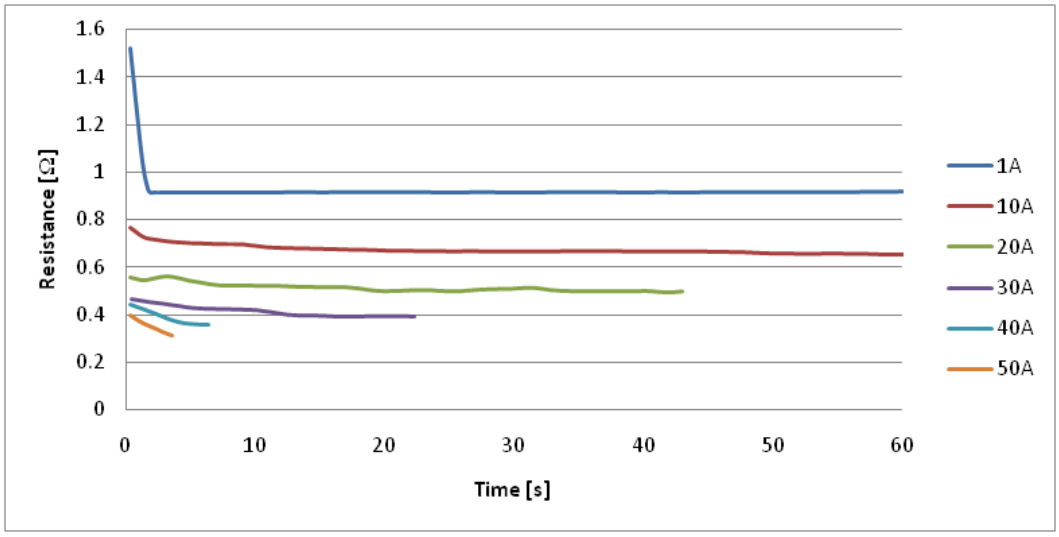

Figure 3.29: Unidirectional Untreated Sample #19: Resistance vs. Time, Steady Current

As seen in Figure 2.29, the resistance is fairly constant for 1-30 A current applications. In these cases, the changes in the current are minimal. Due to the temperature rising quickly for the 40 and 50 A cases, it cannot be determined what the resistance would have been for extended application. It is not likely that the test would be able to be continued for more time because the sample would reach the glass transition temperature as described in Section 2.3.3.3.

The values of the resistance and application time for untreated sample #19 subjected to the current magnitudes listed previously for steady current can be seen in Table 3.10.

Table 3.10: Steady Current Resistance and Application Time for Unidirectional Untreated Sample #19

Resistance [Ω]				
Current [A]	High	Low	Average	Time [S]
1	1.51862	0.91646	0.92379	60
10	0.76589	0.65348	0.67346	60
20	0.56096	0.49599	0.51453	43
30	0.46790	0.39177	0.41297	22
40	0.44187	0.35610	0.38433	5
50	0.39715	0.31187	0.35117	4

When comparing Tables 3.6 and 3.10, the resistance value for the untreated sample at 50 A steady current is approximately 13.5 times greater than sample #12, which had the highest resistance of the three specimens with the same current magnitude. The higher resistance of the untreated sample is due to the fact that the sample did not have a perfectly flat edge on the contact surface and that not all of the conductive carbon fibers were in contact with the copper bus bar. This is due to the preparation process when the samples are cut. In the case of treated samples, the contact edge is treated with a silver conductive epoxy to help flatten the surface and to promote contact with the fibers. Moreover, high contact resistance in the untreated sample led to the rapid increase in the surface temperature. The surface temperature with respect to time for varying current magnitudes can be seen in Figure 3.30.

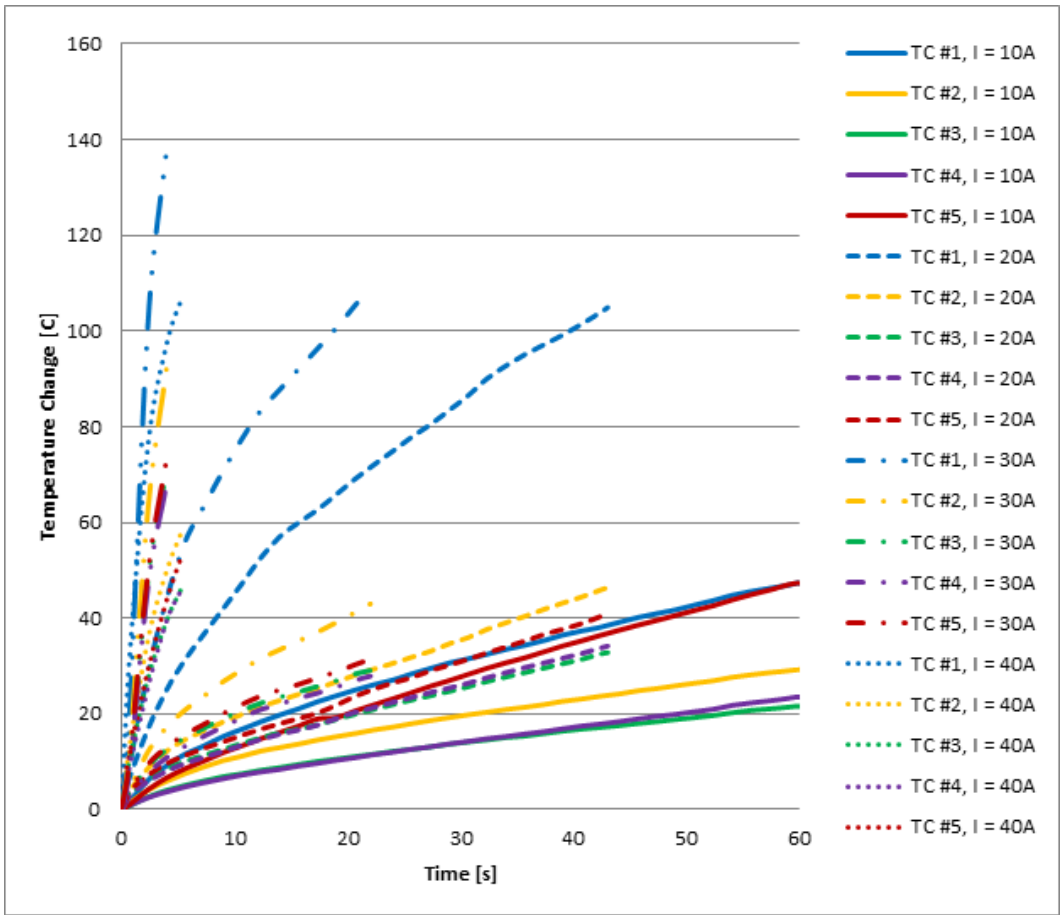

Figure 3.30: Unidirectional Untreated Sample #19: Temperature vs. Time, Steady Current.

3.4 Results of 32-Ply Symmetric Cross-Ply IM7/977-3 Composite Specimens

3.4.1 Electrical Response of 32-Ply Symmetric Cross-Ply IM7/977-3 Composites to Time-Varying Currents

The types of specimens tested next were 32-ply symmetric cross-ply IM7/977-3 composites. These composites, as the name suggests, have fibers orientated in the 0^o direction for the first layer and 90^o direction for the second layer repeated to 16 (plies) and symmetrically repeated for another 16 layers. With this fiber arrangement, one would expect a higher contact resistance of the specimens due to only half of the conductive fibers being available at the composite/copper contact interface. This higher contact resistance would be roughly twice that of the 32-ply unidirectional IM7/977-3 composites. Of the available 32-cross-ply IM7/977-3 composite specimens, three were used to investigate the electrical and thermal response when subjected to time-varying and steady electrical loads using the fully instrumented system as described in Section 2.3.2. Initially, specimens #15, #16, and #17 were tested. As with the 32-ply unidirectional samples discussed earlier, a fourth sample (#18) was tested to ensure that the correct waveform and current amplitude was being applied to the composite specimens by the power supply. This also gave an additional sample to compare resistance against as well as ensure that the temperature in the specimens due to an applied electric current was below both the glass transition temperature of the specimens and the charring temperature of the wooden fixture as noted in Section 2.3.3.3. After analyzing the data, it was determined that a fifth specimen (#22) needed to be tested to validate the results of the experiments as will be discussed later. This sample would only be subjected to steady currents.

According to the procedure outlined in Section 2.4.2, samples #15, #16, and #17 were first subjected to a 1 A steady current for 5 seconds to ensure that all three samples had similar contact resistance. If a sample did not have similar resistance to the others, sample preparation (as described in Section 2.4.1) was repeated. The resistance of the composite samples subjected to the steady current can be seen in Table 3.11.

Table 3.11: 1 A Steady Current Resistance for Symmetric Cross-Ply Composites

Resistance [Ω]			
Sample	Average	Maximum	Minimum
#15	0.08178	0.08503	0.07854
#16	0.05429	0.05460	0.05397
#17	0.08998	0.09200	0.08795
#22	0.09030	0.09052	0.09004

As seen in Table 3.11, the resistance of sample #16 was well below that of the other samples tested. With sample #16 having much lower resistance, an additional sample (#22) was tested. Additionally, in Table 3.11, sample #22 produced similar contact resistance values to samples #15 and #17. With the resistance values of samples #15, #17, and #22 within an acceptable range, a sine wave time-varying current was applied. The shape of the voltage and current, as measured by the DAQ system for sample #17 subjected to sine wave current with $\omega = 50$ Hz and $I_{avg} = 75$ A can be seen in a reduced time step in Figures 3.31 and 3.32, respectively.

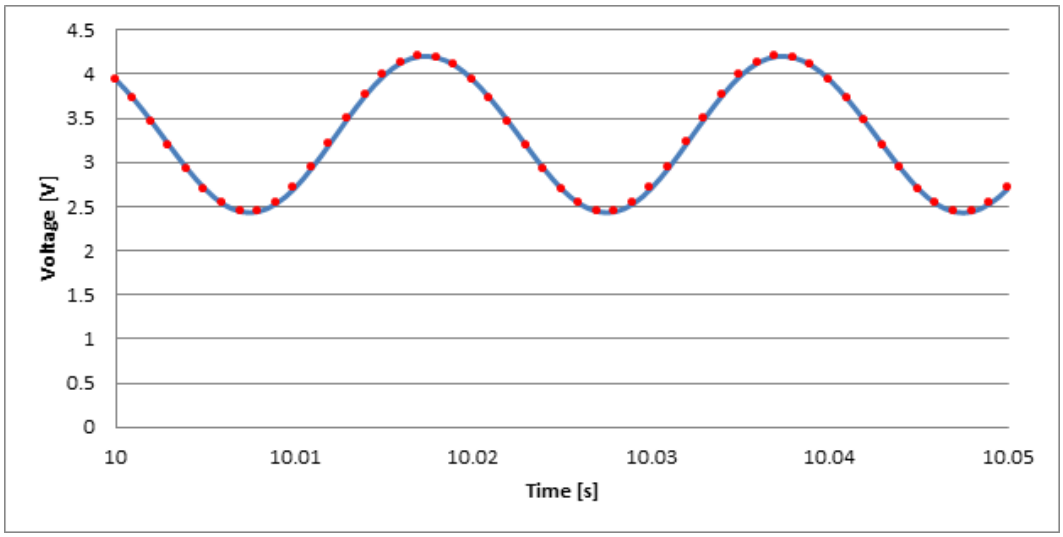

Figure 3.31: Symmetric Cross-Ply Sample #17: Voltage vs. Time, ω = 50 Hz, I_{avg} = 75 A

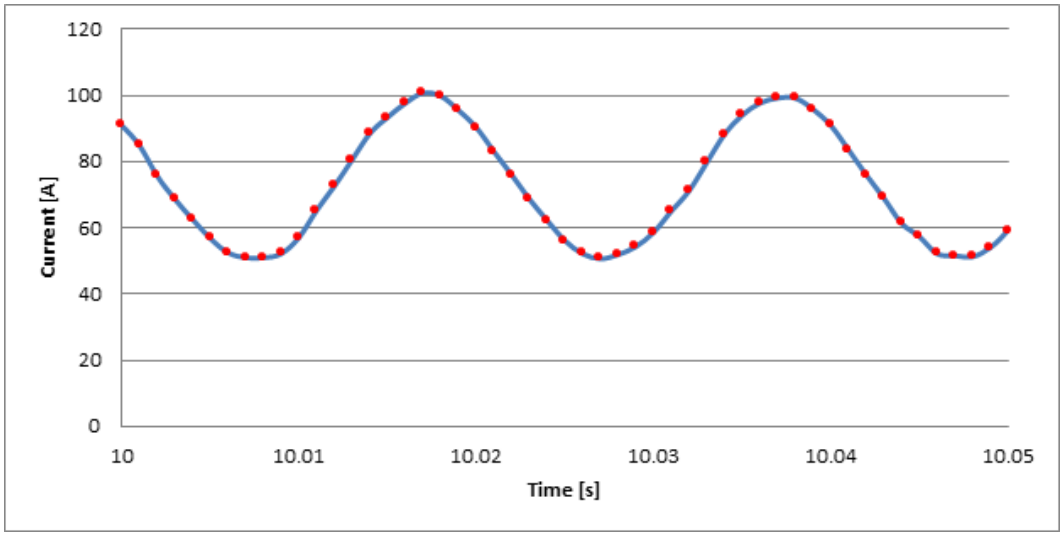

Figure 3.32: Symmetric Cross-Ply Sample #17: Current vs. Time, ω = 50 Hz, I_{avg}= 75 A

The plots of voltage and current as functions of time as shown in Figures 3.31 and 3.32 have a reduced time step to clearly demonstrate that the experimental setup is capturing the time-varying electrical current. Furthermore, the figures also confirm that the sine wave prescribed is what is being applied to the composite specimens. Markers on both figures indicate the time when each measurement was taken. Using the voltage and current measurements, the electrical resistance of the composites subjected to time-varying electrical load could be determined. The general trend of the composite electrical resistance (an average over the sine wave period) as function of time over a 1 minute time for sample #17 subjected to varying current magnitudes at 150 Hz can be seen in Figure 3.33.

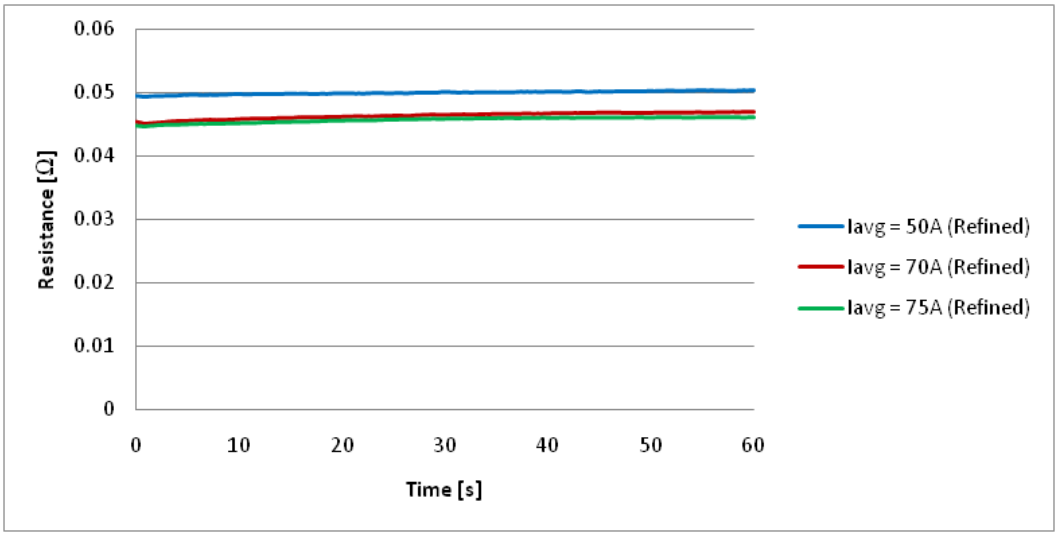

Figure 3.33: Symmetric Cross-Ply Sample #17: Resistance vs. Time, ω = 150 Hz

It should be noted that Figure 3.33 displays the resistance with respect to time using only the filtered and refined data to reduce the amount of data points. This process is required due to high sampling rates and the large amount of data points collected. The time trend of the resistance of symmetric cross-ply composites produced slightly different results than that of the unidirectional composites shown previously in Figure 3.4. As one can see, in the case of cross-ply composites the resistance remains fairly constant throughout the entire experiment. This is different from the unidirectional samples where the resistance sharply increased and eventually lowered or remained steady. As in the case of the unidirectional specimens, the resistance of the cross-ply specimens is dependent on the average value and amplitude of the electric current. Here, higher average current results in smaller resistance, and lower average current results in higher resistance. The results for samples #15 and #22 were very similar to those as shown in Figure 3.33 for sample #17 and were therefore omitted. Sample #16 exhibited a different behavior. Figure 3.34 displays resistance vs. time for sample #16.

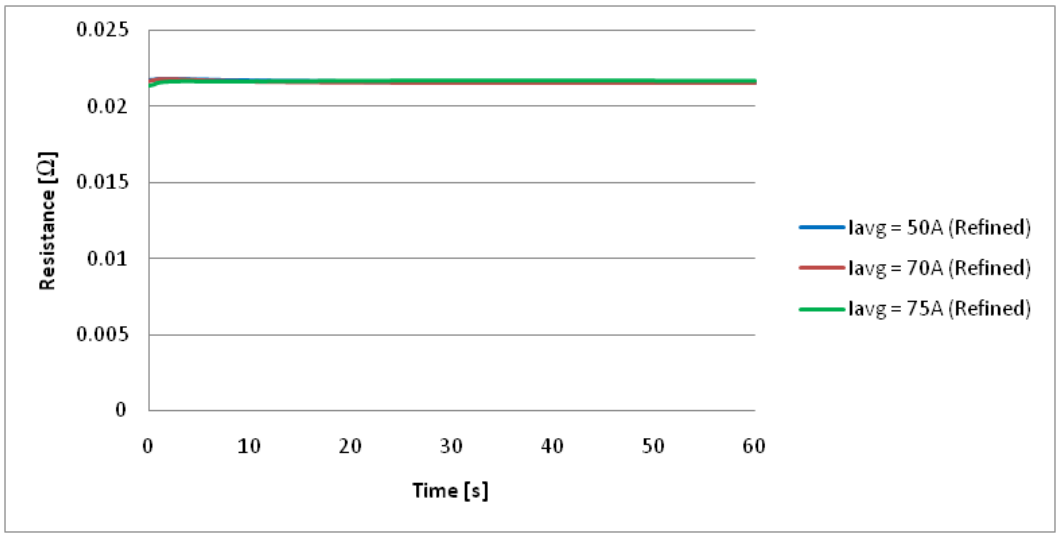

Figure 3.34: Symmetric Cross-Ply Sample #16: Resistance vs. Time, ω = 150 Hz

As shown in Figure 3.34, the resistance follows a trend similar to that of the cross-ply samples #15, #17, and #22. However, the values of the resistance are similar to that of the unidirectional samples #12, #13, and #14. Furthermore, the resistance did not appear to be a function of the average current magnitude. All three average currents, 50, 70, and 75 A, resulted in very similar resistance values. This was found to be the case for all frequencies tested as well as for steady current application. This behavior of sample #16 proved to be inconsistent when compared to other cross-ply samples. Upon testing sample #22 under steady current applications, the result agreed with the behavior of samples #15 and #17. Therefore, the results of sample #16 cannot be considered an accurate representation of the cross-ply sample population. The percentage difference between the lowest and the highest measured contact resistance for each time-varying current experiment can be seen in Table 3.12. Here the highest resistance value is denoted as “High” and the lowest as “Low”.

Table 3.12: Percent Change in Resistance for Symmetric Cross-Ply Composites, Time-Varying Electric Current

Sample #15				
Frequency [Hz]	Average Current [A]	High [Ω]	Low [Ω]	% Difference
25	50	0.0447	0.0438	2.01
	70	0.0406	0.0399	1.64
	75	0.0406	0.0401	1.21
50	50	0.0468	0.0455	2.83
	70	0.0424	0.0413	2.62
	75	0.0419	0.0413	1.44
150	50	0.0483	0.0463	4.41
	70	0.0433	0.0426	1.57
	75	0.0437	0.0427	2.49

Sample #16				
Frequency [Hz]	Average Current [A]	High [Ω]	Low [Ω]	% Difference
25	50	0.0238	0.0233	2.45
	70	0.0226	0.0218	3.77
	75	0.0233	0.0221	5.34
50	50	0.0223	0.0220	1.27
	70	0.0220	0.0215	2.14
	75	0.0220	0.0216	2.24
150	50	0.0218	0.0215	1.32
	70	0.0218	0.0215	1.31
	75	0.0217	0.0214	1.50

Sample #17				
Frequency [Hz]	Average Current [A]	High [Ω]	Low [Ω]	% Difference
25	50	0.0510	0.0474	7.59
	70	0.0455	0.0436	4.33
	75	0.0444	0.0414	7.14
50	50	0.0512	0.0490	4.45
	70	0.0457	0.0446	2.45
	75	0.0457	0.0438	4.47
150	50	0.0505	0.0495	2.02
	70	0.0469	0.0451	4.02
	75	0.0463	0.0447	3.45

Referring to Table 3.12 it can be seen that the resistance for the cross-ply samples remains fairly constant under time-varying current with the largest difference between low and high resistance values being 7.59%. However, the steady current application did tend to produce a resistance that changed with respect to time. In the steady current application, there was a maximum change from low and high resistance of 35.51%. Note that sample #22 is omitted from Table 3.12, as it was only subjected to steady current application. By extracting raw unprocessed data (unfiltered/non-reduced), the shape of the resistance wave can be determined with respect to time. This wave follows the shape of the current applied (sine) due to Ohm's law governing the resistance. The resistance wave shape for sample #15 at ω = 25 Hz, I_{avg} = 50 and 75 A can be seen in Figure 3.35.

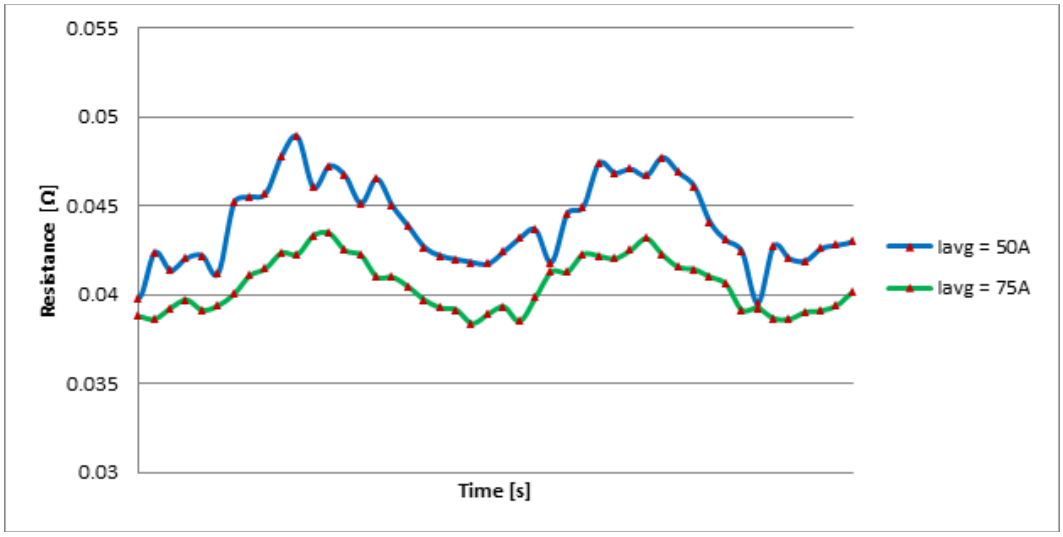

Figure 3.35: Symmetric Cross-Ply Sample #15: Wave Shape, Resistance vs. Time, ω = 25 Hz

It should be noted that, for Figure 3.35, the resistance waves have been time shifted so the resistance peaks for both time-varying currents (I_{avg} = 50 A and I_{avg} = 75 A) can be seen at the same time. The shift was done to analyze the effects of the current amplitude (if any) on the resistance. Here the markers indicate where each measurement during the experiment was taken. It can be seen that the 50 A average current results in higher resistance when compared to the 75 A average current application. Moreover, the shape does not appear as smooth as the voltage and current waves shown in Figures 3.31 and 3.32, respectively. Similar to the unidirectional samples, the cross-ply resistance calculations result in very small changes in resistance at neighboring points. These small changes make plotting difficult when interpolation is used to connect the points for a smooth line. Additionally, any errors in voltage measurements by the U2531A DAQ unit will have a greater error effect on the resistance calculation. It is difficult to distinguish from Figure 3.35, but the "amplitude" of resistance of 50 A average current is slightly larger than that of the 75 A average current. Both average currents in this comparison had the same peak-to-peak current of 50 A as well. This trend was found to hold true for all samples under almost every trial similar to that of the unidirectional samples. However, the difference in "amplitude" is not as noticeable as in the unidirectional experiments. The resistance wave shapes for 70 and 75 A average currents can be seen in Figure 3.36.

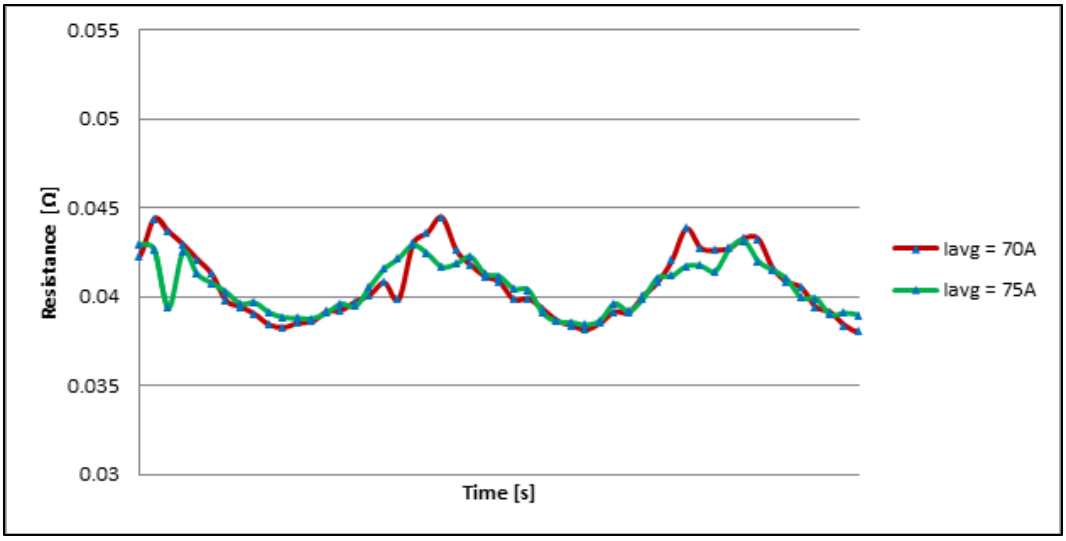

Figure 3.36: Symmetric Cross-Ply Sample #15: Wave Shape, Resistance vs. Time, ω = 25 Hz

As seen in Figure 3.36, the resistance amplitude is greater for 70 A average current than that for 75 A. In this comparison, both current values had different peak resistance at minimum current. This is due to 70 and 75 A having different minimum currents (40 A and 50 A, respectively). Therefore, one would expect that the 70 A average current would have higher peak resistance than the 75 A average current. The minimum resistance values are very similar for both average currents. These minimum resistances occurred at the maximum current application, which was 100 A for both average current applications. It should also be noted that in Figure 3.36 the resistance waves have been time shifted so the resistance peaks can be seen at the same time with markers indicating time when the actual measurements for current and voltage were recorded and the resistances have been calculated.

It has been shown earlier in Figures 3.31 and 3.32 that the system is capable of capturing the waveform applied to the composite specimens by the experimental set-up.

However, as mentioned earlier in Section 3.3.1, it was also important to ensure that the current, voltage, and resistance were being measured in the same phase by the DAQ system. This was verified by scaling the current and resistance to the voltage and plotting them together. This process was performed on many of the experiments to ensure the phase synchronization. A 150 Hz example of such scaling and phase plotting can be seen in Figure 3.37. This plot also shows that the electric resistance is directly related to the amplitude of the applied time-varying current: resistance is in phase with the current, and there is an increase in the resistance as the current magnitude decreases.

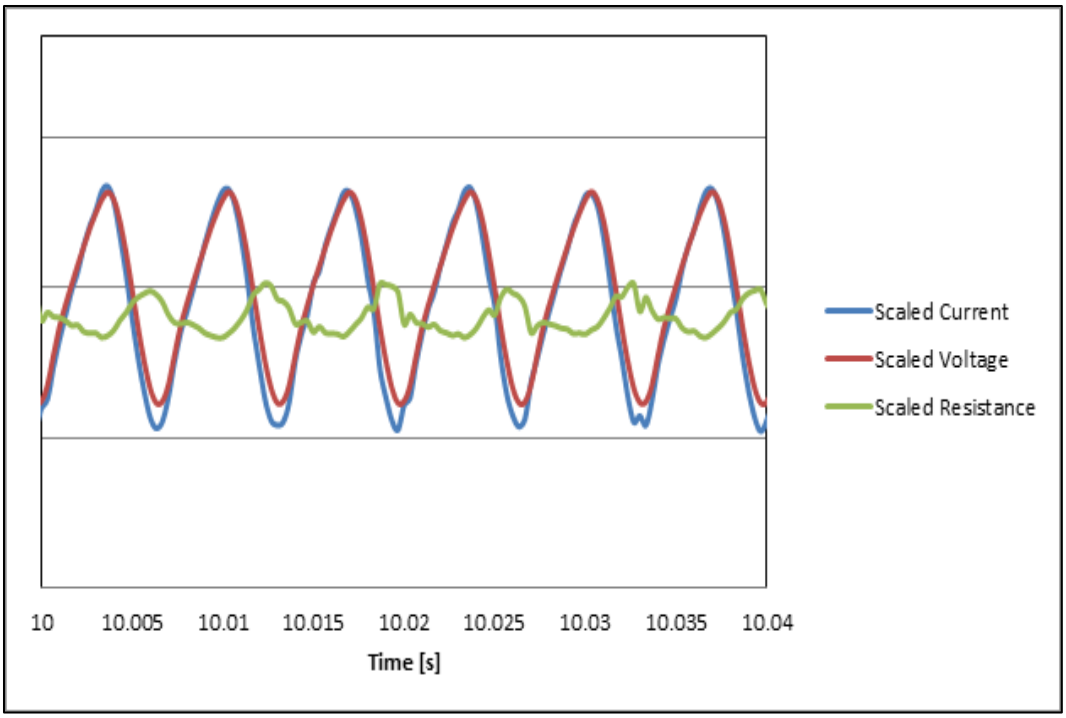

Figure 3.37: Symmetric Cross-Ply Sample #15: Scaled Current, Voltage, and Resistance vs. Time, $\omega = 150$ Hz

3.4.2 Electrical Response of 32-Ply Symmetric Cross-Ply IM7/977-3 Composites to Steady Currents

As in the case of the unidirectional experiments, the cross-ply specimens were also subjected to steady currents of zero frequency (ω = 0 Hz) in addition to the time-varying current application. Figure 3.38-3.41 shows resistance vs. time for samples #15, #16, #17, and #22 subjected to varying magnitudes of steady current.

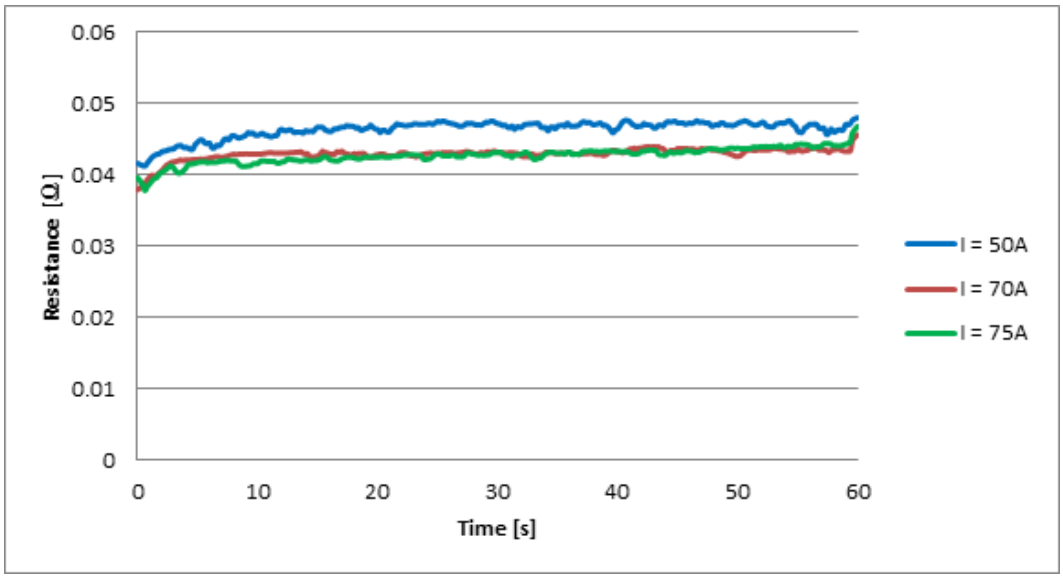

Figure 3.38: Symmetric Cross-Ply Sample #15: Resistance vs. Time, Steady Current

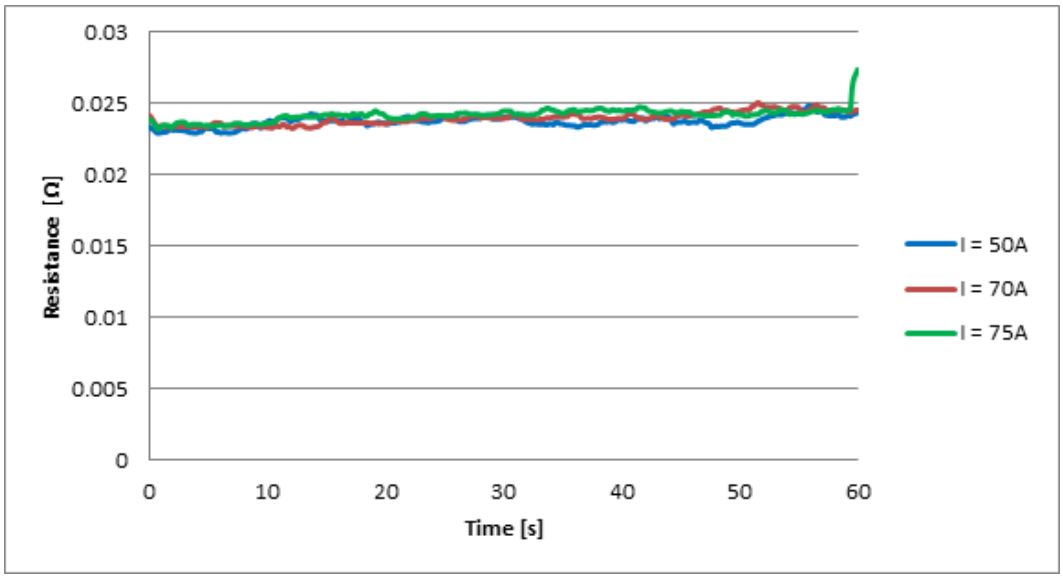

Figure 3.39: Symmetric Cross-Ply Sample #16: Resistance vs. Time, Steady Current

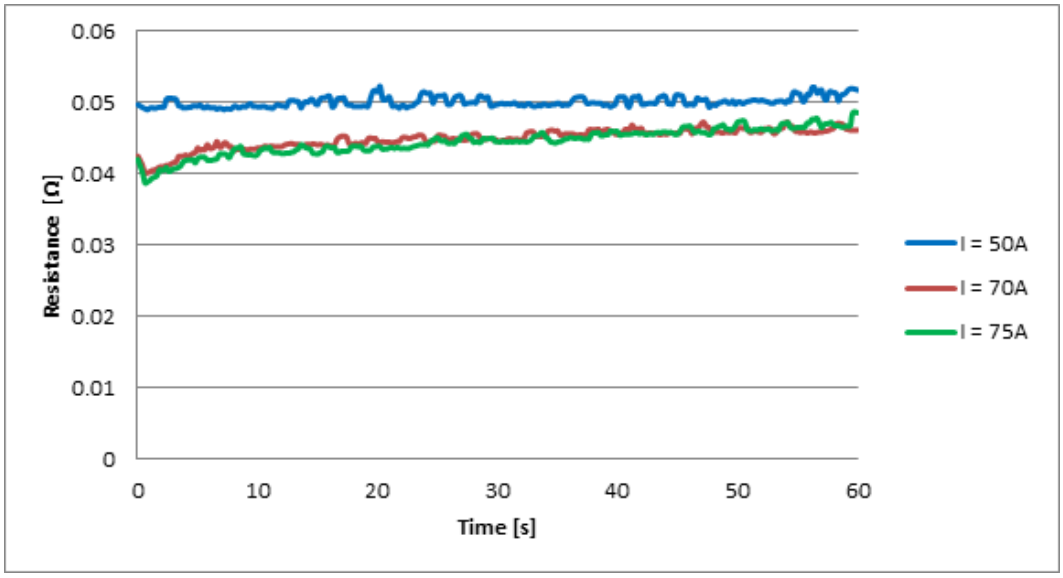

Figure 3.40: Symmetric Cross-Ply Sample #17: Resistance vs. Time, Steady Current

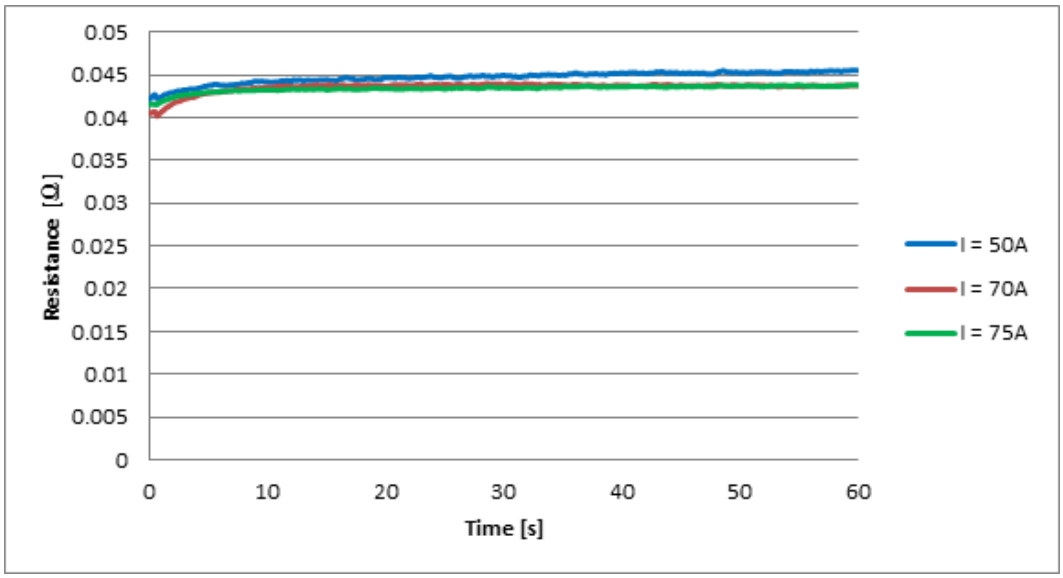

Figure 3.41: Symmetric Cross-Ply Sample #22: Resistance vs. Time, Steady Current

Table 3.13 shows maximum and minimum values of the resistance subjected to 50, 70, and 75 A steady current magnitudes for each sample.

Table 3.13: Steady Current Minimum and Maximum Values of Resistance for Symmetric Cross-Ply Composites

Sample #15				
Frequency [Hz]	Current [A]	High [Ω]	Low [Ω]	Percent Difference
0, Steady	50	0.0480	0.0412	16.53
	70	0.0456	0.0379	20.33
	75	0.0468	0.0378	23.85

Sample #16				
Frequency [Hz]	Current [A]	High [Ω]	Low [Ω]	Percent Difference
0, Steady	50	0.0248	0.0229	8.32
	70	0.0251	0.0233	7.73
	75	0.0274	0.0232	17.89

Sample #17				
Frequency [Hz]	Current [A]	High [Ω]	Low [Ω]	Percent Difference
0, Steady	50	0.0523	0.0490	6.77
	70	0.0472	0.0401	17.94
	75	0.0486	0.0387	25.44

Sample #22				
Frequency [Hz]	Current [A]	High [Ω]	Low [Ω]	Percent Difference
0, Steady	50	0.0456	0.0422	7.92
	70	0.0440	0.0402	9.47
	75	0.0438	0.0416	5.50

Similar to the time-varying current, electrical resistance under steady currents does not stay constant. However, changes in the electrical resistance under steady currents are smaller when compared to time-varying currents (see Figures 3.33, 3.34, and

3.38-3.41). Moreover, electrical resistance under steady current monotonically increases with time, whereas electrical resistance under time-varying currents was not a monotonic function of time. Furthermore, the electrical resistance at the 50 A steady current tends to be higher compared to the 70 A and 75 A currents. This was found to be the opposite for unidirectional samples as the 50 A steady current yielded lower resistance than that of 70 A and 75 A. Additionally the unusual behavior of sample #16 (lower resistance) is obvious when compared to the remaining three samples tested (#15, #17, and #22). Also, the variation in the resistance from sample to sample increases as the current magnitude increases. This variation of the four samples can be seen in Figure 3.42 as resistance vs. time subjected to a 50 A steady current.

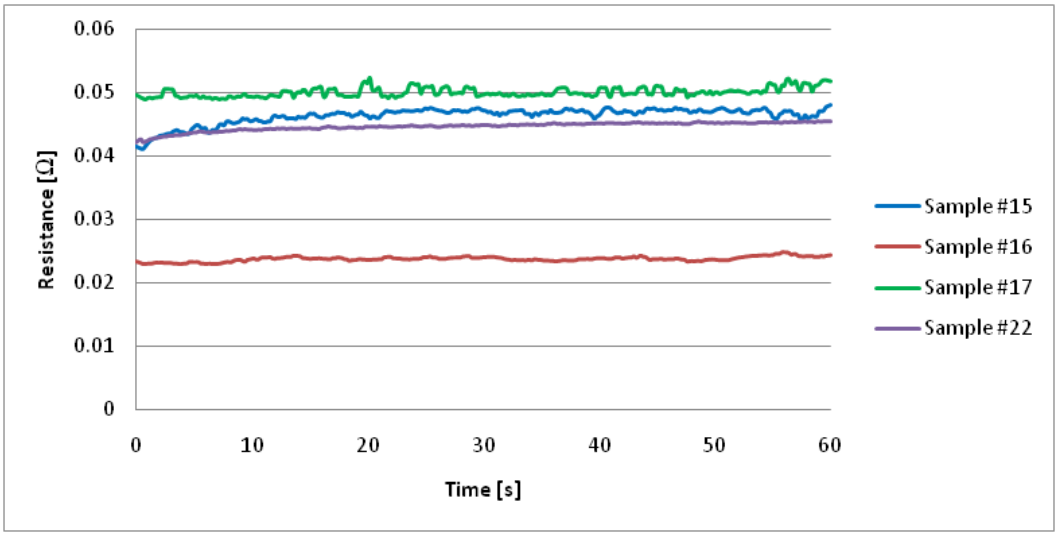

Figure 3.42: Symmetric Cross-Ply: Resistance vs. Time, Steady Current, I = 50 A

In addition to the behavior of the electrical resistance, voltage-current characteristics were examined for all specimens at the onset of the electric current applications and after the electric current had been applied for 1 minute. As emphasized earlier, each specimen undergoing testing was treated following the procedure described in Section 2.4.1 to reduce contact resistance. After that the specimen was placed into the fixture and a steady electric current was applied for 1 minute, while current, voltage, and surface temperature were measured. After that the specimen was allowed to cool back down to ambient temperature (if necessary) and the next test under a higher current magnitude was conducted. As mentioned previously, the minimum tested current was 1 A, which corresponded to the current density of 1312 A/m^2, and the maximum current applied was 75 A, which corresponded to the current density 98425 A/m^2. The current densities were computed by using the composite sample dimensions as shown in Table 3.1 and computing the total contact area by using the thickness and width.

Figures 3.43 and 3.44 reveal the voltage-current relationships for the cross-ply composite specimens measured at the onset of the electric current applications (beginning of experiments, t = 0 sec) and after electric currents were applied for 1 minute (end of experiments, t = 60 sec).

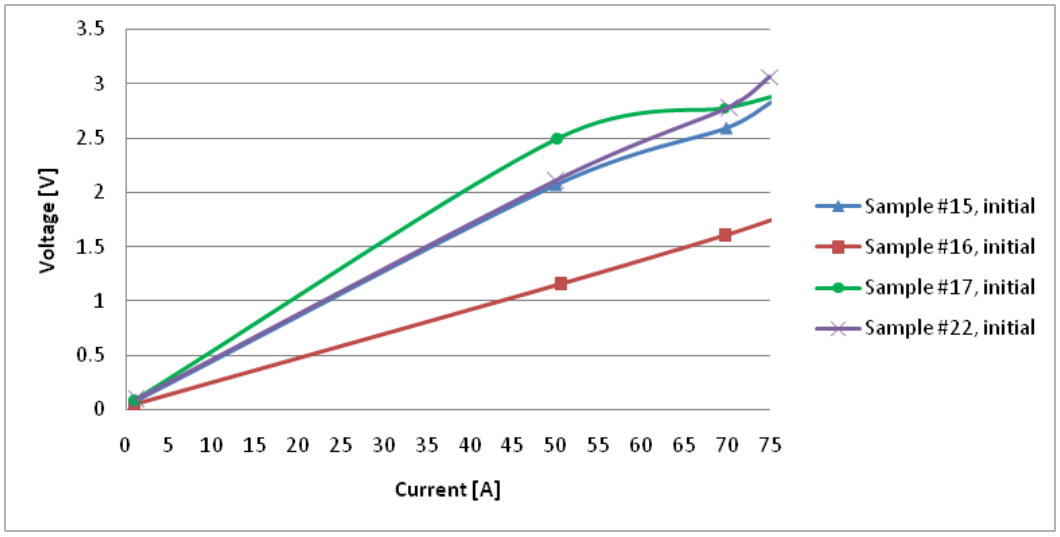

Figure 3.43: Symmetric Cross-Ply: Voltage vs. Current, Steady Currents

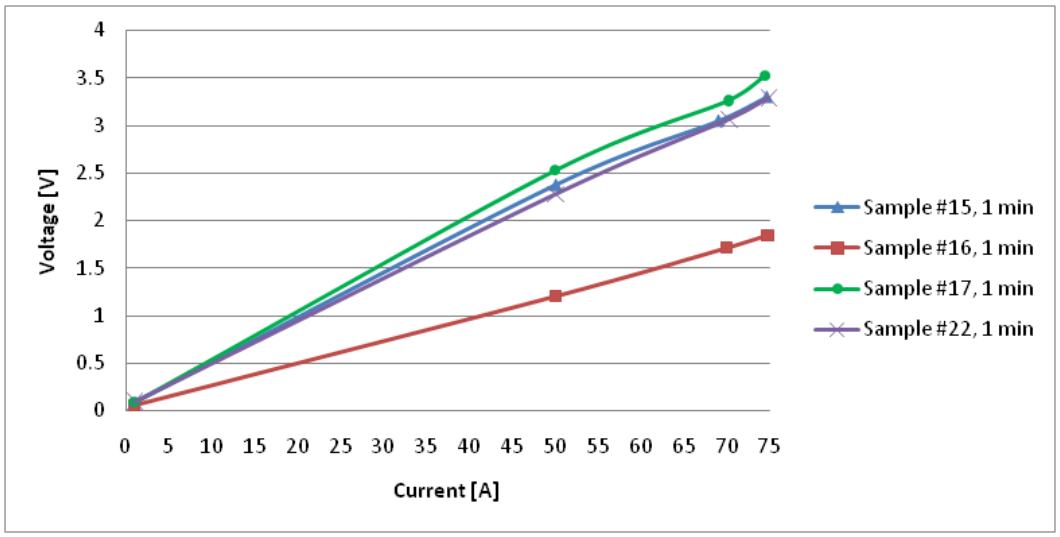

Figure 3.44: Symmetric Cross-Ply: Voltage vs. Current, Steady Currents

Similar to the unidirectional samples, the change in resistance with respect to time in the cross-ply composite specimens has a dynamic resistor effect and not a static or

Ohmic resistance as seen in Figures 3.33 and 3.34 above. However, unlike the unidirectional samples, the initial voltage-current relationship tended to become nonlinear at approximately 50 A. Moreover, the final voltage-current relationship also had a critical value of current at which linear Ohm's law fails and the voltage-current relationship becomes nonlinear. This critical value was also 50 A, which corresponded to a 65617 A/m^2 current density (as described previously). Moreover, it was noticed that below 50 A, electrical resistance changed little over time, while above this value there was an increase in the resistance with time.

3.4.3 Current-Induced Heating of 32-Ply Symmetric Cross-Ply IM7/977-3 Composites

This section presents results of temperature measurement on 32-ply symmetric cross-ply IM7/977-3 composites (samples #15, #16, #17, and #22) subjected to electric currents of various magnitude, frequency, and duration. As mentioned before, the temperature distribution on the surface of composite specimens was measured by five thermocouples. These thermocouples are denoted by the notation as described in Section 3.3.3. Referring to Figure 3.14, shown previously, the location of thermocouple, the copper electrodes, and composite specimen can be seen. The locations of the thermocouples with respect to the left-side copper-composite interface and the desired distance can be seen in Table 3.14.

Unlike the unidirectional samples tested, the thermocouple placement was symmetric with respect to the middle of the specimens for all samples tested. Here, equal distances are present between thermocouple #1 and the copper bar attached on the left and thermocouple #5 and the copper bar attached on the right (see the Figure 3.14 for details).

Table 3.14: Thermocouple Location for Symmetric Cross-Ply Composites

Thermocouple Distance from Interface, x [mm]					
Sample #	TC #1	TC #2	TC #3	TC #4	TC #5
15	25.4	50.8	76.2	101.6	127
16	25.4	50.8	76.2	101.6	127
17	25.4	50.8	76.2	101.6	127
22	25.4	50.8	76.2	101.6	127
Desired	25.4	50.8	76.2	101.6	127

As performed previously with the unidirectional samples, the ambient temperature, $T_{in,}$ was subtracted from the temperature, T, to obtain the temperature change of the composite surface, ΔT. For the cross-ply trials, T_{in}, was $T_{in} = 19^{o}$ C. This leads to the temperature change as dictated by $\Delta T=T-T_{in}$. Figure 3.45 displays the temperature change, $\Delta T,$ measured by the infrared thermocouples (TC#1, TC#2, TC#3, TC#4, and TC#5) vs. time in the 32-cross-ply IM7/977-3 composite (sample #17) subjected to a 150 Hz sine wave electric current with I_{avg}= 75A.

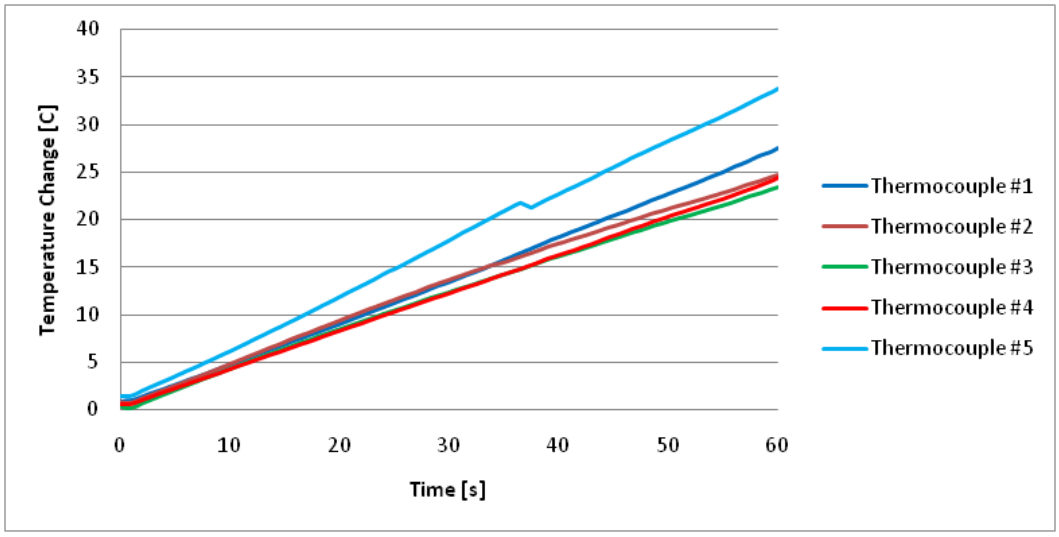

Figure 3.45: Symmetric Cross-Ply Sample #17: Temperature Change vs. Time: ω = 150 Hz, I_{avg}= 75 A

As seen in Figure 3.45, the temperature of thermocouples #1 and #5 measure the highest temperature on the composite surface, #2 and #4 the next highest, and #3 the lowest temperature. This was found to be the same for all samples tested. When comparing the temperature change time history to unidirectional specimens, the temperature rose quicker in the cross-ply specimens due to the increase in the contact resistance. As with the unidirectional samples, there was a temperature gradient present in the composite. This gradient is produced across the composite by current-induced heating. This gradient is formed in the direction of the applied current. Moreover, the same factors found in the unidirectional samples were determined to be the cause of this gradient in the cross-ply specimens. This temperature gradient for sample #15 subjected to a 150 Hz sine wave and I_{avg} = 50 A, after the electric current was applied for 1 minute, can be seen in Figure 3.46.

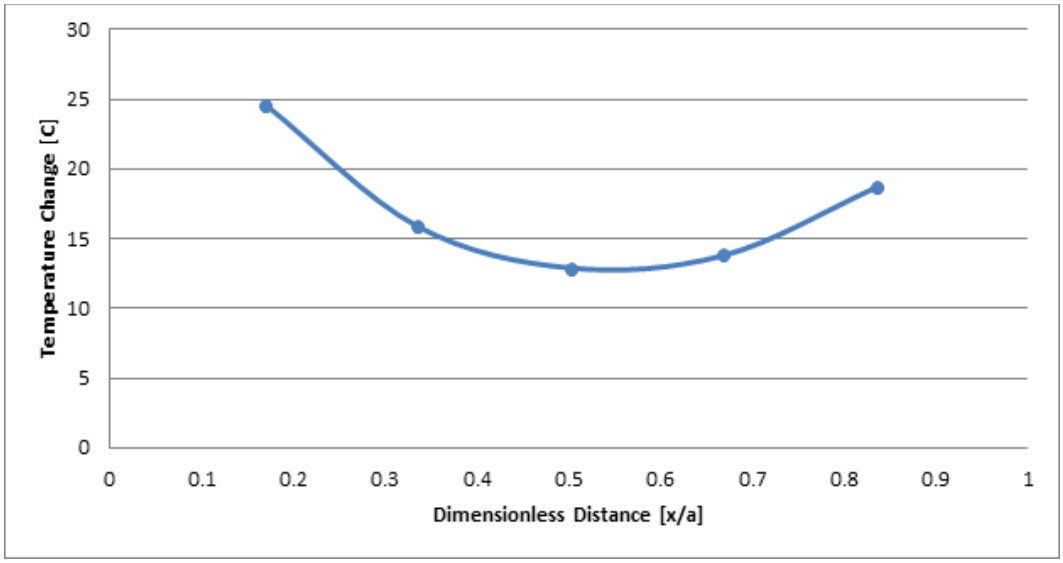

Figure 3.46: Symmetric Cross-Ply Sample #15: Temperature Change vs. Dimensionless Distance: ω = 150 Hz, I_{avg}= 50 A

As seen, the temperature distribution in the plate is not symmetric with the temperature being higher at the left end. This is due to the fact that in all experiments performed in this work the copper bus bar attached to the left end served as the anode, and the copper bar attached to the right end served as a cathode (see Figure 3.14 for details). In both steady and time-varying current experiments, the direction of the current flow did not change, thus leading to different temperatures at the left and right ends of the specimen with the temperature at the anode being higher than at the cathode. Also, any error present in temperature measurement can yield differences in the temperatures at the ends of the plate. Note that in Figure 3.46 the temperature is plotted versus dimensionless distance from the electric contact interface. This "dimensionless distance" is computed by normalizing the distance of the thermocouple measuring location (x) with

the total length of the plate (a) from the anode to the cathode. Similar to the unidirectional samples, the cross-ply samples had dimensions of a = 150 mm (5.91 in). Also, markers indicate the location (dimensionless distance) at which the temperature measurement was taken by the infrared thermocouples on the composite surface. The arrangement of the thermocouples can be seen as shown previously in Figure 3.14. Additionally, the changes in surface temperature were much greater for the cross-ply specimens when compared to the unidirectional samples. This is due to the increase in contact resistance as noted previously. Table 3.15 compares the change in surface temperature, as measured by thermocouple #1, for unidirectional and cross-ply specimens for ω = 25 Hz sine wave current and steady current applications of varying current magnitudes measured at the end of the experiments (60 seconds).

Similar to the unidirectional experiments, temperature measurements have been conducted at other current magnitudes and frequencies listed in Table 3.3. Figure 3.47 shows the results of different current magnitudes of a sine wave with ω = 150 Hz for sample #17.

Table 3.15: Symmetric Cross-Ply and Unidirectional Change in Surface Temperature Comparison of ω = 25 Hz and Steady Current

Frequency [Hz]	Average Current [A]	32-Unidirectional Sample	Maximum Temperature Change [C]		32-Cross-Ply Sample
25	50	#12	12.6	20.4	#15
		#13	15.2	13.1	#16
		#14	5.1	18.2	#17
	70	#12	25.0	36.4	#15
		#13	21.7	25.7	#16
		#14	9.8	28.8	#17
	75	#12	28.3	42.3	#15
		#13	26.0	29.7	#16
		#14	9.7	31.1	#17
0, Steady	50	#12	15.2	22.7	#15
		#13	10.4	13.8	#16
		#14	8.8	16.7	#17
		NA	NA	13.0	#22
	70	#12	34.6	43.9	#15
		#13	20.0	25.9	#16
		#14	19.7	28.0	#17
		NA	NA	23.0	#22
	75	#12	41.1	52.5	#15
		#13	22.5	30.6	#16
		#14	21.5	29.8	#17
		NA	NA	26.9	#22

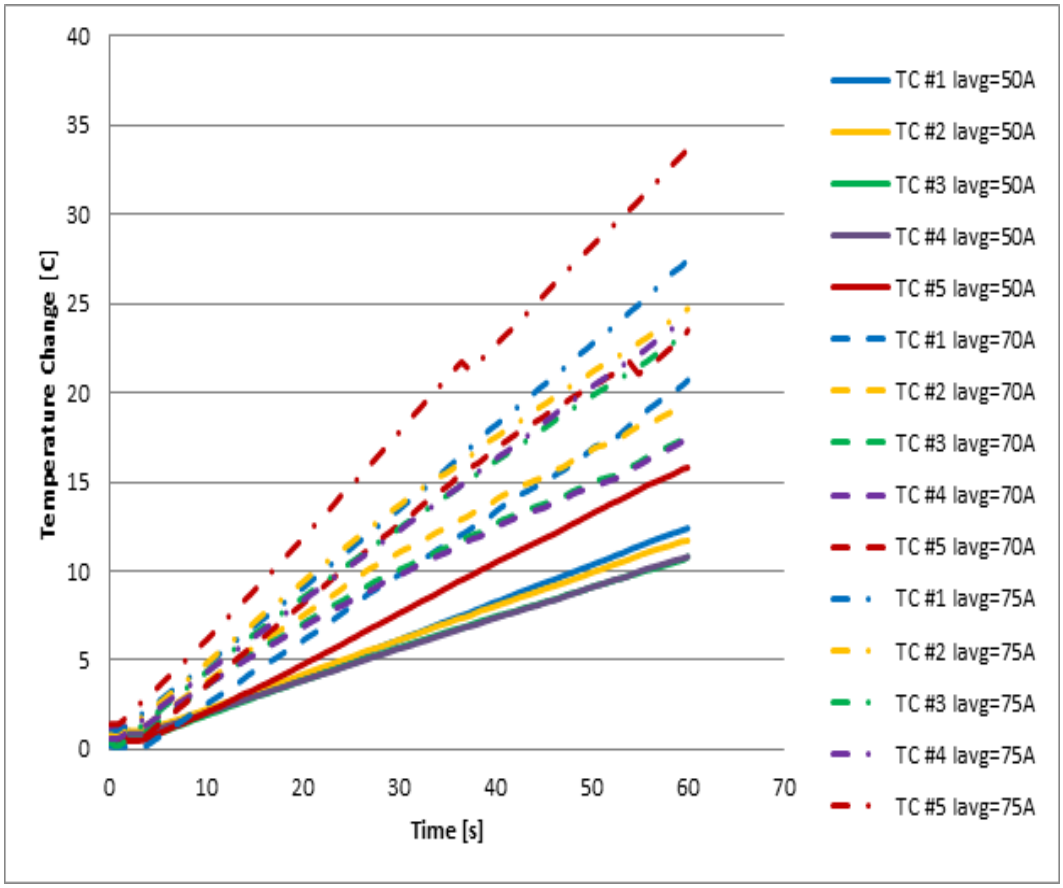

Figure 3.47: Symmetric Cross-Ply Sample #17: Temperature vs. Time, ω = 150 Hz

Figure 3.47 displays the relationship between the average current and temperature change at a frequency of 150 Hz. It can be seen that the higher the current magnitude and the closer the proximity to the contact interface, the greater the change of the composite surface temperature. Figure 3.48 shows the temperature change with respect to dimensionless distance of the thermocouple from the composite and copper bus bar contact interface, with markers indicating the location at which each measurement was

taken. The results are shown for cross-ply samples #15, #16, and #17 subjected to a 50 Hz sine wave and I_{avg}= 75 A.

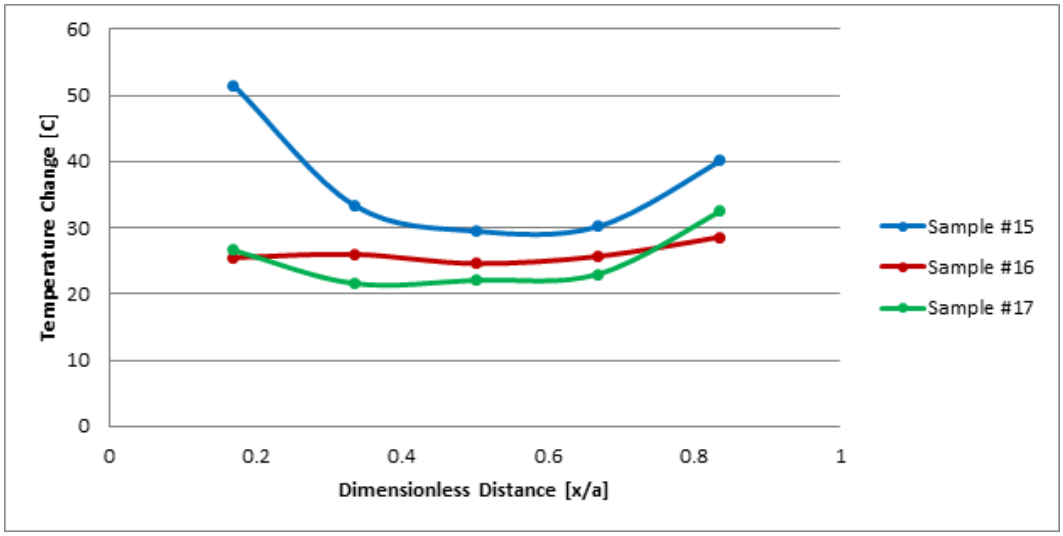

Figure 3.48: Symmetric Cross-Ply: Temperature vs. Dimensionless Distance: ω = 50 Hz, I_{avg}= 75 A

Note that sample #22 is not shown, as this sample was only subjected to steady current applications. As seen in Figure 3.48, each sample exhibited different temperature distributions under the same experimental conditions. Furthermore, it would be expected for samples with higher contact resistance to exhibit higher changes in temperature, as discussed previously in this thesis. This was also found not be the case in the cross-ply specimens. This is seen by comparing sample #15 and #17. Here sample #15 has lower average resistance (0.0417 Ω) than that of sample #17 (0.0454 Ω). Referring back to Figure 3.48, sample #15 resulted in a higher change in surface temperature when

compared to sample #17. Moreover, these characteristic were not found to be constant throughout all of the experiments performed. This, as was the case with unidirectional samples, leads to the assumption that the change in temperature may be a function of the resistance time history as well as differences in Joule heating from sample to sample. As noted earlier, sample #16 exhibited different contact resistance behavior when compared to that of the other three cross-ply samples. This contact resistance difference also resulted in different temperature behavior. As seen in Figure 3.48, sample #16 did not exhibit a temperature gradient seen in samples #15 and #17 as well as the unidirectional samples #12, #13, and #14. There was practically no change in the temperature throughout the length of the composite specimen #16. The time history of the resistance of samples #15, #16, and #17 subjected to sine wave current settings as in Figure 3.48 (ω = 50 Hz, I_{avg} = 75 A) can be seen in Figure 3.49.

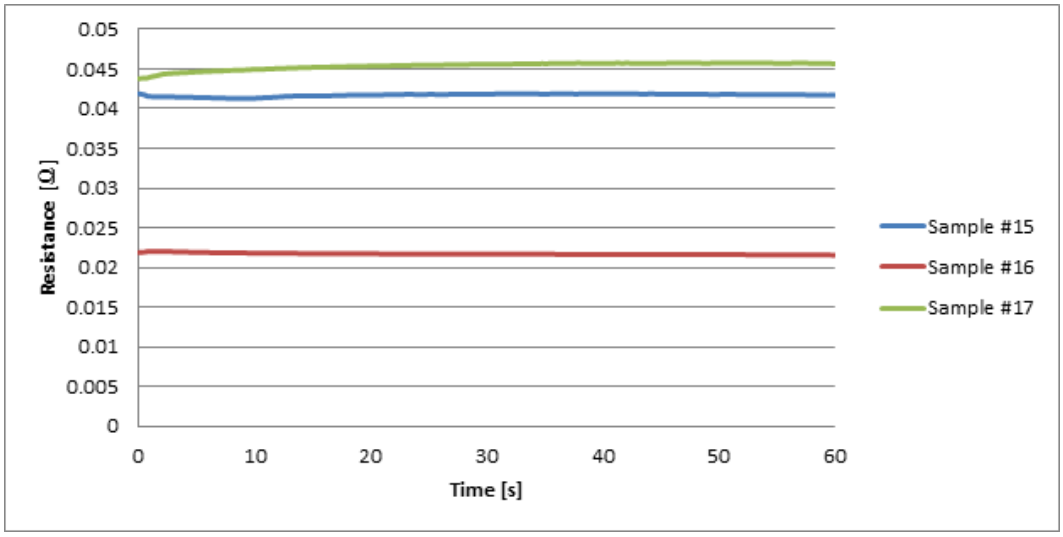

Figure 3.49: Symmetric Cross-Ply: Resistance vs. Time: ω = 50 Hz, I_{avg}= 75 A

The initial, average, and final resistance for samples #15, #16, and #17 subjected to I_{avg}= 75 A and ω = 50 Hz sine wave current can be seen in Table 3.16.

Table 3.16: Initial, Average, and Final Resistance of Symmetric Cross-Ply, I_{avg}= 75 A and ω = 50 Hz

Resistance [Ω]			
Sample	Initial	Average	Final
#15	0.0419	0.0417	0.0417
#16	0.0219	0.0217	0.0216
#17	0.0438	0.0454	0.0457

As noted previously and using Table 3.16 and Figure 3.49, one can see that sample #15 had the lowest resistance through the experiments, excluding sample #16 due to deviant behavior. This, however, did not lead to a lower change in temperature, as sample #15 had the highest change in surface temperature. The resistance trends for the cross-ply samples tended to remain fairly constant throughout the entirety of the experiments. These trends were present in all of the cross-ply experiments. This is in contrast to the unidirectional specimens, where an initial resistance rise was present, followed by a slow fall or leveling off as mentioned previously.

Additionally, similar experiments were carried out for steady current applications. The time history of the change in surface temperature with respect to time for a 50 A steady current application can be seen in Figure 3.50.

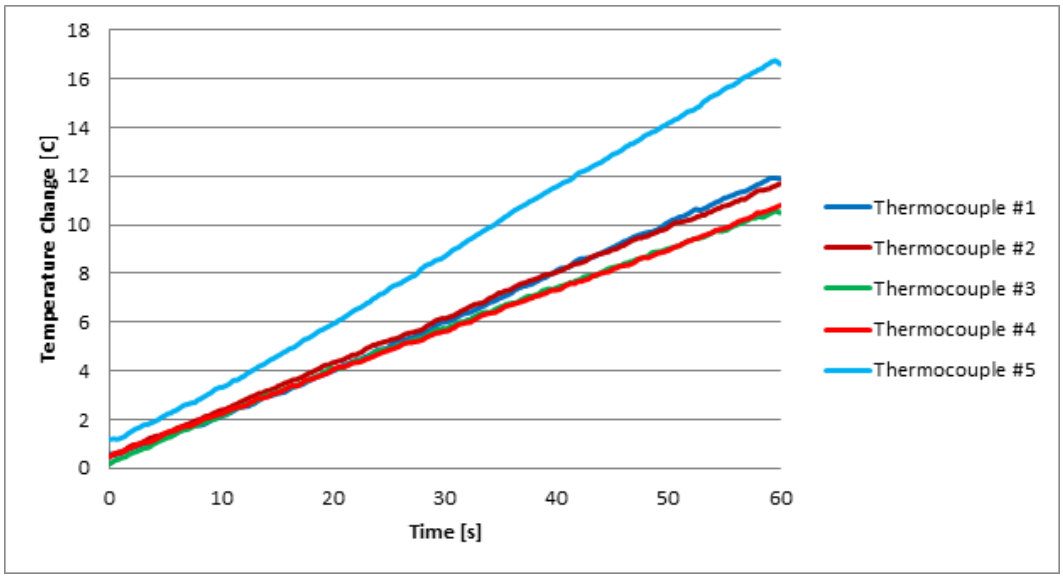

Figure 3.50: Symmetric Cross-Ply Sample #17: Temperature Change vs. Time, Steady Current: I = 50 A

The heating in the composite plates due to the steady electrical current also produced a temperature gradient throughout the length of the plates. This temperature gradient can be seen in Figure 3.51 for 50 A steady current application. The time history of the resistance for this experiment can be seen in Figure 3.52.

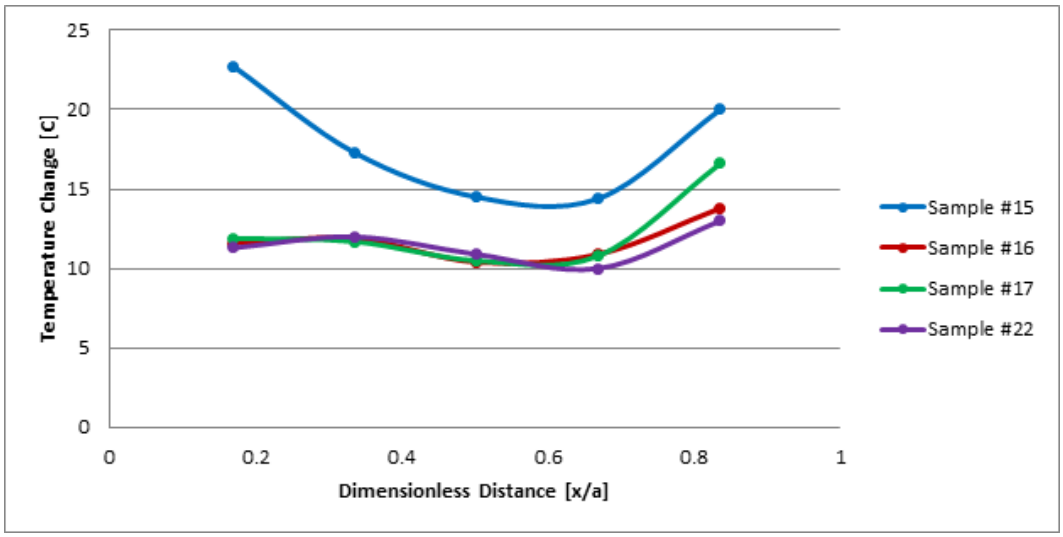

Figure 3.51: Symmetric Cross-Ply: Temperature vs. Dimensionless Distance, Steady Current: I = 50 A

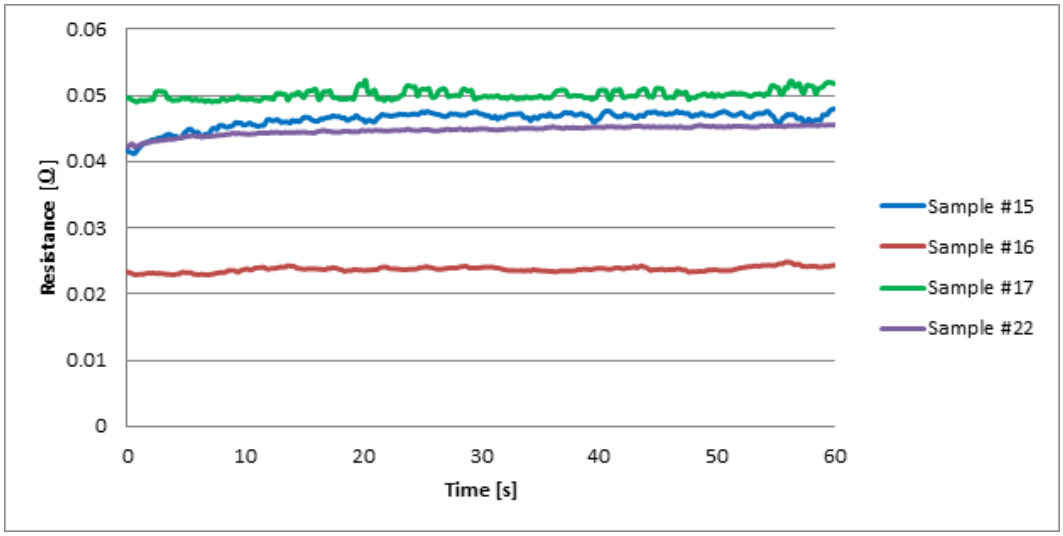

Figure 3.52: Symmetric Cross-Ply: Resistance vs. Time, Steady Current: I = 50 A

Comparing Figures 3.51and 3.52, one can see that the highest resistance measure was for sample #17, followed by #15, #22, and #16. However, this resistance order does not correlate with the change in surface temperature. Here, sample #15 had the highest change in temperature followed by the three remaining samples, which all had similar temperature distributions. Looking at samples #15 and #17, there is a difference of approximately 7.8% in the final resistance (after 1 minute), with sample #17 being greater. However, this lower resistance of sample #15 resulted in a temperature increase of roughly 11^{o} C and 4^{o} C, as measured by thermocouples #1 and #3, respectively. Additionally, the temperature gradient for three of the four samples is different than that observed for the unidirectional samples discussed earlier. Here, the gradient for the cross-ply samples #1, #17, and #22 display different results than sample #15. Sample #15 produces the typical shape of the temperature gradient present in the previous unidirectional trials.

As mentioned earlier with the unidirectional specimens, no correlation was observed between the contact resistance values and the surface temperature change. This is believed to be due to relatively small difference in the resistance of the four samples tested. Therefore, the change in the surface temperature is believed to be a function of the resistance time history as well as any differences in the samples that would have an amplified effect on the Joule heating.

A comparison of the effect of average current on the temperature distribution can be seen in Figure 3.53, along with the resistance time history in Figure 3.54.

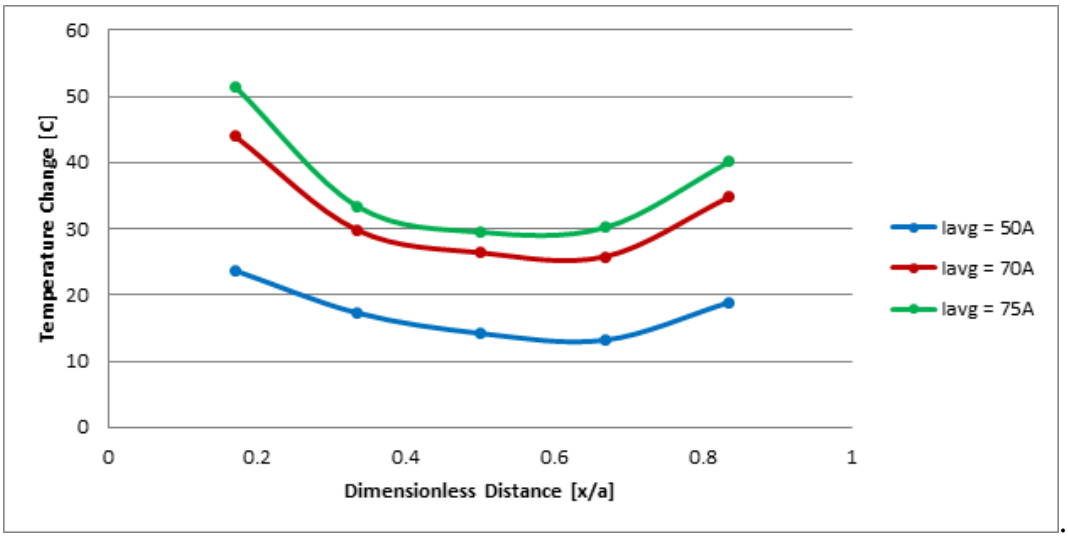

Figure 3.53: Symmetric Cross-Ply Sample #15: Temperature vs. Dimensionless Distance: ω = 50 Hz

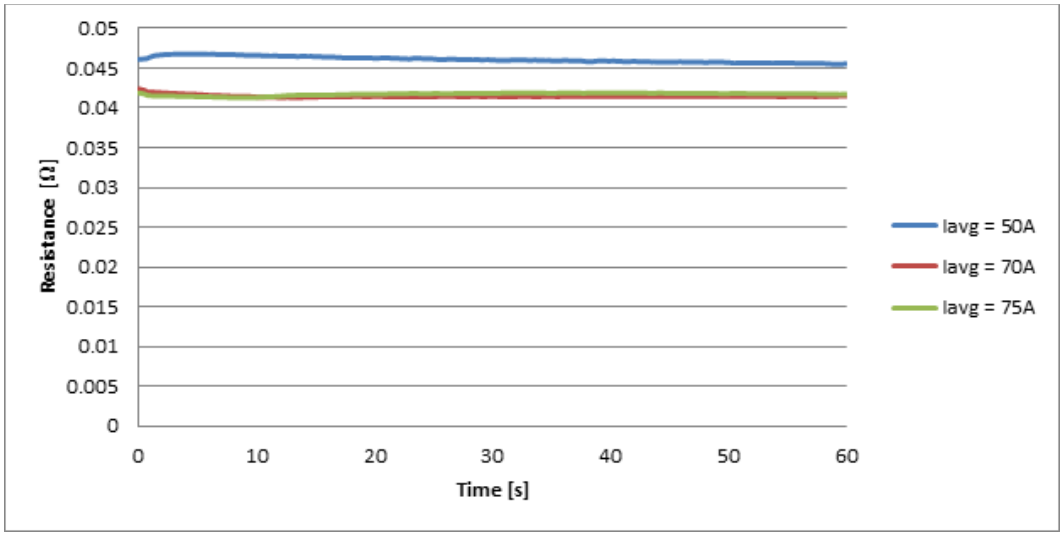

Figure 3.54: Symmetric Cross-Ply Sample #15: Resistance vs. Time: ω = 50 Hz

In Figure 3.53 it can be seen that an increase in the average current directly affects the change in surface temperature of the composite specimens. A decrease in average current from 75 to 50 A resulted in a decrease of surface temperature of approximately 28^{o} C and 15.3^{o} C as measured by thermocouple #1 and thermocouple #3, respectively. This was found to be the case for all samples, experiments, and average currents tested. In Figure 3.54 it can be seen that the resistance remains fairly constant for the entirety of the experiment.

The current/temperature findings above were also confirmed for steady current applications. This temperature relationship with current can be seen in Figure 3.55, as well as the resistance time history in Figure 3.56.

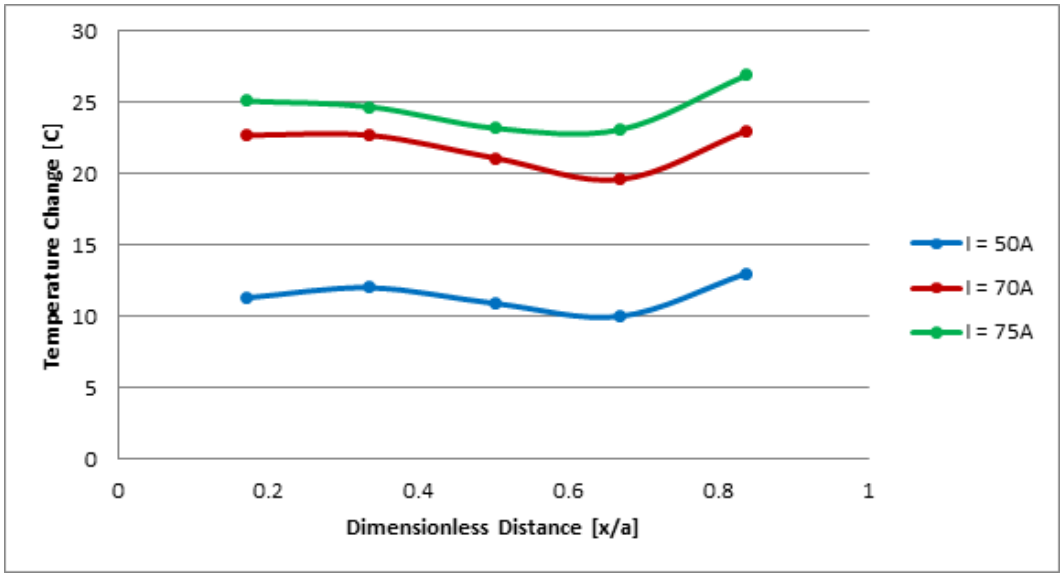

Figure 3.55: Symmetric Cross-Ply Sample #22: Temperature vs. Dimensionless Distance, Steady Current

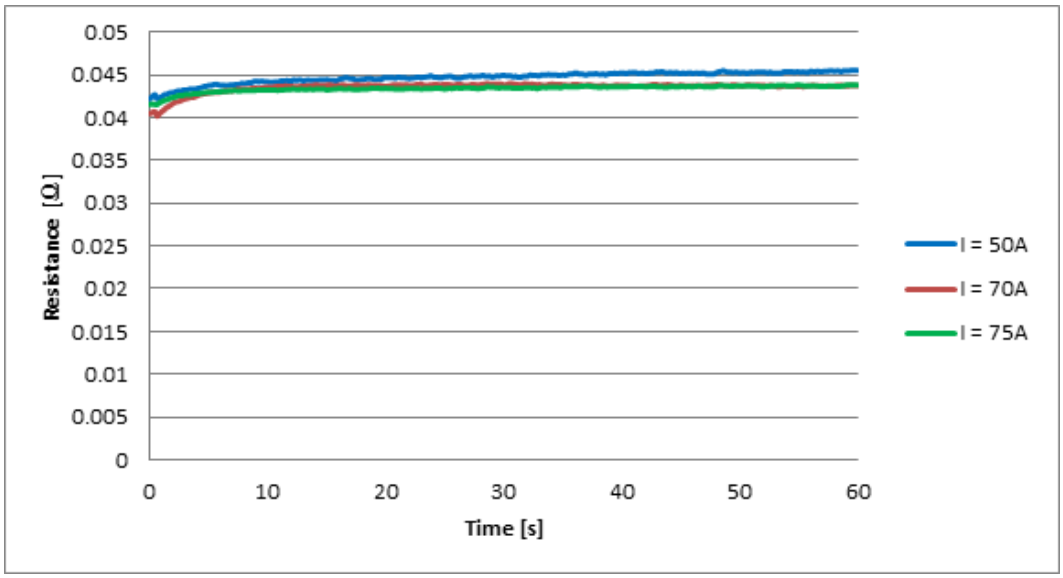

Figure 3.56: Symmetric Cross-Ply Sample #22: Resistance vs. Time, Steady Current

Referring to Figure 3.55, it can be seen once again that decrease in average current (75A to 50 A) results in a decrease in the surface temperature of approximately 14^{o} C and 12.3^{o} C as measured by thermocouple #1 and thermocouple #3, respectively, for sample #22. Figure 3.56 also reveals once again that the resistance during the experiment was fairly constant with very little change throughout the experiment. Note that the resistance for 70 and 75 A is very similar in value, resulting in the two overlapping on the plot.

The effect of frequency on the change in temperature can be seen in Figure 3.57, with markers indicating the location of the temperature measurement. The time history of the resistance associated with the experiment can be seen in Figure 3.58. As noted earlier, the temperature distribution is not symmetric throughout the plate. Figure 3.57 also reveals that frequency does not have a noticeable effect on the temperature distribution of the composite specimens. This was found to be the case for all samples #15, #16, and #17. However, sample #15 exhibited a different behavior at I_{avg} = 75 A

and ω = 25 Hz. Here, the change in temperature was lower compared to the steady current state case at I = 75 A. This situation only occurred in only one sample and one experiment. Therefore, it can be concluded that temperature is not a function of frequency. A summary of the percent differences in temperature from steady to time-varying current (75 A) measured at the end of each experiment (60 seconds) can be seen in Table 3.17.

Table 3.17: Percent Change in Temperature for Symmetric Cross-Ply Composites, 75 A Steady and 75 A Time Varying Electric Currents

Percent Change in Temperature From 75A Steady Current						
Frequency, ω [Hz]	Sample	TC #1	TC #2	TC #3	TC #4	TC #5
25	#15	-19.1	-11.4	-6.6	-7.8	-9.7
	#16	1.5	1.9	3.6	1.1	-2.8
	#17	11.2	10.6	7.5	-0.8	4.2
50	#15	3.7	3.6	9.8	11.4	6.5
	#16	-1.9	4.7	2.8	1.5	-6.3
	#17	10.4	-0.4	1.3	-0.4	8.8
150	#15	7.9	6.9	12.1	17.9	10.6
	#16	1.1	4.3	4.4	0.8	-3.2
	#17	14.0	13.2	7.0	5.4	12.7

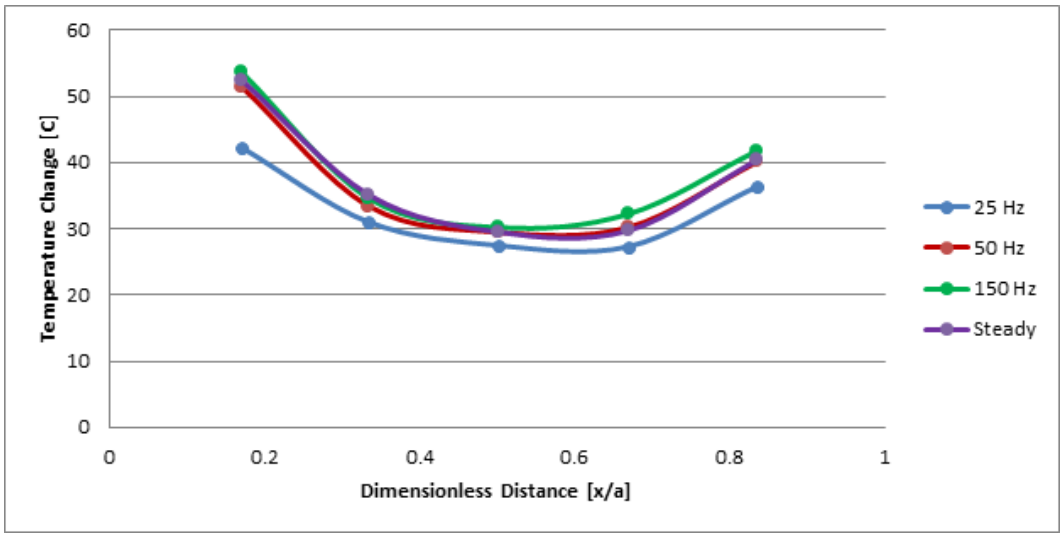

Figure 3.57: Symmetric Cross-Ply Sample #15: Temperature vs. Dimensionless Distance: I_{avg}= 75 A

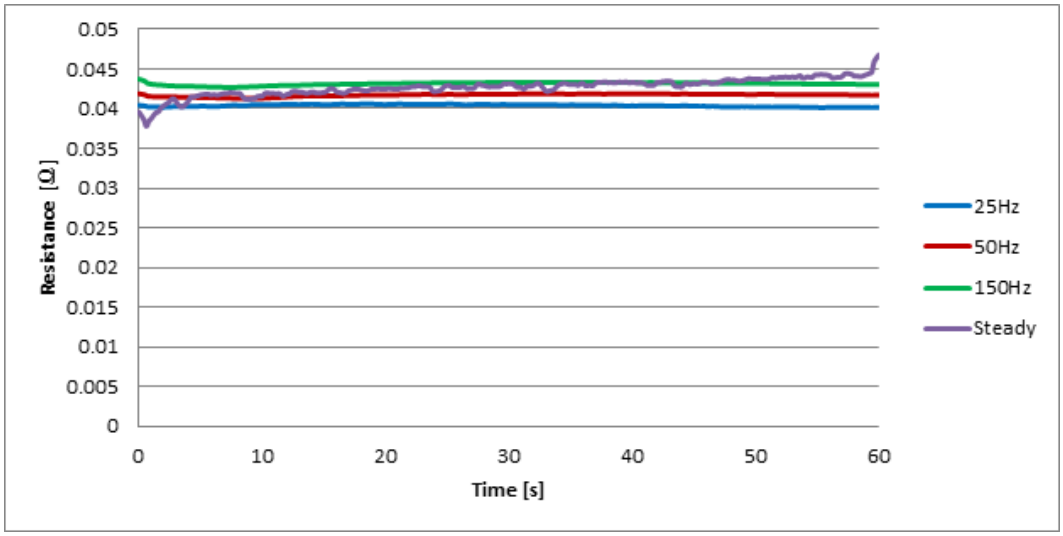

Figure 3.58: Symmetric Cross-Ply Sample #15: Resistance vs. Time: I_{avg}= 75 A

When looking at Figure 3.58, it can be seen that experiments with higher frequencies resulted in higher contact resistance trends, with the steady current having the highest resistance. However, this did not correlate with the change in surface temperature as one might expect as steady current had the second lowest change in surface temperature. As mentioned previously, the relationship between the contact resistance and change in surface temperature is not well defined due to samples having very similar resistance values.

3.5 Experimental Conclusions

3.5.1 Electrical Behavior of IM7/977-3 Composites

A series of electrical characterization tests on IM7/977-3 unidirectional and symmetric cross-ply composite laminates have been performed and the effects of electric current magnitude and duration, electrical resistance, and associated thermal effects have been investigated. After a thorough review of all of the electrical characterization and thermal behavior test results, conclusions can be drawn based off of the electric current characteristics (i.e. different average currents, time-varying frequencies, steady currents) and composite lay-up (unidirectional and symmetric cross-ply).

First, it was found that the electrical resistance for unidirectional specimens subjected to time-varying electrical current tends to increase with time. The resistance starts at an initial value, then sharply rises, and eventually lowers to a steady value. This sharp increase can be as much as 30% from the initial resistance. Frequency did not appear to play a role in the trend of the resistance. Different frequencies at the same average currents tended to produce very similar resistance curves. However, there was a relationship found between the average current and the magnitude of the calculated resistance waveforms. Here, it was found that higher average currents resulted in lower

average resistances. Moreover, it was discovered that the amplitude of resistance tended to be lower for higher average currents compared to lower average currents with the same peak-to-peak current.

Second, for the symmetric cross-ply samples tested, different electrical resistance behavior was noted for applications of time-varying currents. For these fiber orientations, the time history of the resistance remained fairly constant throughout the experiments. Little change (< 8%) was noticed from the beginning of the experiment to the end. Similarly, with the unidirectional samples, very little change in the resistance time history was noticed with a change in the electrical current frequency. Higher resistance values were also calculated at lower average current levels when compared to higher average current levels. A relationship was also found between the average current and amplitude of resistance similar to that of the unidirectional samples. However, this relationship was not as well defined as in the previous case. Additionally, the resistance was also roughly twice as much as the unidirectional samples tested under the same conditions. This was expected as the cross-ply specimens have half of the conducting fibers available for electrical current transfer.

Results of steady current applications for both unidirectional and symmetric cross-ply lay-ups produced different electrical resistance behavior compared to time-varying currents. For both fiber orientations, the electrical resistance under steady current does not stay constant. This was noted as monotonically increasing with time. Furthermore, the calculated electrical resistance was lower when compared to time-varying currents. However, there were some differences in the steady current electrical resistance behavior between the two fiber orientations. For unidirectional samples, the resistance increased with an increase in steady current magnitude. This is in contrast to cross-ply specimens, as a decrease in resistance was noticed with an increase in the steady current magnitude.

Finally, an interesting voltage-current relationship was revealed for steady current application. It was found that the resistance for unidirectional and cross-ply specimens was linear up to a critical value. Once above that value, the relationship becomes nonlinear and linear Ohm's law is no longer valid. This critical value was found to be 50 A for steady current. Furthermore, this critical value also had an effect on the resistance over time. The behavior of the electrical resistance showed very little change under the 50 A critical value over time. However, at or above this value, variations from the initial to the final resistance have been shown.

3.5.2 Thermal Behavior of IM7/977-3 Composites

The electrical current of both time-varying and steady currents results in the electrical energy being converted to Joule heat. The change in temperature due to Joule heat and contact resistance was accurately and consistently measured by the 5 infrared thermocouples used in the experimental set-up. This current-induced heating of the composites resulted in noticeable relationships. First, it was observed for both types of current applications and fiber orientation that an increase in current magnitude (or average current) resulted in an increase in the surface temperature of the composite specimens. Moreover, the temperature distribution across the composite sample in the direction of the applied current is highly non-uniform. Because of contact resistance, the ends closer to the contact interface measured higher temperatures. However, for cross-ply specimens, this increase in temperature was higher for the same current levels compared to unidirectional specimens. This is a result of only half of the conductive fibers being available for electric current conduction in cross-ply samples as compared to unidirectional ones, resulting in a higher current density and higher contact interface heating. Moreover, for the varying frequency range tested, a relationship could not be determined between the frequency and resistance and temperature. Thus, it has been

concluded that that frequency (up to 150 Hz) had no noticeable effect on the resistance or the temperature increase of the composite specimens. This was found to be true for both unidirectional and cross ply samples tested.

The obtained experimental results not only give insights into the electrical and thermal behavior of electrified IM7/977-3 carbon fiber polymer matrix composites, but also provide valuable data for the future development and calibration of models.

CHAPTER 4
SUMMARY AND RECOMMENDATIONS

4.1 Summary

In this work, the electrical characterization and associated thermal effects on IM7/977-3 unidirectional and symmetric cross-ply composite laminates subjected to time-varying and steady currents were studied. A fully automated set-up developed for the electrical and thermal characterizations. Real-time measurements of the electric current, voltage, and temperature made it possible to obtain voltage-current characteristics, time-dependent electrical resistance, and spatial and temporal temperature variations in the composites.

It was found that the electrical resistance of the composites is higher when subjected to the electric current of time-varying frequencies as compared to that of steady currents. Furthermore, the electrical resistance behavior of unidirectional composites differs from that of symmetric cross-ply composite laminates. For unidirectional specimens, the resistance is lower for steady currents and monotonically increases with time. For time-varying frequencies, resistance tends to rise sharply and then settle to a lower value. This is in contrast to symmetric cross-ply specimens where the resistance was roughly twice as much for steady currents, and also monotonically increased with time. However, for time-varying frequencies, the resistance remained fairly "constant" with time. Furthermore, voltage-current relationships for steady current application reveal that there is a critical value at which the relationship becomes nonlinear and the linear Ohm's law is no longer valid.

For current-induced heating, relationships between the current magnitudes for steady currents (average current for time-varying currents), the electrical resistance, and current duration were found. Increases in steady current magnitudes or average currents

resulted in increase of the composite surface temperatures. Additionally, longer applications of current and higher composite resistance also resulted in increased composite surface temperatures. However, for both unidirectional and symmetric cross-ply specimens, it has been concluded that that frequency range tested (up to 150 Hz) had no noticeable effect on the resistance or the temperature increase of the composite specimens.

Finally, a system was created to allow for the time coordination of electrical current application and mechanical impact load. This system allows for a 1 ms time resolution for the impact and current application. Additionally, this system can be removed without affecting the normal operation of the impact tester.

4.2 Recommendations

While performing the electrical characterization and monitoring electric current-induced heating, there were two improvements as well as future investigations that could be performed. These improvements and investigations are:

1. Further develop a method to reduce the contact resistance at the composite-copper contact interface. A reduction in the contact resistance will significantly reduce contact associated heating to further understand the temperature distribution attributed to Joule heating.
2. Incorporate data acquisition, reduction and analysis into one system. The combination of these processes will reduce the amount of time that is spent post-analyzing data.
3. Further explore the electrical characterization and the associated thermal effects on composites subjected to time-varying electrical currents beyond 150 Hz. For this, additional equipment will be needed as the limit of frequency output of the current power supply has been reached.

4. Using the data obtained in this thesis, modify and calibrate finite element model (FEM) developed in earlier studies (Sierakowski et al., 2008, Zantout, 2009) to predict the electric-current-induced temperature distributions in the composites when subjected to time-varying currents.
5. Conduct impact tests on the electrified IM7/977-3 unidirectional and symmetric cross-ply specimens.

APPENDIX A

RESISTANCE DATA SMOOTHING AND REFINEMENT

A.1 Resistance Data Smoothing and Refinement

To simplify the data analysis, the resistance data was post-processed. This was done by averaging the resistance values over set time-steps and then smoothing the averaged data by reducing the amount of data points. The moving average filter calculates the average of a number of points (or of an array) in a time-step (or span) and then repeating at the next time. The simple moving average filter is seen in Equation A.1.

$$MA = \frac{\sum_{j=1}^{n} y_i}{n} \tag{A.1}$$

Here, n represents the time-step and y_i is the function value at the i^{th} step. The array of resistance values and times needed to be averaged over particular time-steps and include the associated time. To compute this average over the entire array, Mathematica computer software was used to determine the new array of averaged values. The Mathematica function call for Equation A.1 can be seen in Equation A.2.

$$MovingAverage[list, r] \tag{A.2}$$

Equation A.2 gives the moving average of *list*, which represents the array of resistance and time values computed by average runs of r elements. In the case for the experiments

performed, *list* would be the array of resistance and time values with a length given by Equation A.3.

$$Length = L_{\exp} x 20 x f \tag{A.3}$$

In this equation, L_{exp} is the length of the experiment in seconds, and f is the frequency of the time-varying signal.

APPENDIX B

MEASUREMENT ERRORS

B.1 Measurement Errors

In the experiments performed in this thesis, there were seven key measurements to be performed. All of these measurements involved measuring and recording voltages. These voltages would be used to compute the current applied and the resistance of the composite sample, as well as the surface temperature. Associated with each type of measurement, there is an expected amount of error and the errors yield uncertainty of the measurement. The goal is to realize these errors and try to minimize them as much as possible. Furthermore, with the amount of uncertainty known, a more thorough analysis of data can be performed to determine if any significant relationships exist.

B.2 Measurement Error Sources

In the performed experiments, the real-time current, resistance and temperature of the composite samples needed to be obtained. These measurements of current and resistance cannot be made directly by the utilized equipment; therefore an alternative approach was used. To determine the current applied to the composite sample, a voltage drop across a precision shunt resistor is measured by the U2351A data acquisition unit (as described in Section 2.3.2.3). Using Ohm's law with this measurement, the current can be determined. The resistance of this shunt resistor was 0.5 mΩ. The maximum current applied to the specimens in any experiment performed was 100 A, resulting in a voltage drop of 0.05 V or 50 mV. A problem with such voltage measurements less than 100 mV is that they are quite susceptible to noise (Figliola, 1995). This becomes even more apparent with lower current applications such as 1 A, resulting in 0.0005 V or 0.5 mV.

Error sources for these measurements are: change in shunt resistance, noise, and analog to digital conversion by the DAQ.

The resistance of the composite specimen is determined by measuring voltage drop across the composite specimen and mathematically calculating the resistance (Ohm's law) by using the current determined previously. The voltage drop measured here was only vulnerable to noise at current applications of 5 A or less, as the minimum resistance of any of the samples tested was approximately 0.02Ω. Sources of error for resistance measurements are: voltage measurement by the DAQ as well as current errors (stemming from DAQ errors), as it is also used to determine resistance (Ohm's law).

Measurements of temperature are performed by the k-type infrared thermocouples and U2536A data acquisition unit (as described in Section 2.3.3) and are inherently subject to the same noise in the current calculation. The range of temperature expected during experiments was ambient to 220^{o}C. This range of temperature for k-type thermocouple output results in voltage ranges of 0.718 – 8.138 mV when referenced at 0^{o}C. However, to avoid the noise due to low voltage measurements, the U2802A signal conditioner was used to amplify (condition) and filter the signal to a voltage (± 10 V) that can be measured by the U2536A more accurately. Errors in temperature measurement can be attributed to infrared thermocouples, signal conditioning, as well as analog to digital conversion by the DAQ.

B.3 Current Error

The error sources listed previously can be used to determine the error bounds of current applied to the composite sample. Current is the first error to be examined as it has an immediate effect on the resistance of the composite specimen. The specifications on the shunt resistance could not be obtained, however it is safe to assume ±0.25% accuracy and 0.002% for every 1^{o}C of temperature change (Current Shunt Resistors,

2010). The temperature change of the shunt was never recorded during experimental testing, so a worst case scenario of 50°C will be assumed. With this worst case, the shunt resistance is 0.5 mΩ ± 0.00175 mΩ. The noise of the low voltage measurements was eliminated by using built in filters and protective shielding of the measurements wires to ensure that any stray signals would not affect the measurement. The final error of the measurement system is the DAQ analog to digital conversion. The analog to digital conversion errors include gain, offset, linearity, quantization, etc. The AMM software performs a self-calibration before each experiment eliminating the gain and offset errors as much as possible. For simplicity only the quantization error will be considered. Therefore the quantization error is the uncertainty of the measurement and is shown in Equation B.1.

$$u_c = e_Q = \pm\frac{1}{2}\left(\frac{E_{FS}}{2^M}\right) \tag{B.1}$$

As seen in Equation B.1, E_{FS} is the full-scale voltage expected to be measured and M is the number of bits of the data acquisition system. An E_{FS} value of 1.25 V is used as this is the measurement range specified in the AMM software and M is equal to the 14-bit resolution of the U2531A. This results in an uncertainty in the measurement of ± 0.038 mV. Using the uncertainty of the resistance and the voltage, the uncertainty of the current using Ohm's law is ± 0.427 A. This is determined by the theoretical voltage drop (50 mV + 0.038 mV) at the largest current expected (100 A) and the minimum shunt resistance (0.5 mΩ – 0.00175 mΩ), as this will result in the largest possible error.

B.4 Resistance Error

With the uncertainty of the current known, the error in the resistance measurement can be determined. The uncertainty for the voltage measured across the composite plate is the same as that for determining the current. However this error will change for every experiment as each sample differs in resistance as well as resistance behavior over time. Therefore, the worst-case scenario will be determined to cover all experimental possibilities. The maximum expected voltage drop across the plate is 10 V. Using Equation B.1, the uncertainty for the voltage across the composite is ± 0.305 mV. The uncertainty in resistance is a propagation of the two previous errors (voltage and current) as the resistance is a function of the two (Ohm's law). The resistance propagation error can be seen in Equation B.2.

$$U_R = \sqrt{\left[\frac{dR}{dV}U_V\right]^2 + \left[\frac{dR}{dI}U_I\right]^2} \tag{B.2}$$

Here, *dR/dV* and *dR/dI* are the derivatives of Ohm's law with respect to voltage and current. U_V and U_I are the uncertainty of voltage and current, respectively. Applying Equation (B.2) leads to Equation (B.3).

$$U_R = \sqrt{\left[\frac{1}{I}U_V\right]^2 + \left[\frac{-V}{I^2}U_I\right]^2} \tag{B.3}$$

Using uncertainties of 10.000305 V for voltage and 0.427 A for current, as well as 10 V and 100 A for V and I parameters, leads to an uncertainty of ± 0.1 Ω due to the propagation of error. This is the largest possible error that can be present during any experiment. The error propagation considers the worst cases for both the voltage and current measurements and how they affect the resistance.

B.5 Temperature Error

Errors in the temperature measurement are straight forward, as the manufacturer of the signal conditioner and the data acquisition system specify a combined accuracy of ± 1.5° C. The infrared thermocouples have specified error of 3% of the reading as described in Section 2.3.3.1. Using the maximum temperature of 150° C the maximum error is ± 4.5° C. The total uncertainty for the measurements is given by Equation B.4.

$$u_c = \pm\sqrt{e_{TC}{}^2 + e_{DAQ}{}^2} \tag{B.4}$$

Here e_{TC} is the error of the infrared thermocouples and e_{DAQ} is the error of the signal conditioner and data acquisition unit. Using the above information, the uncertainty for temperature measurements is ± 4.74° C. Once again this is the maximum uncertainty that can be expected. In the majority of experiments performed the temperature never exceeds 70°C. If this is used as the maximum, the uncertainty can be lowered to ± 2.58° C. The accuracy of the measurement with respect to temperature can be seen in Figure B.1.

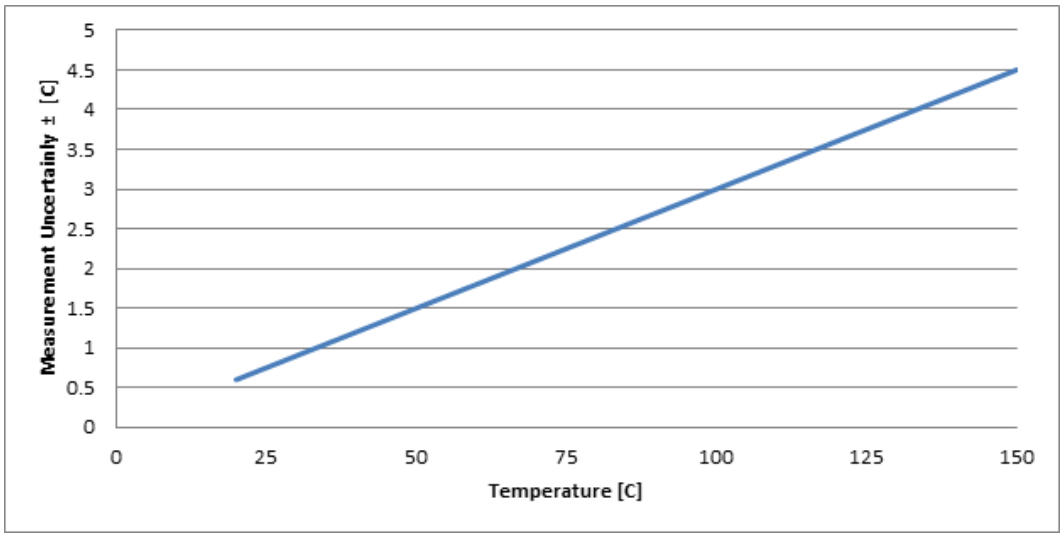

Figure B.1: Measurement Uncertainty vs. Temperature

REFERENCES

Abrate, Serge. IMPACT ON COMPOSITE STRUCTURES. Cambridge: Cambridge UP, 1998. 135-160.

Agilent Technologies. 7 Apr. 2010 <http://www.agilent.com>.
"American Wire Gauge Table and AWG Electrical Current Load Limits with Skin Depth Frequencies." PowerStream Power Supplies and Chargers for OEMs in a Hurry. Web. 20 Aug. 2010. <http://www.powerstream.com/Wire_Size.htm>.

Angelidis N, Khemiri N, Irving PE. Experimental and finite element study of the electrical potential technique for damage detection in CFRP laminates. Smart Materials and Structures 2005; 14: 147-154.

"Arctic Silver Incorporated - Arctic Silver 5." Arctic Silver. 26 Apr. 2010. <http://www.arcticsilver.com/as5.htm>.

“ASTM D 3763-06 Standard Test Method for High Speed Puncture Properties of Plastics Using Load and Displacement Sensors." ASTM International (2006).

“ASTM D 5728-07 Standard Test Method for Impact Resistance of Flat, Rigid Plastic Specimens by Means of a Falling Dart (Tup of Falling Mass)." ASTM International (2007).

"Boeing: Commercial Airplanes - 787 Dreamliner - Background." The Boeing Company. Web. 16 June 2010. <http://www.boeing.com/commercial/787family/background.html>.

Braunovic, Milenko, V. V. Konchits, and Nikolai Konstantinovich. Myshkin. Electrical Contacts: Fundamentals, Applications and Technology. Boca Raton: CRC, 2007. Print.

Chung DDL. Damage detection using self-sensing concepts. Proceedings of IMechE, Part G: Journal of Aerospace Engineering 2007; 221: 509-520.

"Current Shunt Resistors." Digital DC Ammeter, Amp & Watt Hour, Battery Fuel Gauges & Meters. Web. 20 Aug. 2010. <http://www.rc-electronics-usa.com/current-shunt.html>.

"Composites and Advanced Materials." Web. 15 June 2010. <http://www.centennialofflight.gov/essay/Evolution_of_Technology/composites/Tech40.htm>.

“Cycom 977-3 Toughened Epoxy Resin.” Cytec Engineered Materials. 13 Aug. 2010 <http://www.cytec.com>.

Deltec Company. 13 Oct. 2008 <http://www.deltecco.com/>.

"DuPont" DuPont. The Miracles of Science™. Web. 07 June 2010. <http://www2.dupont.com/Plastics/en_US/Products/Delrin/delrin_amer_product.html>.

"Duralco 120" Web. 14 June 2010. <http://www.cotronics.com/vo/cotr/ea_electricalconductive.htm>.

"Dynatup Drop Weight Impact Test Machine Model 8200." Instron. 29 Apr. 2010 http://www.instron.us/wa/library/default.aspx

Figliola, R. S., and Donald E. Beasley. Theory and Design for Mechanical Measurements. New York, NY: J. Wiley and Sons, 1995. Print.

"Hexcel" Hexcel.com - Carbon Fiber and Composites for Aerospace, Wind Energy and Industrial. Web. 09 Aug. 2010. <http://www.hexcel.com/>.

Jones, Robert M. Mechanics of Composite Materials. 2nd ed. New York: Taylor & Francis, 1999. Print.

Joshi, P. B., and P. Ramakrishnan. Materials for Electrical and Electronic Contacts: Processing, Properties, and Applications. Enfield, NH, USA: Science, 2004. Print.

Kruger, Anke. Carbon Materials and Nanotechnology. Weinheim: Wiley-VCH-Verl., 2010. Print.

McMaster-Carr. Web. 26 Apr. 2010. http://www.mcmaster.com

Mohler, J. B. Electroplating and Related Processes. New York: Chemical Publishing, Inc, 1969. Print.

"Mud, Glorious Mud: Homes Made of Earth - Property, House & Home - The Independent." The Independent | News | UK and Worldwide News | Newspaper. Web. 15 June 2010. <http://www.independent.co.uk/life-style/house-and-home/property/mud-glorious-mud-homes-made-of-earth-932752.html>.

"Non-Contact Infrared Temperature Transmitter." Sensors, Thermocouple, PLC, Operator Interface, Data Acquisition, RTD. Web. 27 Apr. 2010. <http://www.omega.com/ppt/pptsc.asp?ref=OS136&ttID=OS136&Nav=>.

Ogasawara T, Hirano Y, Yoshimura A. Coupled thermal-electrical analysis for carbon fiber/epoxy composites exposed to simulated lightning current. Composites Part A-Applied Science and Manufacturing 2010; 41 (8): 973-981.

Paunovic, Milan, and Mordechay Schlesinger. Fundamentals of Electrochemical Deposition. New York: Wiley, 1998. Print.

"Portable Blackbody." Sensors, Thermocouple, PLC, Operator Interface, Data Acquisition, RTD. Web. 07 June 2010. <http://www.omega.com/ppt/pptsc.asp?ref=BB703&ttID=BB703&Nav=>.

Prasse T, Michel F, Mook G, Schulte K, Bauhofer W. A Comparative investigation of electrical resistance and acoustic emission during cyclic loading of CFRP laminates. Composites Science and Technology 2007; 61: 831-835.

Reid, S. R., and G. Zhou. Impact Behaviour of Fibre-reinforced Composite Materials and Structures. Boca Raton: CRC, 2000. Print.

Schulte K, Baron C. Load and failure analysis of CFRP laminates by means of electrical resistivity measurements. Composites Science and Technology 1989; 36(1): 63-76.

Slade, Paul G., ed. Electrical Contacts: Principles and Applications. Danbury: Marcel Dekker Incorporated, 1999.

"Sunstone Engineering - DpInstructions." Sunstone Engineering - Fine Resistance Spot Welders, Weld Heads, and Welding Accessories. Web. 07 Apr. 2010. <http://www.sunstoneengineering.com/site/pages/dpInstructions>.

Sierakowski, Robert L., Igor Y. Telichev, and Olesya I. Zhupanska. "Impact Damage Assessment in Electrified Carbon Fiber Polymer Matrix Composites." American Institute of Aeronautics and Astronautics (2007).

Sierakowski, Robert L., Telitchev, I. Y., and Olesya I. Zhupanska. "On the Impact Response of Electrified Carbon Fiber Polymer Matrix Composites: Effects of Electric Current Intensity Duration." Composites Science and Technology 6 (2008): 639-649.

Swanson, Stephen R. Introduction to Design and Analysis With Advanced Composite Materials. Upper Saddle River, New Jersey: Prentice Hall, 1997. Print.

“Thermocouples." Omega. 26 Apr. 2010
http://www.omega.com/prodinfo/thermocouples.html

Telichev I. Y., Zhupanska O. I. "Experiments in Composite Toughening through Application of an Electrical Field", Technical Report No F08635-03-D-0130/06-0022, AFRL/MN, Eglin AFB, 2007.

Telitchev, I. Y., R. L. Sierakowski, and O. I. Zhupanska. "Low-Velocity Impact Testing of Electrified Composites: Part I-Application of Electric Current." Experimental Techniques (2008a): 35-39.

Telitchev, I. Y., R. L. Sierakowski, and O. I. Zhupanska. "Low-Velocity Impact Testing of Electrified Composites: Part II-Experimental Setup and Preliminary Results." Experimental Techniques (2008b): 53-57. Print.

Vasiliev, Valery V., and Robert M. Jones. Mechanics of Composite Structures. Washington, D.C.: Taylor & Francis, 1993. Print.

Wang D, Chung DDL. Comparative evaluation of the electrical configurations for the two-dimensional electric potential method of damage monitoring in carbon fiber polymer-matrix composite. Smart Materials and Structures 2006; 15: 1332-1344.

Williamson, Darrell. Discrete-time Signal Processing: an Algebraic Approach. London: Springer, 1999. Print.

Zantout, Alan E., and Olesya I. Zhupanska. Electrical and Impact Characterization of Carbon Fiber Polymer Matrix Composites. Thesis. University of Iowa. Dept. of Mechanical Engineering, 2009. Print.

Zantout, Alan E., and Olesya I. Zhupanska. "On the Electrical Resistance of Carbon Fiber Polymer Matrix Composites." ELSEVIER Composites Part A: Applied Science and Manufacturing 41A.11 (2010). Print.

Zhupanska, Olesya I., and Robert L. Sierakowski. "Effects of an Electromagnetic Field on the Mechanical Response of Composites." Journal of Composite Materials 41 (2007): 633-654.

Zhupanska, O. I. "Dynamic Behavior of Carbon Fiber Composites Subject to AC Electromagnetic Fields and Impact Loads." (2009):